**Title**

Unraveling the Role of Endocardial Heterogeneity in Post-EMT Valvulogenesis via Single-Cell Multi-omic Analysis

**Permalink**

**Author**

Merriman, Alexander

**Publication Date**

2023

Unraveling the Role of Endocardial Heterogeneity in Post-EMT Valvulogenesis via Single-Cell Multi-omic Analysis
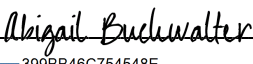
by
Alexander Merriman


DISSERTATION
Submitted in partial satisfaction of the requirements for degree of
DOCTOR OF PHILOSOPHY

in

Developmental and Stem Cell Biology

in the

GRADUATE DIVISION
of the
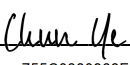UNIVERSITY OF CALIFORNIA, SAN FRANCISCO

Approved:

Abigail Buchwalter
_____
Chair

Deepak Srivastava
_____

Daniel Wagner
_____

Chun Ye
_____

_____
Committee Members

# Acknowledgements

As I conclude this phase of my training, I cannot help but feel overwhelmed with gratitude. There are numerous individuals who have played an indispensable role in shaping my path, encouraging my aspirations, and supporting me through the countless trials and triumphs over the past four years. Therefore, I dedicate this acknowledgement to express my profound appreciation for those who have been there for me.

First and foremost, I extend my deepest appreciation to my thesis advisors, Deepak and Jimmie. Through your exceptional guidance, patience, and dedication to mentorship, you have challenged me to push the boundaries of my knowledge and given me the freedom to develop not only as a scientist, but also as a person. I aspire to run a lab as you do, encouraging my students to pursue their interests and provide the supportive environment that allows them to flourish.

To my incredible parents, who have loved me, made sacrifices for me, and always believed in my dreams, thank you. Your unwavering support and encouragement have been critical throughout my academic journey. Every achievement I've made is a testament to your endless love and unwavering support. Thank you for instilling in me the values of resilience, determination, and never giving up.

To my amazing friends, who have been with me through thick and thin, thank you for your unwavering camaraderie and for always being there for me. Your support, our never-ending adventures, and venting sessions have kept me going. You've filled this journey with warmth and unforgettable memories.

**Abstract**

**Unraveling the Role of Endocardial Heterogeneity in Post-EMT Valvulogenesis**

**via Single-Cell Multi-omic Analysis**

**Alexander Merriman**

Valvular heart disease is a major source of morbidity and mortality with an anticipated increase in prevalence secondary to an aging population and increase in survivorship for patients with congenital disease. Living tissue engineered heart valves are a promising regenerative medicine-based therapeutic objective, but require further developmental studies to become a clinical reality. While many of the molecular regulators of endocardial cushion formation via endocardial-to-mesenchymal transition (EMT) have been identified, much remains to be understood about post-EMT valvulogenesis. In this study, we have interrogated the later stages of valvulogenesis to understand the molecular mechanisms of valve formation and how these mechanisms are disrupted in the context of disease. Leveraging a combination of single-cell RNA and chromatin accessibility sequencing in the developing mouse heart, we identified a novel, rare valvular endocardial subpopulation with a unique transcriptional profile comprised of highly specific developmental signaling pathway genes. These cells are first detectable after valve primordia formation at embryonic day 12.5 and are spatially localized at the leading edge of the developing leaflets. Temporally-restricted ablation of this rare subpopulation results in perinatal lethality and dysplastic valve development, characterized by thickened, immature leaflets associated with valvular stenosis and regurgitation. These dysplastic features are consistent with the features of several congenital valvulopathies including Ebstein's anomaly, and pulmonary or aortic valve stenosis. Lineage tracing analysis revealed that these cells are neural crest-derived,

providing the first evidence of a neural crest-to-endocardial transition. Neural Crest-specific deletion of Pthlh, a marker gene for this rare subpopulation, similarly results in perinatal lethality and dysplastic valve development, implicating a previously undescribed neuroendocrine peptide hormone signaling pathway in the regulation of valvulogenesis. Loss of neural crest-derived Pthlh signaling was associated with a cell autonomous down-regulation of several marker genes and a disruption in valvular myocardial BMP signaling, a previously described pathway required for valvular growth and remodeling. Single-cell RNA sequencing analysis of a human fetal heart with hypoplastic left heart syndrome and critical aortic stenosis demonstrated a depletion of this cell population in the diseased aortic valve relative to the other three healthy valves, suggesting these cells may be required for human valvular development. This study establishes that this rare, highly secretory neural crest-derived endocardial subpopulation and the Pthlh signaling pathway are critical to valve morphogenesis and provide new avenues for investigation into the pathogenesis of human congenital heart defects.

**Table of contents**

**List of Figures**

**Chapter 1 – Introduction**

**Chapter 2 – Analysis of wild-type murine post-EMT valvulogenesis**

**Chapter 3 – Perturbation of *Pthlh*+ Valvular Endocardial Cells**

**Chapter 4 – Pthlh+ Valvular Endocardial Cells during Human Development & Disease**

**List of Abbreviations**

AV – Atrioventricular

BMP – Bone morphogenetic protein

CHD – Congenital Heart Disease

CNCC – Cardiac neural crest cell

DAR – differentially expressed region

E – Embryonic Day

EMT – endocardial-to-mesenchymal transition

ENDC – Endocardial-derived cell

EPDC – Epicardial-derived cell

FISH – Fluorescent *in situ* hybridization

HLHS – Hypoplastic Left Heart Syndrome

Multiome – Single-cell ATAC and Gene Expression Co-Assay

OFT – Outflow Tract

scRNAseq – Single-cell RNA sequencing

scATACseq – Single-cell ATAC sequencing

TFG-β – Transforming growth factor β

VEGF – Vascular endothelial growth factor

# Chapter 1

# Introduction

**1.1 Congenital Heart Disease**

Congenital heart disease (CHD) refers to a wide array of structural abnormalities present at birth that impact cardiac function[1]. It is the most common congenital anomaly with a prevalence of approximately 1% of live births, increasing to 2.5% of live births when including bicuspid aortic valves[2,3,4]. Despite vast improvements in medical and surgical management of these patients, CHD continues to be a major source of morbidity and mortality[5,6,7]. Congenital heart defects can range from a simple septal defect to complex lesions that require multipart reconstructions or transplantation, in some cases. Congenital valve defects, accounting for approximately 20-30% of CHD cases, are often associated with the some of the highest morbidity and mortality rates[8,9].

Heart valves are complex structures within the heart that serve the critical function of maintaining unidirectional blood flow throughout the cardiac cycle. The adult heart has two sets of valves, the atrioventricular valves and the semilunar valves. The atrioventricular valves are positioned between the atria and ventricles with the mitral valve on the left side of the heart and the tricuspid valve on the right side of the heart. Similarly, the semilunar valves are positioned between the ventricles and great vessels with the aortic valve on the left side of the heart and the pulmonary valve on the right side of the heart. Developmental errors can result in a spectrum of valve disease that include stenosis, regurgitation, or atresia. Valvular stenosis occurs with the valve opening is narrowed, preventing blood from easily flowing through the valve. Regurgitation occurs when the valve fails to close properly, leading to backflow of blood to the preceding cardiac chamber. The last and most severe development defect is atresia, where the valve fails to form entirely.

One such example of a severe congenital valvulopathy is hypoplastic left heart syndrome (HLHS), characterized by the underdevelopment of the left side of the heart, including the left

ventricle, aortic valve, and mitral valve[10]. The 'no flow, no grow' hypothesis proposes the notion that improper development of the aortic and/or mitral valve results in poor flow through the left ventricle[11]. This hemodynamic disruption subsequently results in ventricular hypoplasia, leaving the patient with a single developed, functioning ventricle that postnatally needs to be surgically attached to systemic circulation in a series of three open-heart surgeries[12].

Unfortunately, treatment options for valvular CHD are limited, often requiring surgical replacement with suboptimal prostheses that can require chronic anticoagulation, increase risk of infection, and often require re-replacement[13]. Children who undergo surgical valve replacement often require numerous open-heart procedures by the time they reach adulthood, secondary to the failure of the valve prosthesis to grow with the patient[14]. Tissue engineering has emerged as a promising strategy for generating living valve replacements; however, the optimal cellular source remains to be identified[15]. To advance this therapeutic to the clinic, further developmental studies of valvulogenesis are required that will aid in the elucidation of pathogenic mechanisms of congenital valvulopathies which may be leveraged in regenerative medicine-based therapies.

While it is known that genetic factors, environmental factors, and their interaction play an important role in the development of CHD, the precise etiology of most cases remaining unknown[16,17]. Environmental contributors to CHD include maternal diabetes[18], rubella infection[19], smoking[20], obesity[21], vitamin deficiencies[22], and fetal teratogen exposures such as thalidomide[23], alcohol[24], and lithium[25]. Genetic causes of CHD are numerous and include chromosomal abnormalities (e.g. trisomy 21, trisomy 18), copy number variants (e.g. 22q11.2 deletion syndrome, 1p36 deletion), and monogenic etiologies[16,17,26,27]. Pathogenic variants have been identified in a number of molecular regulators including cardiac transcription factors (e.g. TBX5[28], GATA4[29], NKX2.5[30]), cell signaling pathways (e.g. NOTCH[31], BMP[32], VEGF[33]), and structural

proteins (e.g. MYH6[34], MYH7[35]). Improvements in next generation sequencing technologies have resulted in decreased sequencing costs and increased collection of significant amounts of genomic information from thousands of patients with CHD[36,37,38]. Despite the increase in availability of these data, limitations still exist in the prioritization and functionalization of these variants, both coding and non-coding. As such, further developmental studies that provide critical spatiotemporal information about transcriptional states and chromatin accessibility would aid tremendously in elucidating the molecular mechanisms of CHD.

## 1.2 Overview of Valvulogenesis

Valvulogenesis is the complex process by which the heart valves develop during embryonic development. During murine development, at approximately embryonic day (E) 8.5, the primitive heart tube forms which consists of an inner layer of endocardial cells surrounded by an outer layer of myocardial cells[39]. By E9.5, not long after primitive heart tube formation, valvulogenesis commences as endocardial cushions begin to form in the atrioventricular (AV) canal and outflow tract regions of the heart tube through myocardial secretion of proteoglycan-rich extracellular matrix, known as the cardiac jelly (**Fig. 1.1 A, B**)[40,41]. These endocardial cushions are subsequently cellularized via a process of endocardial-to-mesenchymal transition (EMT).

In the atrioventricular canal, there are a total of four endocardial cushions: the superior, inferior, left lateral, and right lateral cushions. All four of these cushions will undergo proliferation, differentiation, compaction, delamination and ultimately remodel giving rise to the valve leaflets, chordae tendineae, and annulus fibrosus of the mature atrioventricular valves, with some caveats (**Fig. 1.1 C, D**)[42]. By E10.5, the superior and inferior (major) cushions are mostly formed, populated by endocardial-derived cells (ENDCs) and will fuse to form the atrioventricular

4

mesenchymal complex that contributes to septation at the core of the heart, the septal leaflet of the

tricuspid



**A** Atrioventricular valves

Early | EMT | Remodeling | Mature

**B** Semilunar valves

Early | EMT | Excavation | Mature

**C**

ICC
sAVC
llAVC
CTC
iAVC
rlAVC

Preseptation

**D**

Anterior cusp
Left cusp
Right cusp
Left coronary cusp
PV
Right coronary cusp
Noncoronary cusp
AoV
Anterior leaflet
Mural leaflet
MV
TV
Aortic leaflet
Posterior leaflet
Annulus fibrosus
Septal leaflet

Postseptation

**Figure 1.1 Overview of valvulogenesis.**

**A,** Cartoon representation of atrioventricular valvulogenesis beginning with emergence of cardiac jelly between the endocardium and myocardium of the primitive heart tube, cellularization of the cushion via endocardial-to-mesenchymal transition (EMT), remodeling and delamination into leaflet and chordae tendineae structures, completed by postnatal remodeling. **B,** Cartoon representation of semilunar valvulogenesis, which follows a similar pattern as atrioventricular valvulogenesis, but differs in the excavation stage, notably lacking chordae tendineae. **C,** Cartoon representation of the endocardial cushions prior to fusion. **D,** Cartoon representation of the endocardial cushion derivatives following fusion and remodeling. AVC, atrioventricular cushion; s, superior; i, inferior; rl, right lateral; ll, left lateral; CTC, conotruncal cushion; ICC, intercalating cushion; AoV, aortic valve; PV, pulmonary valve; MV, mitral valve; TV, tricuspid valve. (Fig 1.1 A, B Adapted from Rosenthal & Harvey, 2010[41]; Fig. 1.1 C, D Adapted from MacGrogan et al., 2014[42])

valve, and the aortic leaflet of the mitral valve. The mesenchyme of lateral cushions will continue to receive additional input from epicardial-derived cells (EPDCs) through E12.5; however, these cushions do not contribute to the atrioventricular mesenchymal complex, but rather give rise to the anterior and posterior leaflets of the tricuspid valve and the mural leaflet of the mitral valve[43].

The semilunar valves form in a very similar process as to the atrioventricular valves, with some notable differences. By E11.5, the outflow tract has a total of four cushions: two cono-truncal cushions that fuse to form the aortico-pulmonary septum and two intercalating cushions that do not fuse but do contribute to semilunar leaflet formation. These cushions are populated by mesenchymal populations derived from both the endocardium and cardiac neural crest cells (CNCCs)[44]. Rather than delaminating from the underlying myocardium with sub-valvular chordae tendineae, the semilunar valves undergo a poorly understood process of excavation that yields free leaflets and the sinuses of Valsalva – the future location of the coronary artery ostia.

At the conclusion of valvulogenesis, all four valves contain mature, highly organized leaflets with a trilaminar extracellular matrix structure surrounded by an endocardial layer. Valve leaflets are composed of three layers: the atrialis (atrioventricular) or ventricularis (semilunar) layer, the spongiosa layer, and the fibrosa layer[45]. These layers have distinct ECM compositions

and mechanical properties, which contribute to the overall function of the valve. The atrialis/ventricularis layer is an elastin-rich layer on the inflow side of the leaflet subjected to laminar flow. The spongiosa layer is rich in proteoglycans that provide the valve with compressibility and cushioning. Lastly, the fibrosa layer is composed of collagen and elastin fibers that provide the valve with mechanical strength and durability.

In addition to the complex cellular and molecular processes involved in valvulogenesis, mechanical forces also play a critical role in valve development[46,47]. Hemodynamic flow through the developing heart provides mechanical cues that influence the differentiation and remodeling of endocardial cushions, valve leaflets, chordae tendineae, and annulus fibrosus. It has been shown sheer stress responsive transcription factor, *Klf2*, is required in a subset of inflow-sided valvular endocardial cells that are subject to laminar flow[48]. This mechanosensitive transcription factor up-regulates *Wnt9b* that mediates paracrine signaling between these endocardial cells and the underlying mesenchymal cells. Deletion of these transcription factors or loss of downstream *Wnt9b* leads to improper mesenchymal compaction and valvular morphogenesis resulting in midgestational demise. Moreover, ectopic valvulogenesis has been induced with modulation of mechanical forces during zebrafish heart development[49]. As such, disruptions in hemodynamic flow can lead to valve malformations and other congenital heart defects.

In summary, valvulogenesis is a complex process that involves the coordinated differentiation, proliferation, and remodeling of cells and ECM to form functional heart valves. Disruptions in valvulogenesis can lead to congenital heart defects, including valve malformations, that can have significant clinical consequences. Additionally, congenital valve defects can predispose patients to VIC dysfunction during tissue homeostasis as contributory to the pathogenesis of degenerative valvulopathies[31,50,51].

### 1.3 Molecular Regulators of Valvulogenesis

Endocardial cushion formation is the first and most well-studied stage of valvulogenesis. The molecular regulation of endocardial cushion formation is complex and involves the interplay of various signaling pathways, transcription factors, and extracellular matrix components. Some of the most well-studied regulators include bone morphogenetic protein (BMP) signaling, transforming growth factor (TGF)-β signaling, Notch signaling, and vascular endothelial growth factor (VEGF) signaling.

Initiation of valvulogenesis begins with cardiac jelly secretion by the valvular myocardium, giving rise to the endocardial cushions. This cardiac jelly secretion is secondary to AVC and OFT myocardial-derived *Bmp2* signaling, which promotes expression of hyaluronan synthase 2 (*Has2*)[52,53]. Loss of BMP ligands (e.g. *Bmp2*, *Bmp4*) or receptors (e.g. *Alk2*, *Bmpr1a*, *Alk5*) have resulted in impaired or absent cushion formation and midgestational lethality[54]. Moreover, in the AVC, *Bmp2* signaling through its receptor *Bmpr1a* also promotes AV myocardial identity through the upregulation of AVC-specific transcription factors *Tbx2*/*Tbx3* and repression of chamber-specific gene programs[55,56,57,58].

Following the establishment of a competent valvular myocardium and cardiac jelly swelling, several signaling mechanisms have been identified that induce endocardial cells to undergo epithelial-to-mesenchymal transition (EMT). One of the signaling pathways that has been linked to EMT-initiation is TGF- β[59]. This process involves the loss of cell-cell contacts and the acquisition of migratory and invasive properties through upregulation of *Twist1* and *Snai1*, allowing the endocardial cells to transform and migrate into the cardiac jelly[60]. Similar to loss of BMP signaling genes, loss of TGF-β ligands (e.g. *Tgfb2*[61]), receptors (*Tgfbr2*[62]), or intracellular

signaling mediators (e.g. *Smad4*[63]) result in incomplete cushion formation and midgestational lethality, highlighting this critical signaling pathway's role in the initiation of EMT. Notch has also been implicated as a signaling pathway necessary for promoting EMT gene programs in endocardial cells, where it has been speculated that Notch may act to sensitize cells to receiving TGF- β signals[64].

While TGF-β signaling appears to promote EMT, VEGF signaling has been demonstrated to be a negative regulator of EMT, where premature induction of myocardial VEGF signals inhibited cushion formation[65]. It was subsequently shown that endocardial cells upregulate *Nfatc1* secondary to received VEGF signals[66]. *Nfatc1* has been demonstrated to broadly mark the valve endocardium; however, not all of these cells undergo EMT. The mechanism regulating which endocardial cells undergo EMT is not fully understood; however, several regulators of this process have been defined. A more recent study elegantly demonstrated that a subset of cells have open chromatin in an enhancer within the *Nfatc1* gene body, where *Nfatc1* acts to suppress EMT gene programs[67].

Unlike the EMT phase, many of the molecular regulators of post-EMT valvulogenesis are largely unknown. During post-EMT valvulogenesis, the cushions fuse and the cushion mesenchyme undergoes further proliferation, differentiation, delamination or excavation into free leaflets, and proceed to mature into the postnatal period. Studies have implicated some of the pathways that have been implicated in the EMT phase of valvulogenesis such as VEGF[68] and BMP[69]. In fact, it is for this exact reason that much remains to be understood about this stage of valvulogenesis. If there are stage-specific roles for the same genes, then these previous studies lacking temporally-inducible models of gene function would fail to characterize their prospective role at later stages of valve development. Understanding molecular regulators of post-EMT

valvulogenesis is a critical objective, as it is thought that defects impacting this stage could underly the pathogenesis of congenital valvulopathies.

## 1.4 Lineage Heterogeneity in Valvulogenesis

In addition to the aforementioned open questions related to molecular regulators of post-EMT valvulogenesis, there also exists a long-standing question related to the potential functional significance of differential lineage contribution to the leaflet mesenchyme. As summarized in section 1.2, it is known that epicardial-derived cells preferentially colonize and give rise to the parietal leaflet mesenchyme of the atrioventricular valves[43], while the neural crest contributes mainly to the semilunar valves[44]. There is some controversy in the field regarding neural crest contributions to the atrioventricular valve mesenchyme, with several studies coming to opposite conclusions[44,70,71]. The functional significance of these differential lineage contributions remains uncharacterized; however, given the predisposition of certain valves and leaflets to congenital and degenerative disease, the etiology of the mesenchyme likely plays a role. Recent technological advancements have made answering these long-standing questions possible.

## 1.5 Single-cell Genomics

Historically, researchers have performed studies on large groups of cells in bulk assays, providing an average view of gene expression and molecular events occurring within a tissue or organ. However, advances in single cell sequencing technologies have allowed for the generation of high-resolution transcriptomic and epigenomic data from individual cells[72]. The advent of high-throughput single-cell (sc) sequencing technologies has permitted the unbiased measurement of thousands of features per cell for thousands of cells at a time, enabling the generation of high-

dimensional transcriptional data (scRNAseq), epigenetic data (scATACseq)[73], and spatiotemporal data (spatial transcriptomics)[74], defining individual cell states at previously unavailable resolutions[75]. These novel single-cell assays can be readily combined with existing prospective lineage tracing approaches, permitting the association of cell state information with cell fate determinations[76,77]. Furthermore, these data can be integrated with human genetics analyses, in which genomic mutations are mapped onto the biological networks constructed from our multi-omic profiling strategies, permitting a dissection of the underlying biological architecture of human disease[78]. In this thesis, we have leveraged novel multi-omic technologies in concert with existing lineage tracing methods to address longstanding questions in the field of developmental cardiac biology.

One of the primary benefits of single cell technologies is the ability to identify and characterize previously unknown cell types within a tissue or organ. For example, recent studies have identified a rare cell type implicated in cystic fibrosis pathogenesis[79]. Thus, single cell technologies have allowed for the characterization of rare cell types that may be missed in traditional bulk sequencing approaches. In the context of developmental biology, another key benefit of single cell technologies is the ability to track developmental trajectories of individual cells. This has been particularly useful in studying zebrafish gastrulation[80]. Single cell technologies have also allowed for the study of cellular heterogeneity in disease states. For example, single cell sequencing has revealed significant heterogeneity in cancer cell populations, providing insights into tumor development and progression[81,82]. Similarly, single cell technologies have been used to study immune cell function in autoimmune disease[83].

One of the challenges of single cell technologies is the generation of large amounts of data. A single experiment can generate thousands or even millions of data points, which requires

sophisticated computational and bioinformatics tools to analyze[85,86]. To overcome these challenges, many computational pipelines have been developed which have been used in this thesis to study valvulogenesis. We have used these novel technologies to explore novel cellular heterogeneity, previously undescribed signaling pathways, and molecular mechanisms of disease, all in the context of valvulogenesis.
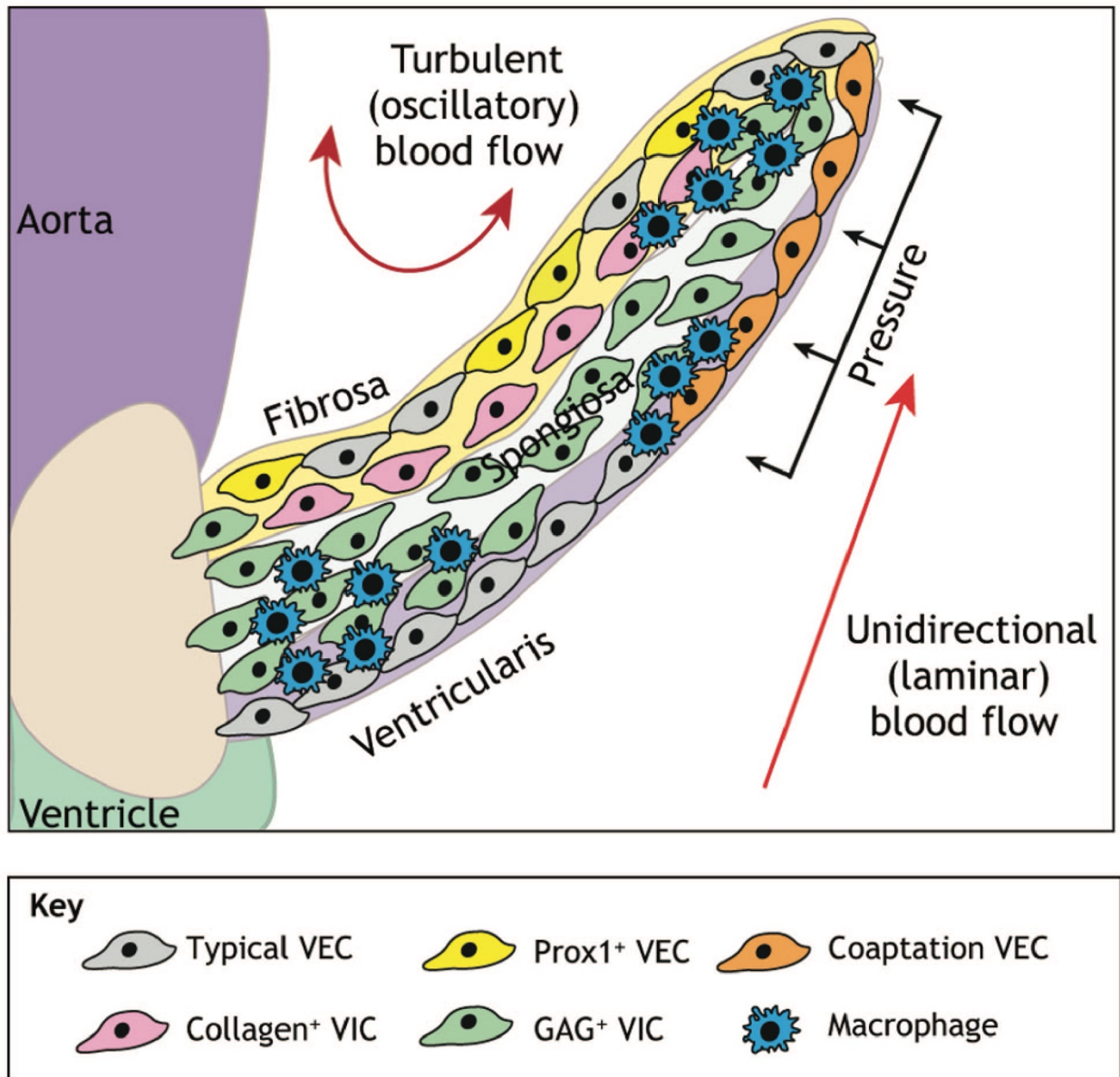


**Fig 1.2 Cellular heterogeneity in the postnatal remodeling valve**

**A,** Cartoon representation of a postnatal aortic valve displaying heterogenous endocardial, interstitial, and immune cell populations. (Adapted from O'Donnell et al., 2020)[88]

As it pertains to the application of single-cell technologies to study valvulogenesis, a recent study characterized novel heterogeneity in postnatal aortic and mitral valves at P7 and P30 (**Fig 1.2**)[87,88]. This critical study identified subpopulations of valvular endocardium, valvular interstitial cells, and immune cells. The onset and functional significance of this heterogeneity remains to be understood; however, these questions can be addressed with the additional resolution afforded by single-cell genomic technologies. Gaining a deeper understanding of the mechanisms underlying the specification of distinct valvular subpopulations during development and how they contribute to the formation of mature, competent valve structures could offer valuable insights that may be relevant to a broad array of disease states.

## 1.6 Specific Aims

It is clear that valvular heart disease presents a serious public health issue given the highly morbid and mortal nature of the disease and raising prevalence secondary to an aging population and an increase in survivorship of patients with congenital disease. As such, I have chosen to focus my thesis work on the molecular mechanisms of valvulogenesis. The advent of single-cell sequencing technologies has enabled the study of cellular phenotypes at a previously unavailable resolution, presenting an opportunity to re-visit and address longstanding questions in the field of developmental biology. My aim has been to utilize these innovative technologies to gain a better understanding of post-EMT valvulogenesis, a developmental stage that still holds many unanswered questions, and to identify new molecular regulators in this process.

In this thesis, we have leveraged a combination of scRNAseq and scATACseq to study both murine and human valve development. We have identified a novel, rare cell type whose specification is spatiotemporally restricted to post-EMT valvulogenesis. This cell type is present in human valve development and appears to be depleted in the context of human disease. Ablation of this population during development results in congenital valvulopathy phenotypes. Moreover, we have demonstrated that this novel cell type is derived from the neural crest, representing the first evidence of neural crest-to-endocardial transition. Furthermore, loss of neural crest-derived Pthlh signaling, a marker gene for this rare population, similarly results in a congenital valvulopathy phenotypes. Multi-omic analysis of neural crest Pthlh-deficient embryos revealed dysregulated BMP signaling in the valvular myocardium, providing a mechanistic framework for Pthlh regulation of valvulogenesis. The definition of this novel cell type and signaling pathway in the context of valve development opens new avenues of investigation into the pathogenesis of congenital valvulopathies and could lead to improvement in our capacity to diagnose, treat, and prevent human disease.

# Chapter 2

## Analysis of wild-type murine post-EMT Valvulogenesis

**2.1 Rationale**

There exist many longstanding questions related to the molecular regulation of post-EMT valvulogenesis. While it is known that the endocardium, epicardium, and neural crest contribute to the valvular mesenchyme, the functional significance of this differential lineage contribution remains to be determined[43,44,71]. Moreover, an initial single-cell study of postnatal valvular remodeling revealed heterogeneity in several cell types, raising new questions about the onset and distinct roles of these subpopulations[87]. Single cell genomic tools enable the dissection of cellular heterogeneity and the study of rare cell types, and in doing so, allows us to begin answering these questions. The first objective of my thesis was to develop a wild-type single cell transcriptional atlas at E12.5 and E17.5, in an effort to define cellular heterogeneity and identify novel molecular regulators of post-EMT valvulogenesis.

**2.2 Identifying Embryonic Day 12.5 Endocardial Cushion Cell Populations via scRNAseq**

To generate an atlas of post-EMT valvulogenesis, we began by performing single cell RNA sequencing (scRNA-seq) on two micro-dissected C57BL6 whole mouse hearts at embryonic day 12.5 (E12.5). This time point coincides with the end of EMT and the transition to post-EMT growth and remodeling, with ENDCs, EPDCs, and CNCCs populating the endocardial cushion mesenchyme[89]. The two biological replicates were sequenced, processed, and filtered for quality control metric resulting in a 13,926 cell Seurat object[85]. This object subsequently underwent normalization via cell cycle regression and unsupervised clustering into sixteen distinct clusters (**Fig. 2.1A**). Amongst these sixteen clusters, we identified four main 'super-clusters' representative of known cardiac cell types including: myocardium, endocardium, epicardium, and mesenchyme.

16
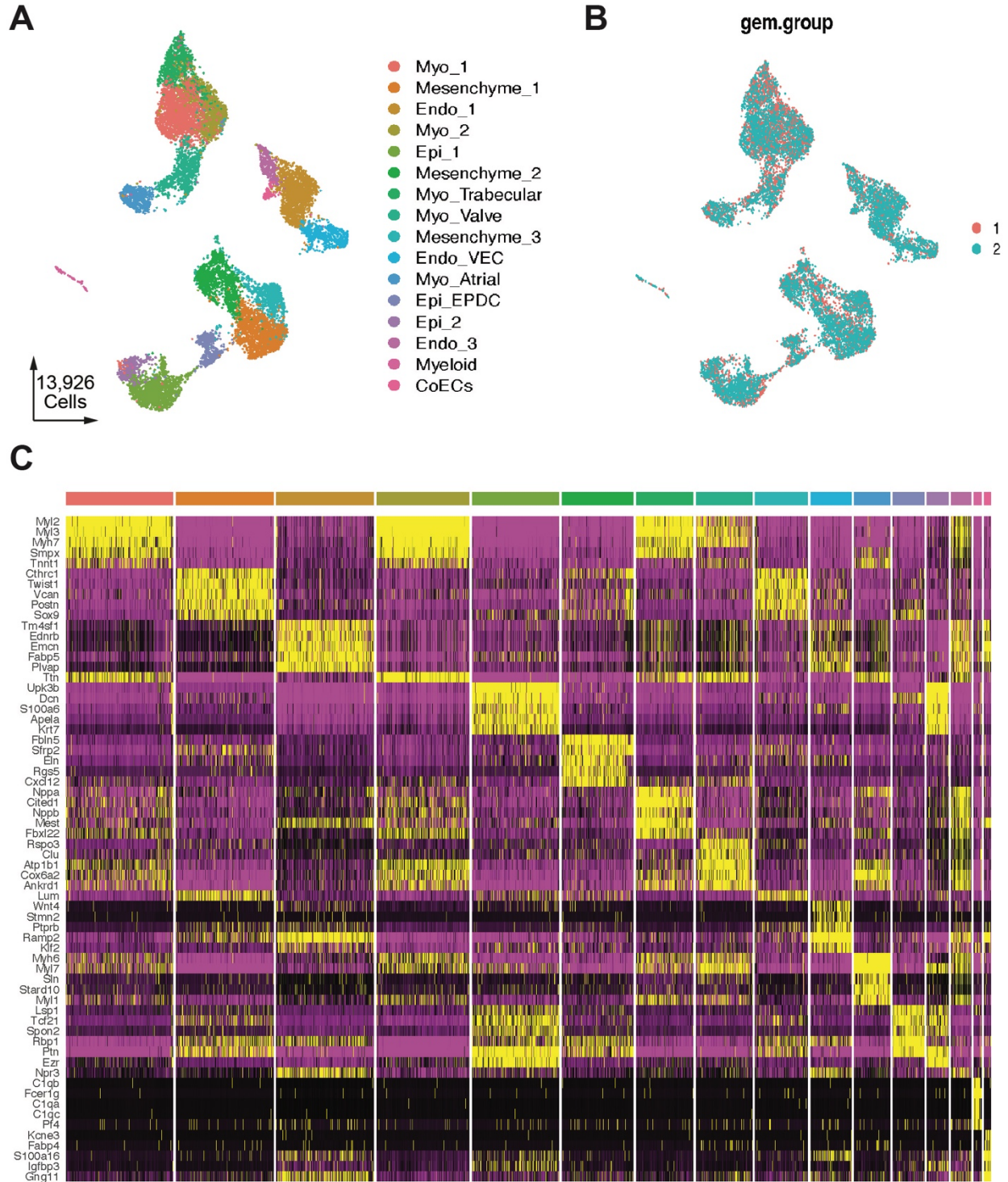
**Fig 2.1 Identification of Cardiac Cell Types at Embryonic Day 12.5**
**A,** UMAP plot of all captured cardiac cell populations colored by cluster. **B,** UMAP plot of all captured cardiac cell populations colored by biological replicate. **C,** Expression heatmap of top 5 marker genes for each cluster. Myo, myocardium; Endo, endocardium; Epi, epicardium; VEC, valvular endocardial cell; EPDC, epicardial-derived cell; CoEC, coronary endothelial cell.

17

Within these super-clusters we identified five myocardial, four endocardial, four mesenchymal, two epicardial, and one immune cell cluster. Both biological replicates contributed roughly equally to each cluster, indicating low sample-to-sample variability during sample and sequencing library preparation (**Fig. 2.1B**). To broadly annotate each of the sixteen clusters, we identified marker genes for each cluster and cross-referenced the literature for prior cell type annotations (**Fig 2.1C**).
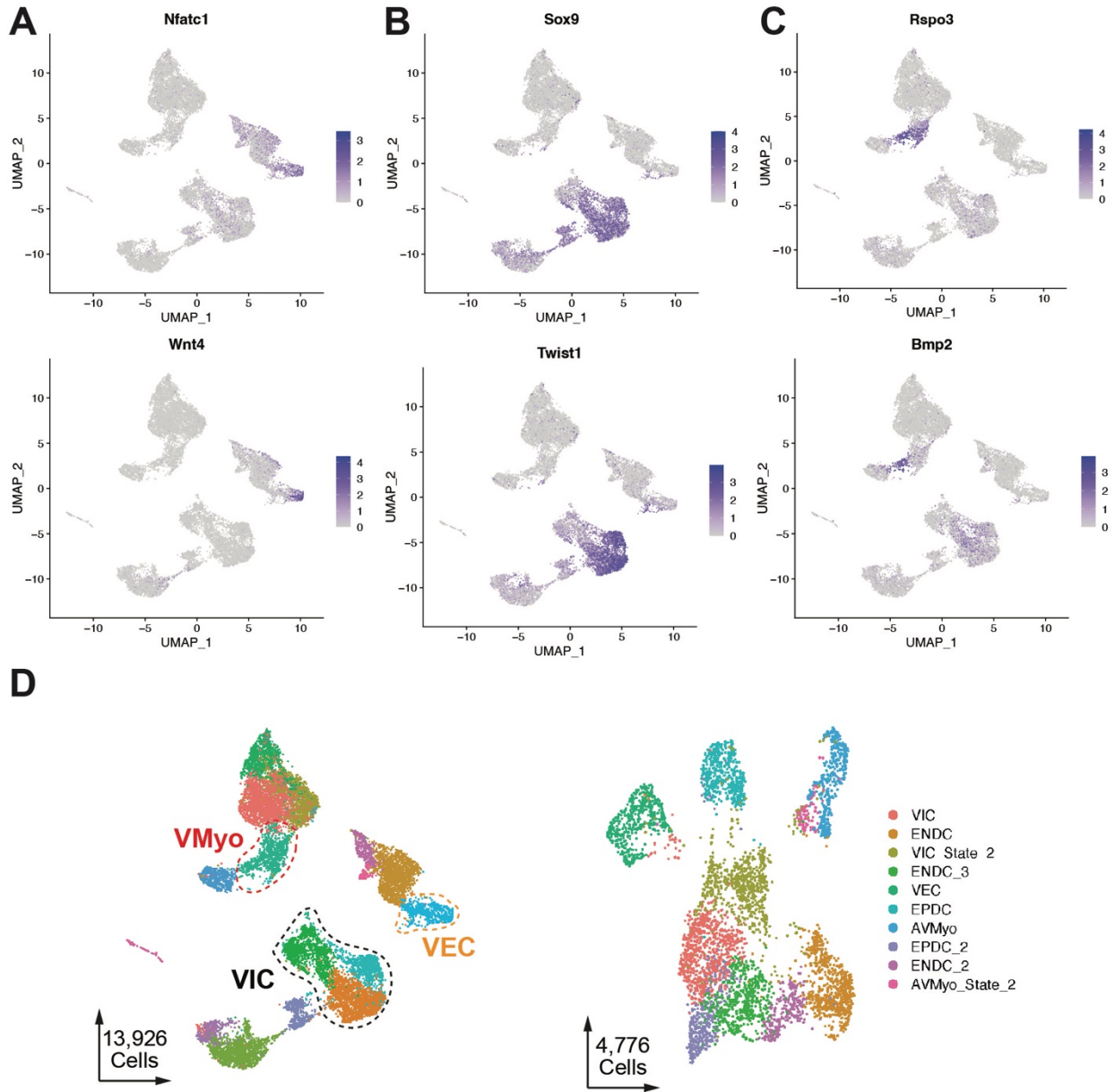


**Fig 2.2 Computational dissection of valvular cell types**

**A,** UMAP plot of valvular endocardial cell markers, *Nfatc1* and *Wnt4*. **B,** UMAP plot of mesenchymal cell markers, *Sox9* and *Twist1*. **C,** UMAP plot of valvular myocardium markers, *Rspo3* and *Bmp2*. **D,** Computational sub-setting of whole heart Seurat object into valvular cell type Seurat object. VMyo, valvular myocardium; VEC, valvular endocardial cell; VIC, valvular interstitial cell; ENDC, endocardial-derived cell; EPDC, epicardial-derived cell.

To focus our analysis on valvular cell types, we used previously annotated marker genes computationally subset valvular cell types from the other cardiac cells present in the Seurat object. We identified the valvular endocardium via expression of *Nfatc1*[90] and *Wnt4*[91], the valvular mesenchyme via expression of *Sox9*[92] and *Twist1*[93], and the valvular myocardium via expression of *Rspo3*[94] and *Bmp2*[52] (**Fig 2.2 A, B, C**). Following identification of these cell types, we computationally subset these cells into a new valvular cell type Seurat object (**Fig 2.2D**). This process was performed to enrich our downstream analysis for valve-related molecular regulators, given the relatively low number of valve cells relative to the whole heart. Notably, despite *a priori* knowledge that there are multiple lineage origins for the cardiac mesenchyme, we were unable to transcriptionally distinguish which cluster originated from which lineage. Thus, to be safe not to exclude potentially relevant mesenchymal subpopulations, we included all four mesenchymal clusters in the valvular cell type Seurat object. This new valvular Seurat object was then re-clustered and revealed eight distinct cell type populations. The valvular myocardium and one of the mesenchymal clusters, VIC, each generated two transcriptionally similar clusters that differed mainly by cell cycle gene expression. As such, they were annotated as the same cell type and given the suffix state 1 or state 2.

**2.3 Identifying Novel Cell – Cell Interactions during Post-EMT Valvulogenesis**

To identify novel signaling interactions regulating post-EMT valvulogenesis, we applied the computational pipeline CellChat to the valvular cell type Seurat object[95]. CellChat infers statistically and biologically significant cellular communication by leveraging single cell expression data of ligand – receptor combinations between and within clusters to identify paracrine and autocrine signaling interactions, respectively. We first performed cellular communication analysis that sorted the ten clusters into four secretory patterns based on the similarity and level of expression of ligands in each cluster (**Fig 2.3 A**). A river plot was generated to graphically demonstrate the sorting of clusters into secretory patterns and then identify the signaling pathways that define each of these four patterns. To validate this computation pipeline, we first searched for previously annotated signaling pathways that have been implicated in the regulation of valvulogenesis near this timepoint. Indeed, Cellchat identified the Notch and Wnt signaling pathways as high confidence marker pathways for patterns 4 and 2, respectively[64,91]. Network centrality analysis of the Notch pathway identified a distinct mesenchymal ligand secreting population, ENDC, with the primary receiver as the VEC cluster (**Fig 2.3 B**). Analysis of the Wnt pathway identified the VECs as the sole Wnt secreting population, with several receiving clusters – the highest being the valvular myocardium and a subset of the mesenchyme, VIC_State_2. These analyses are consistent with numerous studies that have previously implicated these pathways in the regulation of valvulogenesis, as was reviewed in Chapter 1.3.

To identify novel regulators of post-EMT valvulogenesis, we manually examined the marker pathways for each pattern, prioritizing non-ECM, paracrine pathways without prior annotation in valve development. Two pathways caught our attention – the parathyroid hormone

Outgoing communication patterns of secreting cells



**A**

**B**

NOTCH signaling pathway network

WNT signaling pathway network

**C**

PTH signaling pathway network

CALCR signaling pathway network
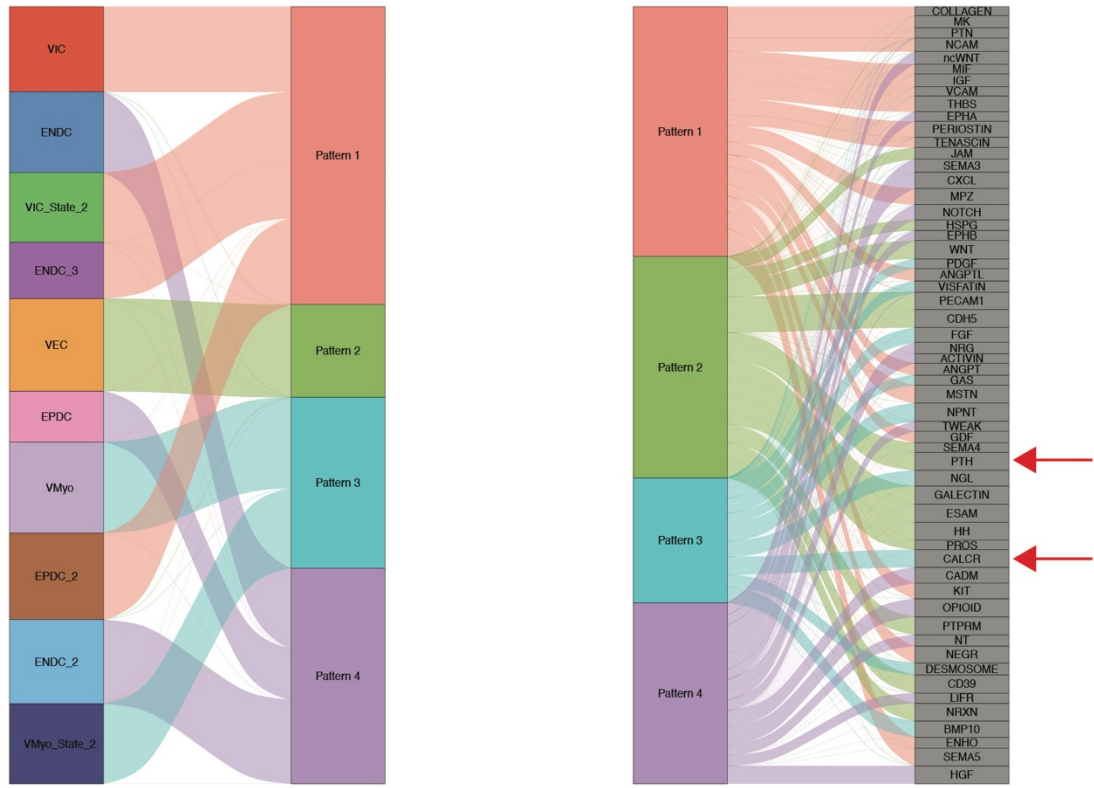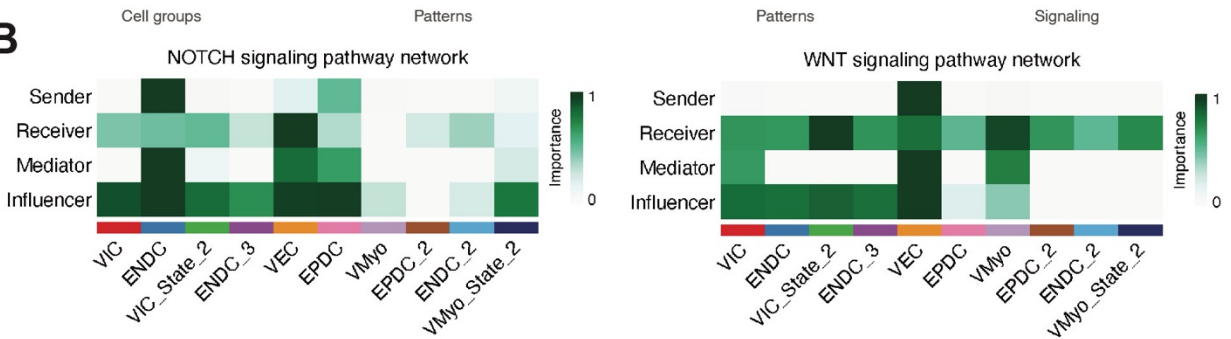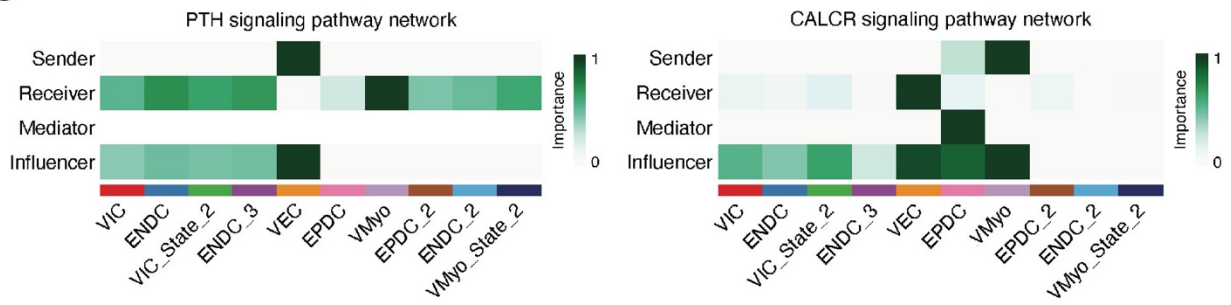
**Fig. 2.3 E12.5 Valvular Cell – Cell Communication Analysis**
**A,** River plot showing the inferred outgoing communication patterns of secreting cells (L), and the signaling pathways that define each communication pattern (R). **B,** Heatmap showing the relative importance of each cell group based on the computed four network centrality measures of previously annotated valvulogenesis-regulating signaling pathways, Notch (L) and Wnt (R). **C,** Heatmaps showing the relative importance of each cell group based on the computed four network centrality measures of novel putative valvulogenesis-regulating signaling pathways, PTH (L) and CALCR (R). PTH, parathyroid hormone; CALCR, calcitonin receptor.

(PTH) pathway and the calcitonin receptor (CALCR) pathway, which marked pattern 2 and 3, respectively. Network centrality analysis of the PTH pathway identified a putative interaction between the VEC-derived parathyroid hormone-like hormone (*Pthlh*) ligand and parathyroid hormone 1 receptor (Pth1r)-expressing valvular myocardium and mesenchyme (**Fig 2.3 C**). Analysis of the CALCR pathway identified a reciprocal putative interaction between the valvular myocardium-derived adrenomedullin (*Adm*) ligand and the *Calcrl/Ramp2* co-receptor expressing VECs. Interestingly, the paralogous of *Pthlh* and *Adm*, parathyroid hormone and calcitonin, play an important antagonist role in calcium and bone homeostasis systemically[96,97]. These proteins are thought to have evolved for local paracrine tissue effects; the role of these neuroendocrine peptide hormones in valvulogenesis remains to be understood.

Despite both pathways being attractive candidates to pursue, we ultimately chose to pursue studying *Pthlh*^{+} cells and the PTH signaling pathway for several reasons. First, in the context of mammary bud outgrowth, *Pthlh* has previously been annotated as modulating mesenchymal cell responsiveness to BMP signaling via upregulation of *Bmpr1a* leading to an increase in *Msx2* expression, thus driving mesenchymal cell maturation[98,99]. Both BMP signaling and *Msx2* have been demonstrated as being important regulators of valvular mesenchyme differentiation[69,100]. Importantly, a mouse model of Ebstein's anomaly, a congenital valvulopathy with a specific defect in post-EMT valvulogenesis, was generated through AV myocardial deletion of *Bmpr1a*[57].

Second, this gene has been shown to be an important regulator of endochondral bone formation[101]. Much work has been done to understand the gene regulatory network in bone development involving feedback loops between *Pthlh* and *Ihh*, mediated by *Gli3* and *Trps1*. It is known that there exists considerable overlap between the gene regulatory networks regulating bone and valve development[102,103]. Moreover, whole organism knockout of *Pthlh* results in perinatal cyanosis and lethality. The cause of this lethality was initially attributed to some form of mechanical failure inhibiting respiration given the expression of *Pthlh* in the developing ribs[104]. However, congenital heart defects would present in a very similar manner and would be difficult to rule out without a functional assay, such as fetal echocardiography, to assess valve function.

Another recent study found a *Pthlh*[+] skeletal stem population in the resting zone of developing long bones that gives rise to osteoblasts and marrow stromal cells[105]. These skeletal stem cells have been shown to require a Wnt inhibitory environment to function properly and give rise to columnar chondrocytes; Wnt agonism results in decreased progeny from the *Pthlh*[+] stem cell population[106]. This again forms an interesting corollary with valve development, in which maternal exposure to lithium, a Wnt agonist, results in a 1000x increase in risk of having a child with Ebstein's anomaly[25]. Furthermore, the expression of the *Pthlh* receptor, *Pth1r*, has previously been shown to be highest in the endocardial cushions in the developing heart, suggesting this candidate signaling pathway may play a role in the regulation of valvulogenesis[107].

Lastly, recent studies of human congenital heart defects have placed an emphasis on endocardial dysfunction playing an important role in the pathogenesis of human disease[108]. With the recent discoveries of postnatal valvular endocardial heterogeneity and biomechanical endocardial patterning during development, we elected to focus our attention on this novel endocardial ligand and the cell type that expresses this gene.

**2.4 *Pthlh*⁺ Valvular Endocardial Cells are Highly Secretory and Spatiotemporally Restricted**

To identify which cells express *Pthlh* during cardiogenesis, we queried our whole heart Seurat object for *Pthlh* expression and, much to our surprise, found that only 0.84% (117 cells) express this novel gene (**Fig. 2.4 A**). All of these cells exist in the cluster we annotated as valvular endocardium via *Nfatc1*⁺/*Wnt4*⁺ co-expression. To identify when *Pthlh*⁺ cells are first observed during cardiogenesis, we assembled and queried an atlas of wild type scRNAseq datasets at seven time points during cardiogenesis from three studies: E7.75, E8.25, and E9.25 from De Soysa et al.[109], E10.5 and E11.5 from Ranade et al.[110], and E12.5 and E17.5 from our study presented here. We found there to be a robust increase in *Pthlh*⁺ cells between E11.5 and E12.5, temporally coinciding with the end of EMT and the progression into post-EMT valvulogenesis (**Fig. 2.4 B**). To better understand how these cells differ from other endocardial cells, we performed differential gene expression analysis between *Pthlh*⁺ and *Pthlh*⁻ endocardium (**Fig 2.4 C**). We found that these cells are marked by the expression of a number of highly specific signaling ligands including: *Wnt9b*, *Dhh*, *Nppc*, *Wnt4*, *Jag1*, *Wnt11*, in addition to several retinoic acid signaling genes (**Fig 2.4 D**). Notably, these cells are also marked by down-regulation of important endocardial genes such as *Emcn*[111] and *Ednrb*[112]. The unique transcriptional signature of this cell population raises many interesting questions related to its function during development.

**A** Pthlh

**B** Pthlh

**C** Pthlh⁺ vs Pthlh⁻ Endocardium

**D** Wnt9b          Dhh          Nppc
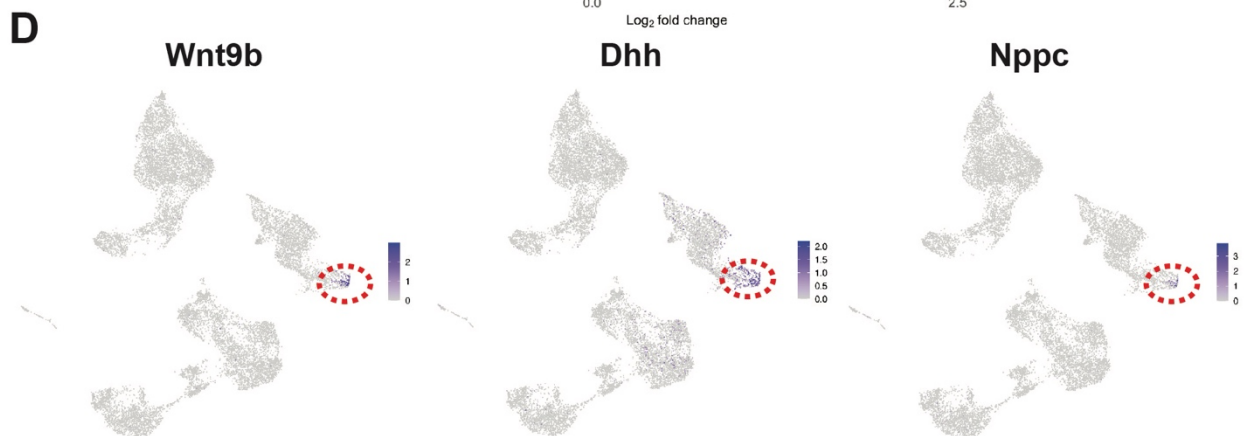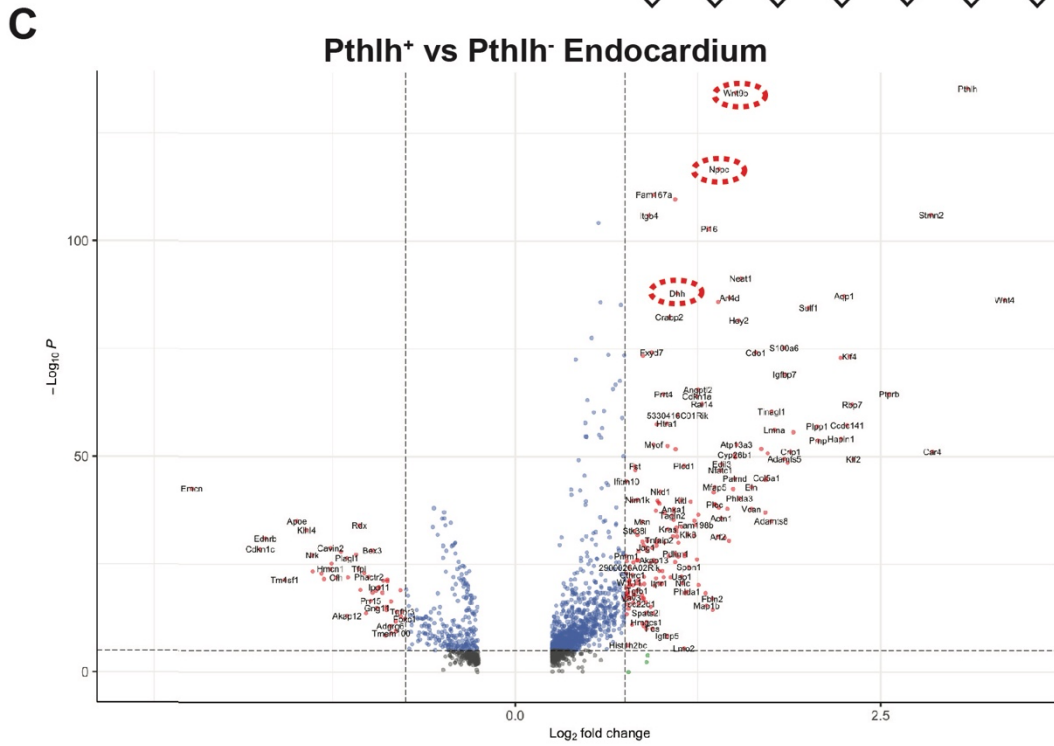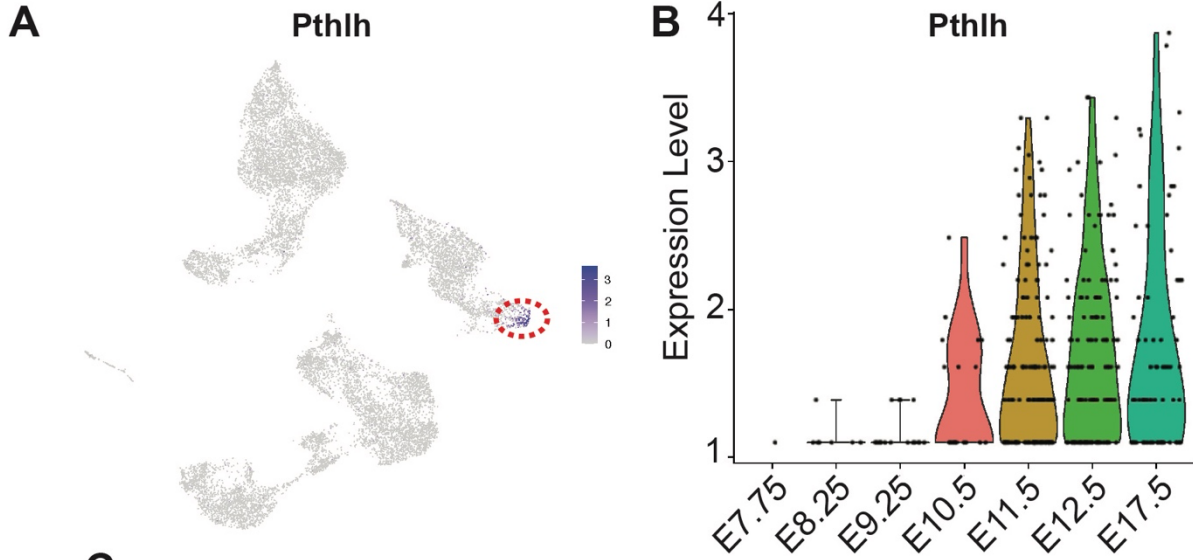
**Fig 2.4 Pthlh+ cells represent highly secretory, temporally-restricted subpopulation**
**A,** UMAP plot of *Pthlh* expression at E12.5. **B,** Violin plot of *Pthlh* expression during cardiogenesis. **C,** Volcano plot of differentially expressed genes between Pthlh+ and Pthlh-Endocardium (FCcutoff = 0.75). **D,** UMAP expression plots for co-expressed developmental signaling ligands, Wnt9b(L), Dhh (C), and Nppc (R), in Pthlh+ cells.

One of the limitations of scRNAseq is the loss of spatial information during sample preparation. Therefore, to validate our single cell findings and identify the spatial localization of Pthlh^{+} cells, we performed fluorescent *in situ* hybridization (FISH) for *Pthlh* mRNA via RNAscope on E12.5 and E18.5 heart sections[113]. At E12.5, we identified *Pthlh+* cells on the endocardial surface of the atrioventricular and outflow tract cushions, localized to the cushion endocardium most distal to the valvular myocardium and nearest the opposing cushion (**Fig. 2.5 A**). At E18.5, we identified *Pthlh+* cells highly localized to the coaptation surface of the valve leaflets across all four valves (**Fig. 2.5 B**). We further validated our scRNAseq data by performing FISH for *Dhh* and *Wnt9b* at E12.5 on both atrioventricular and outflow tract cushions, where we visualized an overlapping, yet broader, expression domain with *Pthlh* expression (**Fig. 2.5 C**). Thus, through a combination of scRNAseq and traditional FISH, we have identified a rare, highly secretory subpopulation that is spatially-restricted to the valve leaflet and temporally-restricted to post-EMT valvulogenesis (**Fig. 2.5 D**).

**A** E12.5

OFT

OFT Cushion / Distal OFT / Proximal OFT

Pthlh / DAPI

AVC

RA / LA / AVC / RV / IVS / LV

**B** E18.5

AoV

Pthlh

Tricuspid Valve

**C** E12.5

OFT

OFT Cushion / Distal OFT / Proximal OFT

Dhh / DAPI

Wnt9b

AVC

RA / LA / AVC / RV / IVS / LV

**D**

PTHLH

Chamber Myocardium
Valvular Myocardium
Valvular Endocardium
Pthlh+ Valvular Endocardium
Valvular Mesenchyme

**E**

| Lymph VEC | VEC | Coapt VEC |
|-----------|-----|-----------|
| Lsamp | Bmx | Prnp |
| Pdgfra | Nrp1 | Pthlh |
| Enpp2 | Cpe | Anxa1 |
| Prox1 | Cd200 | Fxyd5 |
| Postn | Col3a1 | Slc9a3r2 |
| Rdx | Fmo2 | Wnt9b |
| Ednrb | Selp | Pi16 |
| Fn1 | Rspo3 | Crip1 |
| Ahsg | Bgn | Dkk2 |
| Ebf1 | Calcrl | Nts |
| Ephx2 | Edn1 | Palmd |
| Zfp36l1 | Apoe | Ly6a |
| Fbn2 | Col14a1 | Hapln1 |
| Lrg1 | Icam1 | Ly6c1 |
| Epha7 | Id2 | Plk2 |
| Tshz2 | Vwf | Ptprr |
| Akap12 | Npr3 | Sorbs2 |
| Efnb2 | Clec14a | Podxl |
| Ugcg | Hlf | Sulf1 |
| Rgs16 | Fgl2 | Serpinb1a |

Lymph-VEC / VEC / Coapt-VEC

**D** Prox1 **E** Emcn **F** Hapln1  P30 AoV

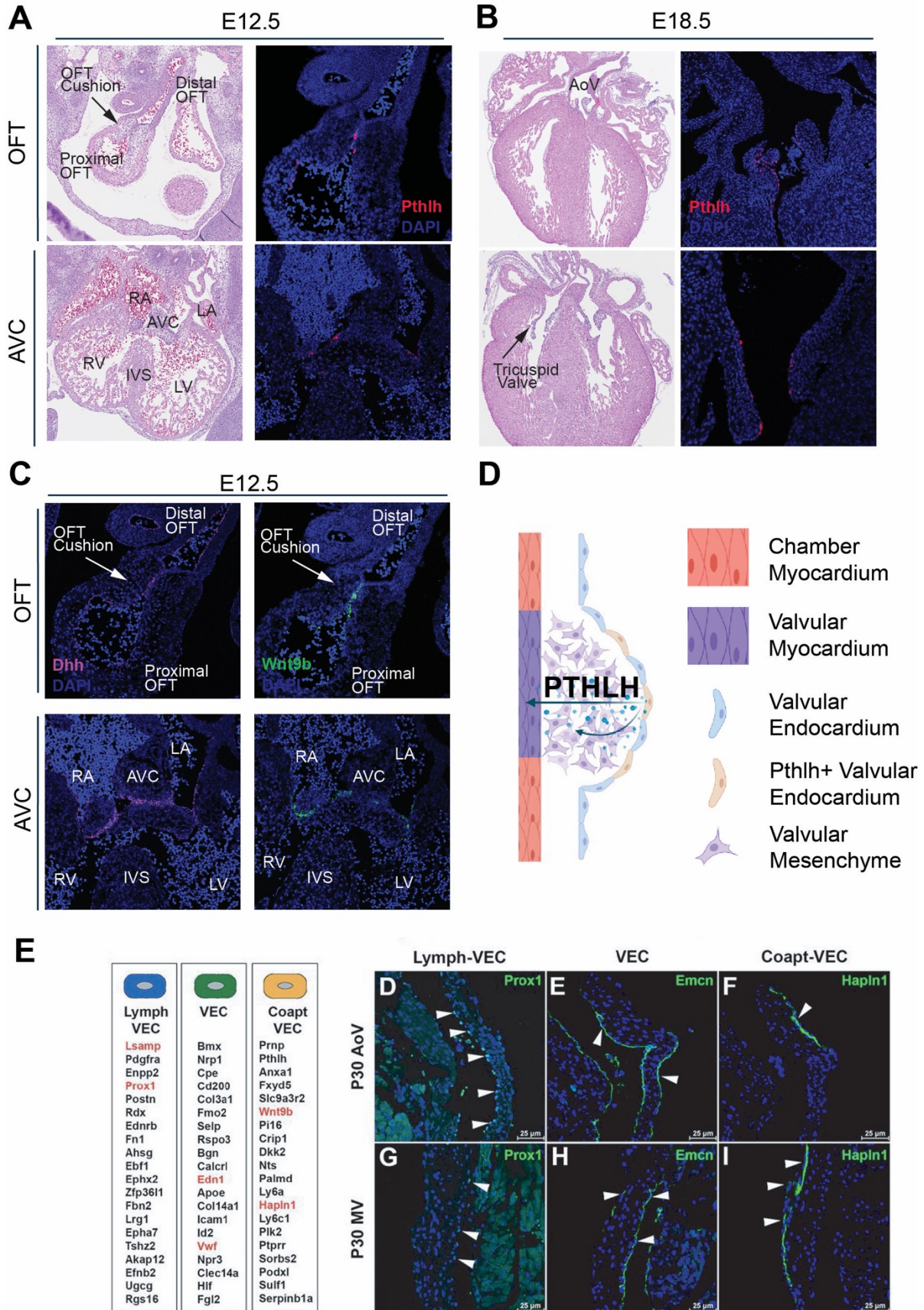**G** Prox1 **H** Emcn **I** Hapln1  P30 MV

25 µm

27

**Fig 2.5 Pthlh+ cells represent spatially-localized valvular endocardial subpopulation**
**A,** *Pthlh* expression via in situ hybridization in the OFT and AVC cushions at E12.5 with accompanying H&E stained section. **B,** *Pthlh* expression via in situ hybridization in the OFT and AVC cushions at E18.5 with accompanying H&E stained section. **C,** *Dhh* and *Wnt9b* expression via in situ hybridization in the OFT and AVC cushions at E12.5. **D,** Cartoon representation of Pthlh+ valvular endocardial cells interacting with underlying mesenchyme and myocardium at E12.5. **E,** Marker genes and accompanying immunofluorescence staining of a single marker gene for each endocardial subpopulation for both P30 aortic (AoV) and mitral (MV) valves. (Adapted from Hulin et al., 2019)[87]

Furthermore, to determine if *Pthlh*+ VECs are a transient developmental population or if they persist into the postnatal period, we cross referenced our E12.5 and E17.5 scRNA-seq data with previously published P7 and P30 data (**Fig. 2.5 E**)[87]. We found that the marker genes for E12.5 *Pthlh*+ VECs display a high degree of concordance with the marker genes for the coaptation VECs found at P7 and P30, implying that these cells are developmentally established at the completion of endocardial cushion formation and persist late into postnatal remodeling and into adult life.

## 2.5 Exploring the chromatin accessibility signature of *Pthlh*⁺ VECs

Given the unique transcriptional signature and spatiotemporal specificity of this novel, rare cell type, we next sought to characterize the chromatin accessibility landscape and identify candidate transcription factors that aid in the specification of *Pthlh*⁺ VECs. To accomplish this objective, we used the 10X gene expression and chromatin accessibility co-assay (10X multi-ome). The advantage of this assay is that it measures both transcriptional and chromatin accessibility data from the same cells, rather than independently performing scRNAseq and scATACseq on different cells from the same sample. This experimental feature thus avoids the need for computational imputation of cluster identities from transcriptional data onto the chromatin accessibility data, an imperfect process that has variable success rates dependent upon the biological context. This is

especially advantageous when studying a rare cell type, as is the case here with *Pthlh*[+] VECs, as ATAC data is notoriously sparse and we want to be certain we have identified the correct cell population.

We micro-dissected two C57BL6 whole mouse hearts at E12.5 as a pilot multi-ome experiment. Following nuclei isolation, gem preparation, and library construction, the pooled library for the two biological replicates was sequenced, processed, and filtered for quality control metric resulting in a 7,844 nuclei ArchR object[86]. Latent semantic indexing dimensionality reduction was performed to identify a total of fifteen distinct clusters in this ArchR object, represented in UMAP space incorporating both RNA and chromatin accessibility information (**Fig. 2.6 A**). Cluster-specific transcriptional and chromatin accessibility features were identified and cell types were annotated using the same marker genes as used in the annotation of the E12.5 scRNAseq Seurat object (**Fig. 2.6 B**).

While we found expression of *Pthlh* to be restricted to a small subset of cluster 9, we were surprised to find a broader degree of accessibility for the *Pthlh* gene body outside of cluster 9 (**Fig. 2.7 A, B**). It can be difficult to interpret scenarios when transcriptional state and chromatin accessibility state do not align. In the case of cluster 9, we find a high degree of accessibility in the subset of cells that express *Pthlh.* However, in clusters 15 and 16 we identify a high degree of *Pthlh* gene body accessibility in mesenchymal cells that do not express *Pthlh*. One could hypothesize that the *Pthlh* gene body accessibility in these cells could precede expression of the gene; however, both our scRNAseq and *in situ* hybridization data indicate that the valve mesenchyme does not express *Pthlh* at later timepoints during valvulogenesis. Conversely, this *Pthlh* gene body accessibility could be a remnant of a past transcriptional state. Again, this hypothesis does not seem likely as previously published scRNAseq data of cardiogenesis fails to

ATAC Z-Scores
99177 P2GLinks
−2 2

RNA Z-Scores
99177 P2GLinks
−2 2

groupBy

C1   C13   C2   C7
C10  C14   C4   C8
C11  C15   C5   C9
C12  C16   C6

30
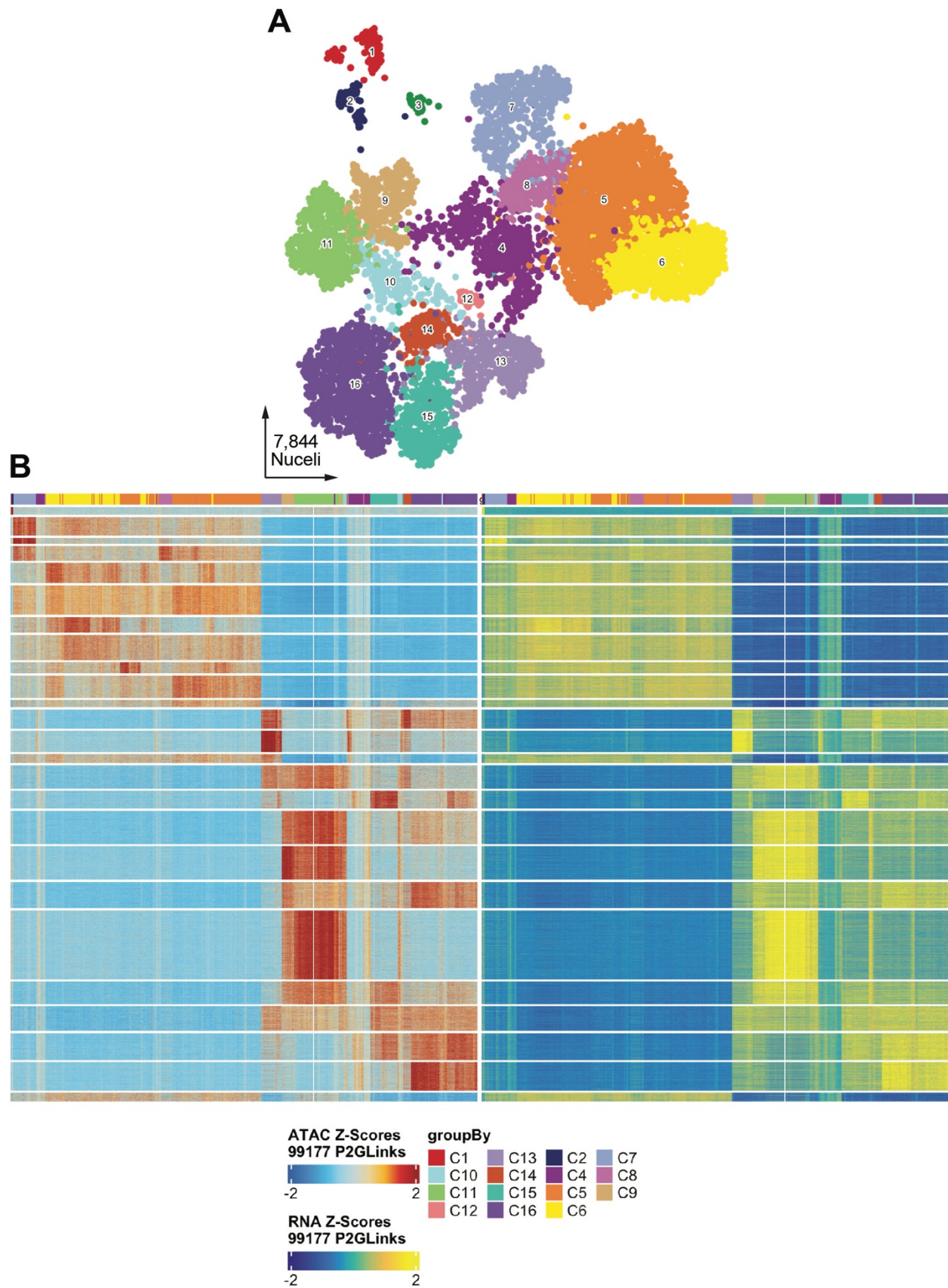
**Fig 2.6 Identification of cardiac cell types via single-cell Multi-ome**
**A,** UMAP plot representing captured cardiac cell types colored by cluster, incorporating both chromatin accessibility and gene expression data. **B,** Marker peak heatmap and gene score heatmap for each cluster.

identify *Pthlh*[+] populations prior to E12.5. This remains an open question in our analysis of wild-type valvulogenesis, as to the potential significance of *Pthlh*-accessible populations that do not express *Pthlh*.
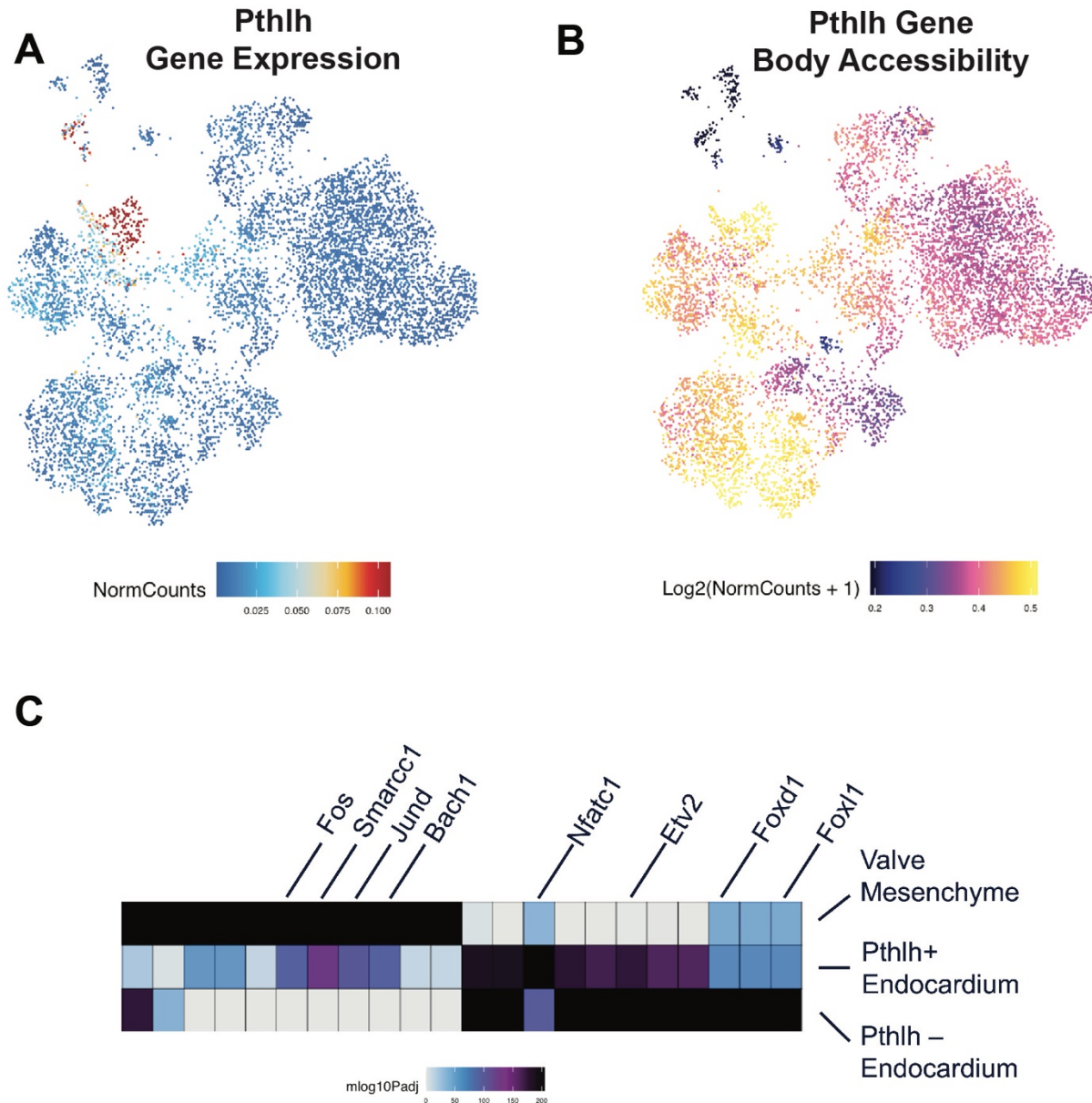


**Fig 2.7 Transcription factor motif enrichment analysis of *Pthlh*[+] VEC Marker Peaks**

**A,** UMAP plot of *Pthlh* expression. **B,** UMAP plot of *Pthlh* gene body chromatin accessibility. **C,** Heatmap plot of transcription factor motif enrichment in marker peaks for the valve mesenchyme, *Pthlh*⁺ endocardium*, and Pthlh*⁻ endocardium*.*

To identify prospective lineage-defining transcription factors that aid in the specification of *Pthlh*⁺ VECs, we performed transcription factor motif enrichment analysis on the differentially accessible regions of chromatin for each cluster. This analysis revealed an enrichment for *Nfatc1* motifs and a stark decrease in fox-family transcription factor accessibility within *Pthlh*⁺ endocardium relative to *Pthlh*⁻ endocardium (**Fig. 2.7 C**). Moreover, *Pthlh*⁺ VECs shared motif enrichment for a number of transcription factors that are also enriched within the valvular mesenchyme clusters including *Fos/Jun*, *Smarcc1*, and *Bach1*. Using our E12.5 wild-type scRNAseq data to validate these findings, we identified a lack of *Foxc1* expression and a high level of *Bach1* expression within the *Pthlh+* VECs (**Fig. 2.8 A**). Moreover, we took an orthogonal approach to validate our scRNAseq data with fluorescent *in situ* hybridization and found a lack of overlap in the *Pthlh* and *Foxc1* expression domains, both at E12.5 and E18.5 (**Fig. 2.8 B**). *Bach1* has previously been demonstrated to impede angiogenesis *in vivo*, and was mechanistically characterized to be a Wnt signaling repressive transcription factor *in vitro*[114]. This forms yet another interesting connection both with prior studies of *Pthlh+* skeletal stem cells in mice that require Wnt inhibitory environments and the wealth of literature related to Wnt-mediated regulation of valvulogenesis. Thus, *Bach1* and absence of *Foxc1* serve as interesting candidate transcriptional regulators that may play a role in the specification of *Pthlh*⁺ VECs.
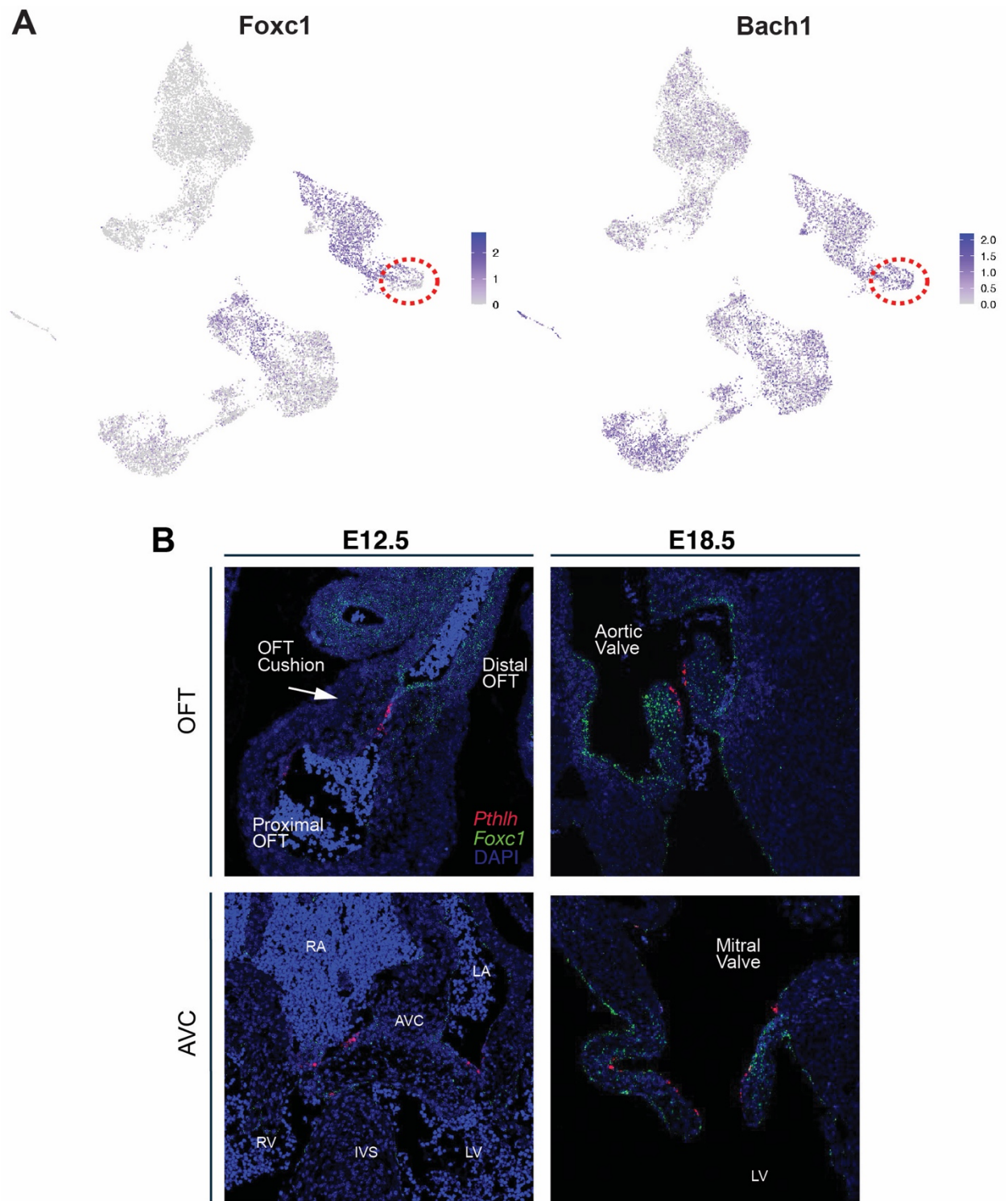
**Fig 2.8 Identification of candidate lineage-specifying transcription factors**
**A,** UMAP plot of *Foxc1* and *Bach1* expression at E12.5. **B,** *Pthlh* and *Foxc1* expression via in situ hybridization in the OFT and AVC cushions at E12.5 and E18.5.

**2.6 Dissecting Embryonic Day 17.5 Mesenchymal Cell Heterogeneity**

To complete our atlas of post-EMT valvulogenesis, we performed scRNAseq on two micro-dissected C57BL6 whole mouse hearts at embryonic day 17.5 (E17.5). This time point coincides with the end of end of embryonic valvulogenesis characterized by fully formed, mobile valve leaflets that will subsequently undergo postnatal remodeling[71]. Similar processing as before was applied to this timepoint and resulted in a Seurat object of 10,286 cells from which we identified nineteen distinct clusters (**Fig. 2.9A**). Given prior annotation of *Pthlh* signaling modulating mesenchymal and chondrocyte differentiation, we focused our attention on the identification of mesenchymal subpopulations that may be impacted in perturbation models of this novel neuroendocrine hormone signaling pathway.

**A**     E17.5 scRNAseq UMAP

**B**     E17.5 Mesenchyme Sub-Cluster

**C**

**Fig 2.9 Identification of Cardiac Cell Types at Embryonic Day 17.5**
**A,** UMAP plot of all captured cardiac cell populations colored by cluster. **B,** UMAP plot of all captured mesenchymal cell populations colored by cluster. **C,** Expression heatmap of top 5 marker genes for each mesenchymal cluster.

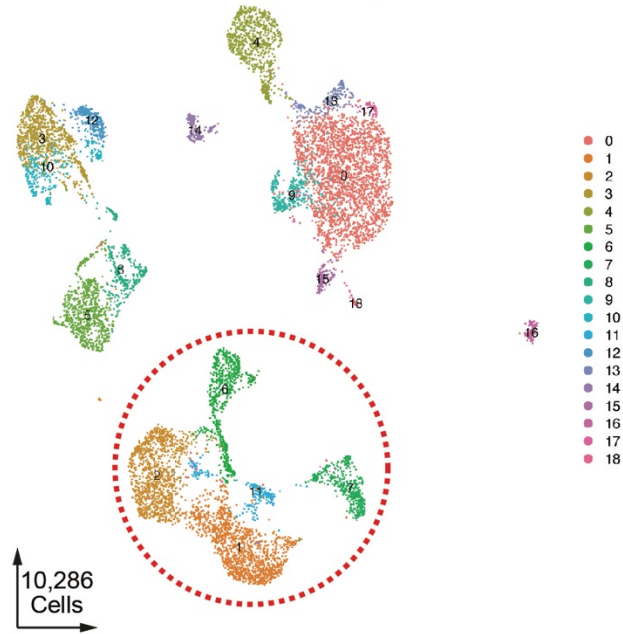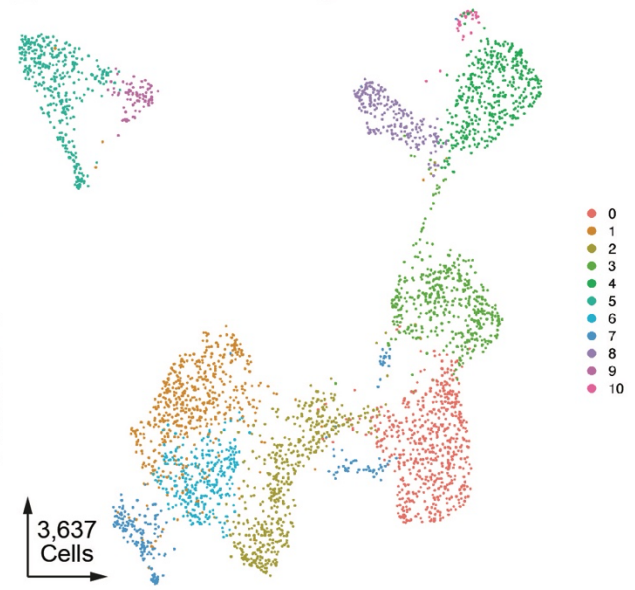Using *Col1a1* expression as a broad mesenchymal cell marker, we subset clusters 1, 2, 6, 7, and 11 into a separate mesenchymal Seurat object containing 3,637 cells. We re-clustered this new mesenchymal Seurat object and identified 11 distinct clusters with unique transcriptional marker genes (**Fig 2.9 B, C**). We cross referenced these marker genes with prior bulk RNAseq data that compared the transcriptional profile of E17.5 valves with E12.5 endocardial cushion tissue[115]. We then leveraged fluorescent *in situ* hybridization on E18.5 aortic valve sections to spatially localize these genes in search of leaflet-specific mesenchymal marker genes. To our surprise, several of the genes previously annotated as most-upregulated in the E17.5 had little to no expression in the leaflet and were mainly in the valve annulus or great vessel media including *Aspn*, *Ptprz1*, and *Sfrp2* (Fig. 2.10 A). Of the genes we identified as being expressed within the leaflet mesenchyme, we found *Cthrc1* to have the highest level of expression within the hinge region of the leaflet, proximal to the annulus (**Fig. 2.10 B**). Moreover, *Dpt* appeared to robustly label both the leaflet mesenchyme in addition to the epicardium*,* while *Col14a1* appeared to mark the leaflet, annulus, and great vessel mesenchyme. Of all of the genes we tested, the most specific valve leaflet mesenchymal marker was *Adamts19*, a gene that has previously been implicated as a genetic cause of progressive human valve disease and as a novel marker of valvular interstitial cells. Identification of these validated marker genes for heterogeneous mesenchymal populations will enable us to interrogate mesenchymal cell maturation in future *Pthlh* signaling perturbation models.
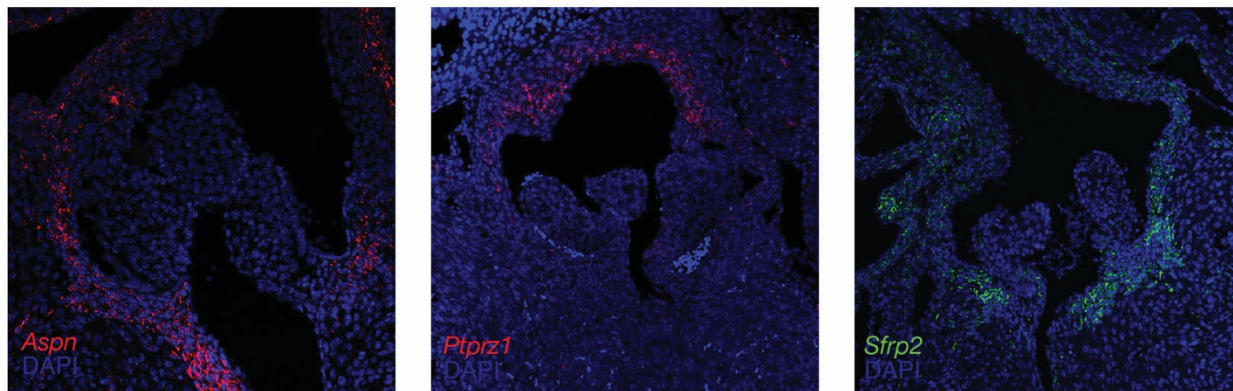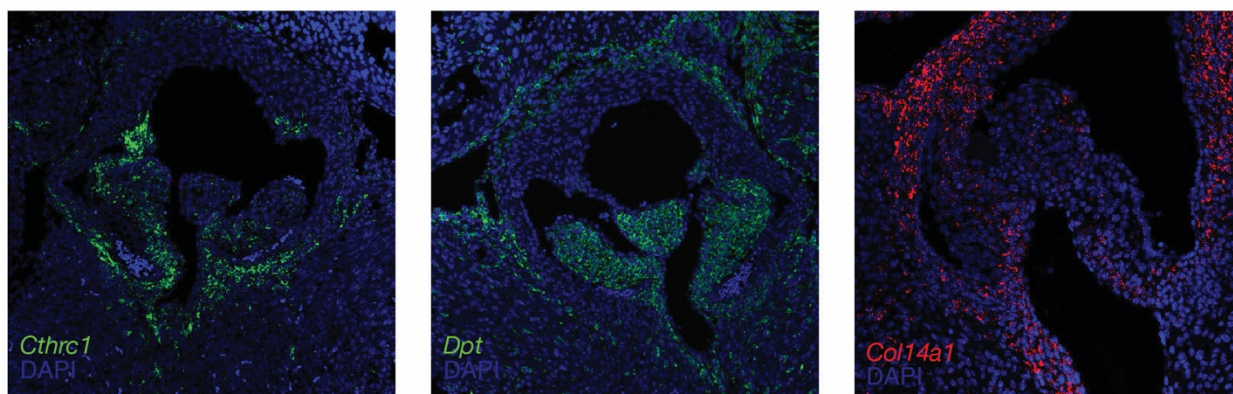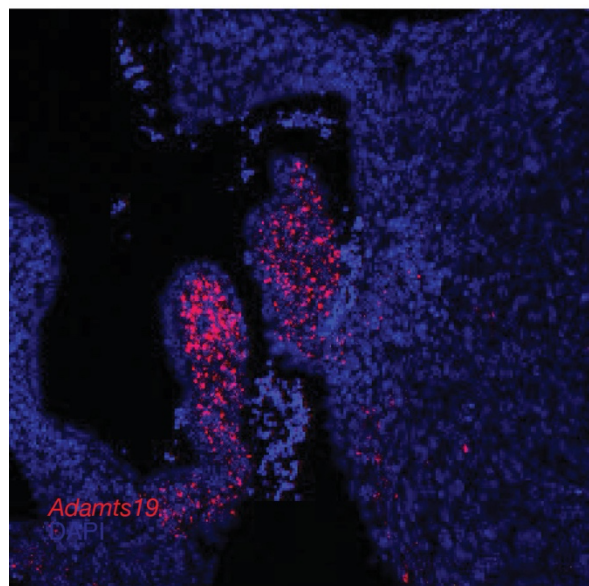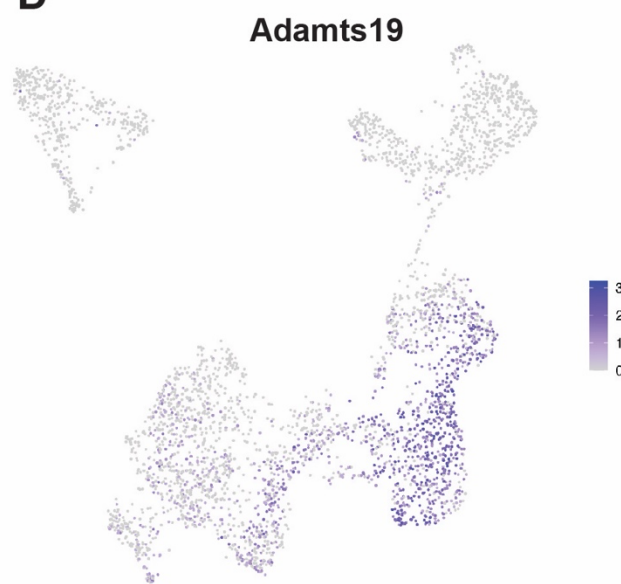
**Fig 2.10 Validation of mesenchymal subpopulations via *in situ* hybridization**
**A,** *Aspn, Ptprz1,* and *Sfrp2* expression via in situ hybridization in the Aortic valve at E18.5. **A,** *Cthrc1, Dpt,* and *Col14a1* expression via in situ hybridization in the Aortic valve at E18.5. **A,** *Adamts19* expression via in situ hybridization in the Aortic valve at E18.5. **D,** UMAP plot of *Adamts19* expression at E17.5 in mesenchymal cell populations.

## 2.7 Conclusions

Through the application of single-cell technologies to a poorly understood stage of valvular development, we were able to fill several important knowledge gaps and identify interesting, new questions to pursue. First, we identified novel cellular heterogeneity in the valvular endocardium at E12.5 that persists long into the postnatal period in mice. The rare nature of this novel population, representing less than 1% of cells in the developing heart, highlights the need for single cell genomics to detect and study rare populations of cells. Previous bulk assays easily would have been unable to detect such a small signal, as compared to more abundant cell types.

This subpopulation is temporally-restricted to post-EMT valvulogenesis and spatially-restricted to the leading edge of the developing cushion endocardium and is further restricted to the coaptation surface of the leaflet later in development. This is a unique microenvironment that experiences not only laminar sheer stress from blood flow, but also the mechanical stimulus of leaflet coaptation, when the valve closes each cardiac cycle. This highly degree of spatial localization to such a unique biomechanical niche opens many interesting questions related to the specification of this cell type. While the role of the sheer stress-responsive *Klf2* and downstream target, *Wnt9b*, have been described, the functional role of this cell type during later stages of valvulogenesis and postnatally remains to be understood[48]. Moreover, we identified candidate transcription factors that may play a role in the specification of this unique cell type through integrated scRNA/ATACseq analysis with the 10X multi-ome assay.

Secondly, we succeeded in our objective of identifying two new candidate molecular regulators of post-EMT valvulogenesis, both previously undescribed neuroendocrine peptide hormones, *Pthlh* and *Adm*. Ultimately, we have focused our studies on the former; however, both present interesting new avenues of investigation. Functional characterization of *Pthlh+* valvular endocardial cells and the *Pthlh* signaling pathway will be the focus of the subsequent chapter.

# Chapter 3

## Perturbation of Pthlh-positive Valvular Endocardial Cells

## 3.1 Rationale

My next objective was to define the role of Pthlh-positive valvular endocardial cells during development for several important reasons. First, the marker gene, *Pthlh*, exhibits a high degree of spatio-temporal specificity to the process we are attempting to study, post-EMT valvulogenesis. Moreover, this gene has prior annotation as a modulator of BMP signaling, a pathway well annotated in the formation and maturation of the endocardial cushion[69], further making this an attractive candidate to characterize. As such, we sought to characterize the role of this population using a combination of mouse genetic models, single-cell multi-omics, and traditional lineage tracing techniques.

## 3.2 Ablation of Pthlh-positive Valvular Endocardial Cells

To test the requirement of *Pthlh*[+] VECs during valvulogenesis, we devised an ablation experiment using a tamoxifen-inducible Pthlh[CreER] mouse line in conjunction with a RosaDTA mouse line (**Fig. 3.1 A**)[105,116]. We induced ablation of *Pthlh*[+] VECs beginning at E10.5 and continued daily until E14.5. Our rationale was that we would pre-load the tamoxifen to initiate ablation of these cells as soon as *Pthlh* begins to be transcribed. To balance ablating this population without causing too much tamoxifen-induced toxicity, we ceased injection at E14.5, which produced a temporally-restricted, transient ablation of the population centered on the time at which these cells first appear based on our scRNAseq atlas data. Initial litters displayed perinatal cyanosis and lethality, consistent with the whole-organism Pthlh knockout phenotype[104]. After determining
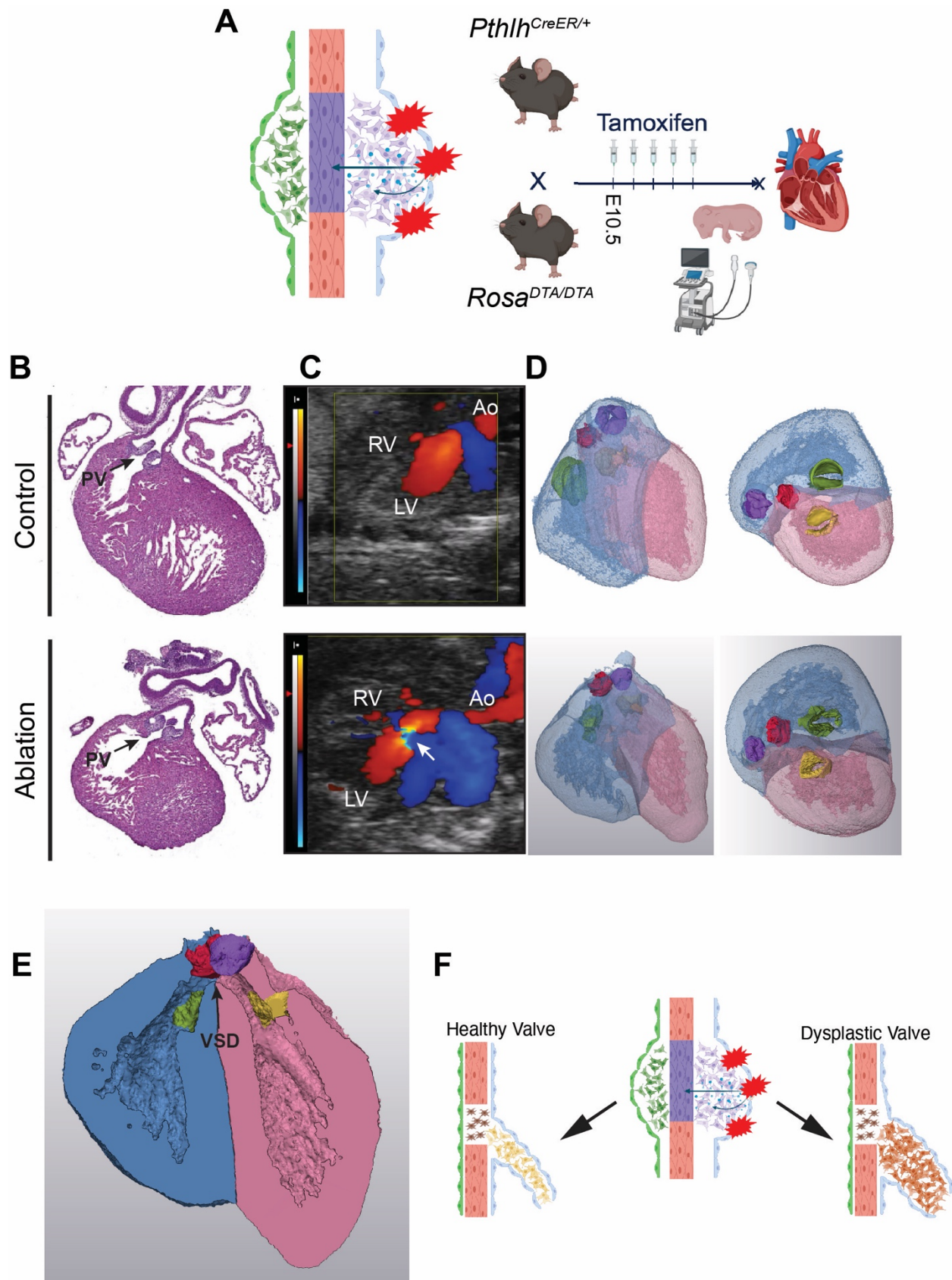
**A**

*Pthlh^{CreER/+}*

Tamoxifen

E10.5

*Rosa^{DTA/DTA}*

**B**

Control

PV

Ablation

PV

**C**

Ao

RV

LV

RV

Ao

LV

**D**

**E**

VSD

**F**

Healthy Valve

Dysplastic Valve

**Figure 3.1: *Pthlh*⁺ valvular endocardial cells are essential for post-EMT valvulogenesis**
**A,** Cartoon representation of the *Pthlh*⁺ valvular endocardial cell ablation model. **B,** H&E stained sections of Pthlh^{CreER-/+};ROSA^{DTA/+} (control) and Pthlh^{CreER+/+;}ROSA^{DTA/+} (ablation) pulmonary valves (PV). **C,** fetal echocardiograms of developing semilunar valve function from control and ablation littermates at E18.5. **D,** 3-D reconstructions of E18.5 mouse heart micro-CT scans from control and ablation littermates. Aortic Valve, red; Pulmonary Valve, purple; Mitral valve, yellow; Tricuspid Valve, green; Right Ventricle, blue; Left Ventricle, pink. **E,** 3-D reconstruction of E18.5 mouse heart micro-CT scan demonstrating VSD. **F,** Cartoon representation of dysplastic valve development secondary to loss of *Pthlh*⁺ valvular endocardial cells.

perinatal lethality, we subsequently screened for functional valvular phenotypes via fetal echocardiography at E18.5, and then micro-dissected and sectioned the embryonic hearts to screen for histologic phenotypes. Histologic analysis revealed that ablation of *Pthlh*⁺ VECs resulted in valvular dysplasia characterized by thickened, "immature"-appearing leaflets, most severely impacting the semilunar valves (**Fig. 3.1 B**). Subsequent review of fetal echocardiograms of ablation and control littermates revealed turbulent flow across the aortic valve in 4-chamber view, suggestive of a functional valvular phenotype that is concordant with the histologic phenotype we observed (**Fig. 3.1 C**). To gain a better understanding of the 3-dimensional morphometric changes to the semilunar valves, E18.5 mouse hearts were stained with phosphotungstic acid and imaged via microCT[117], which subsequently were transformed into 3-dimensional models from which surface area to volume ratios were derived (**Fig. 3.1 D**). We found that *Pthlh*⁺ VEC ablated pulmonary valves had a 1.6x-fold increase in surface area to volume ratio as compared to control littermates. Additional phenotype outcomes we observed include sub-aortic VSD, over-riding aorta, tricuspid valve tethering, and secondary ventricular remodeling (**Fig. 3.1 E**). Thus, loss of *Pthlh*⁺ VECs induce features of several human congenital heart defects such as congenital aortic stenosis, tetralogy of Fallot, and Ebstein's anomaly, suggesting this perturbation model may be well-suited to study the pathogenesis of congenital heart defects. This experiment established that

these cells are essential during valve development and loss of *Pthlh*[+] VECs results in dysplastic valvulogenesis (**Fig. 3.1 F**).

### 3.3 Determination of *Pthlh*[+] Valvular Endocardial Cell Origin

Given the striking phenotype we observed secondary to ablation of this rare subpopulation, we next sought to determine what is the cellular contribution of *Pthlh*[+] VECs during development and test the extent of our ablation. With this objective, we crossed the Pthlh[CreER] mouse line to an Rosa26[Ai6/Ai6] (ZsGreen) fluorescent reporter line[118], using the same TAM injection scheme as for the ablation model. To our surprise, the Pthlh[CreER] mouse line labeled not only the anticipated mesodermal structures (e.g. extremity long bones), but also a number of neural-crest derived structures including dorsal root ganglia, craniofacial derivatives, and midbrain (**Fig 3.2 A, B**). This unexpected result raised the interesting possibility that the endocardial population we are studying is neural crest-derived. A re-evaluation of the differentially expressed genes between Pthlh+ and Pthlh- VECs revealed an up-regulation of a number of nervous system-specific genes including *Stmn2*[119], *Nts*[120], *Prnp*[121]. This is in addition to the previously recognized down-regulation of endocardial/endothelial markers such as *Emcn* and *Ednrb* (**Fig. 2.4 C**). Notably, stathmin 2, *Stmn2*, is a microtubule-associated protein that has been annotated as playing a role in neural growth[122], in addition to osteogenesis[123], and has been associated with Down's syndrome[124] – a chromosomal aneuploidy associated with a 40-50% incidence of congenital heart disease[125]. Review of our scRNAseq data for *Stmn2* expression demonstrated restriction of *Stmn2* expression to the same valvular endocardial cell cluster as *Pthlh* (**Fig. 3.2 C**). Fluorescent *in situ* hybridization for *Stmn2* expression at E12.5 demonstrated localization to both central and peripheral nervous system (neural crest-derived) structures, in addition to the cushion endocardial overlapping with the *Pthlh*

expression domain (**Fig 3.2 D**). Furthermore, this lineage tracing result provides a new perspective

from which to view the multiomics data and transcription factor motif enrichment analysis of cell

type-specific marker peaks derived from our E12.5 wildtype single cell chromatin accessibility
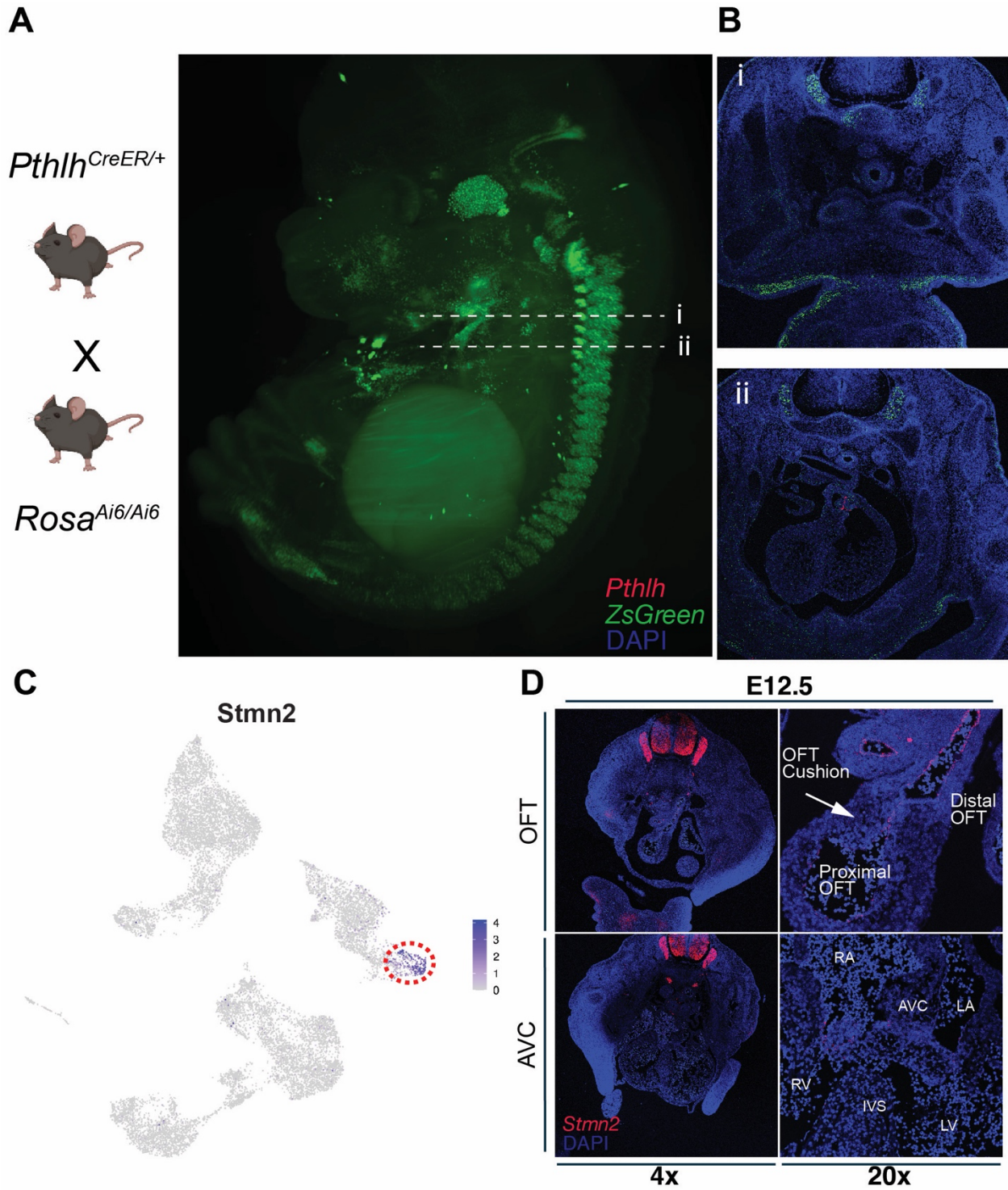
**Figure 3.2: *Pthlh* expression marks both mesodermal and neural crest-derived tissues**
**A,** Lightsheet image of a cleared Pthlh^CreER+/+;ROSA^Ai6/+ E14.5 embryo. **B,** *ZsGreen* and *Pthlh* expression via in situ hybridization of axial sections at multiple levels from a Pthlh^CreER+/+;ROSA^Ai6/+ E14.5 embryo. **C,** UMAP plot of *Stmn2* expression at E12.5. **D,** *Stmn2* expression via in situ hybridization in the OFT and AVC cushions at E12.5 at 4x and 20x magnification.

and gene expression data. We had originally hypothesized that the chromatin accessibility differences we observed were secondary to specification of *Pthlh*+ VECs from an endocardial precursor and acquiring some mesenchymal transcriptional and chromatin accessibility traits. It is entirely possible that the opposite is true, in that *Pthlh*+ VECs had mesenchymal characteristics as a neural crest-derivative and acquired endocardial traits as this population migrated and incorporated into the valvular endocardium. Taken together, these data raise the interesting possibility that *Pthlh*+ VECs have a distinct neural crest origin as compared to the other valvular endocardial cells.

To test this hypothesis and determine the origin of *Pthlh*+ VECs, we performed a lineage tracing experiment with the Wnt1Cre2 line that has been shown to be more neural-crest specific than previous Wnt1Cre lines[126]. We found co-localization of *Pthlh* and *ZsGreen* expression, providing further evidence of a neural crest origin for *Pthlh*+ VECs (**Fig. 3.3 A**). Furthermore, to test for endocardial contributions to this lineage, we are currently in the process of leveraging a tamoxifen-inducible Cdh5CreER mouse line and are pulsing tamoxifen for transient induction at E8.5 and E9.5, before *Pthlh*+ cells co-express *Cdh5*[127]. To further validate our lineage tracing results, we reprocessed two previously published independent FACS-sorted neural crest-derived scRNA-seq datasets generated using a different Wnt1Cre mouse line[128] than the one we used in our own lineage trace experiment, and a tdTomato reporter[129]. The first dataset we analyzed prepared their samples by FACS-sorting tdTomato+ cells from pooled, microdissected embryonic hearts at several developmental timepoints[129]. We focused our analysis on the E17.5 timepoint,

searching for cells with a similar transcriptional identity to the *Pthlh*[+] VECs we identified in our

own scRNAseq experiment. Analysis of the E17.5 neural crest pulse-seq data revealed a subset of

cells to be dual positive for *Pthlh* and *Stmn2* (**Fig. 3.3 B**). The second dataset we re-processed

differed from the first, in that the authors focused on early cardiogenesis timepoints E8.5, E9.5,

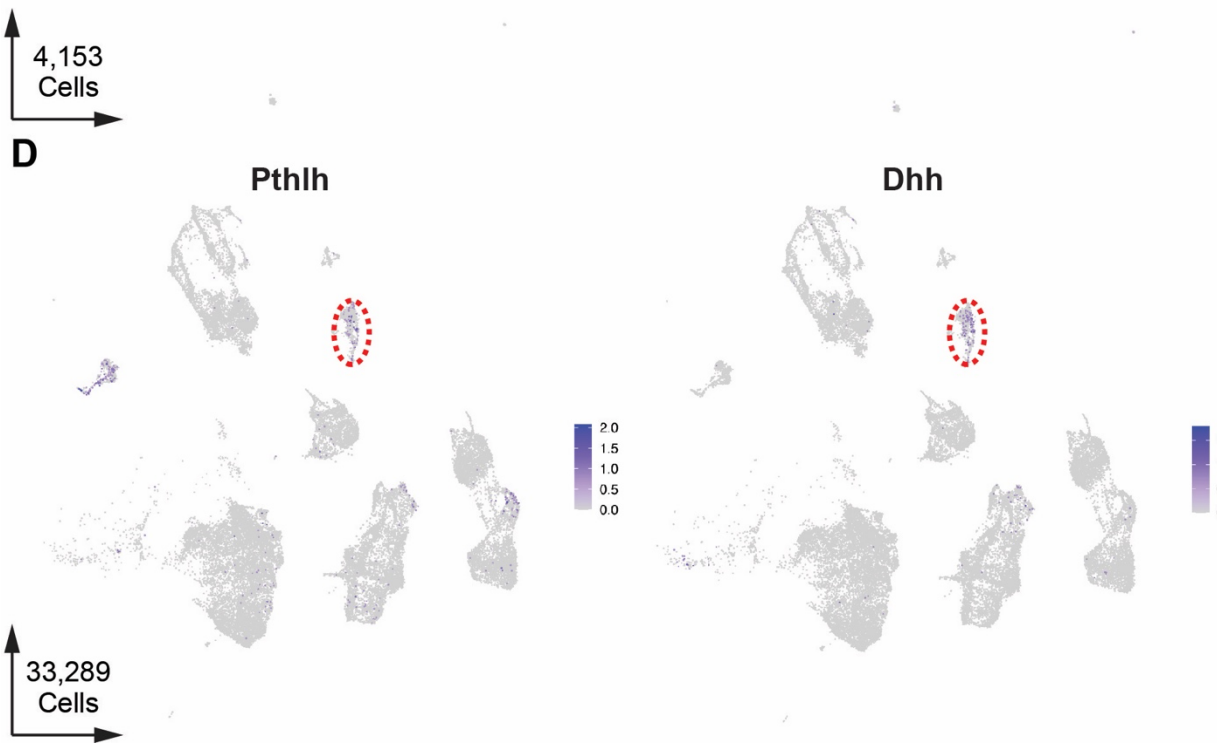and E10.5. Furthermore, in their sample preparation they purposefully included extra-cardiac
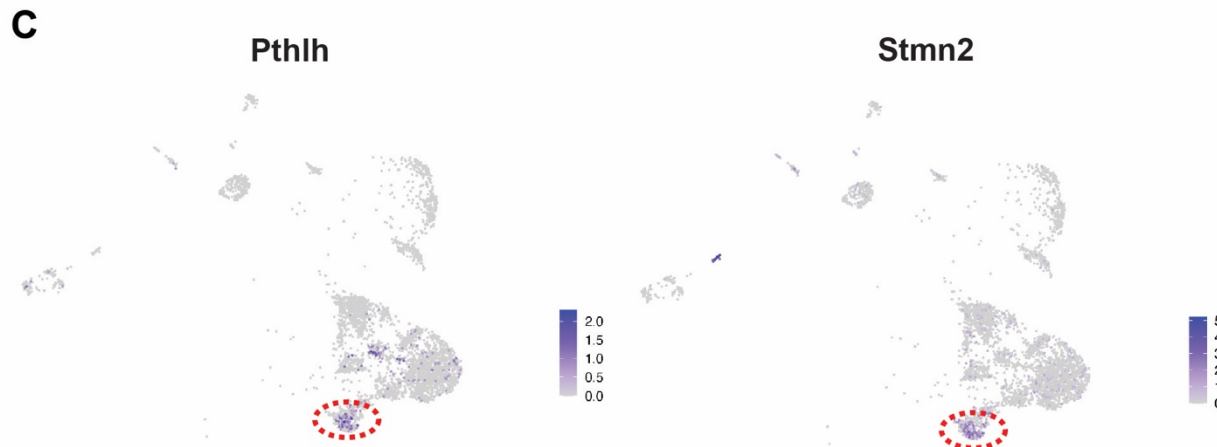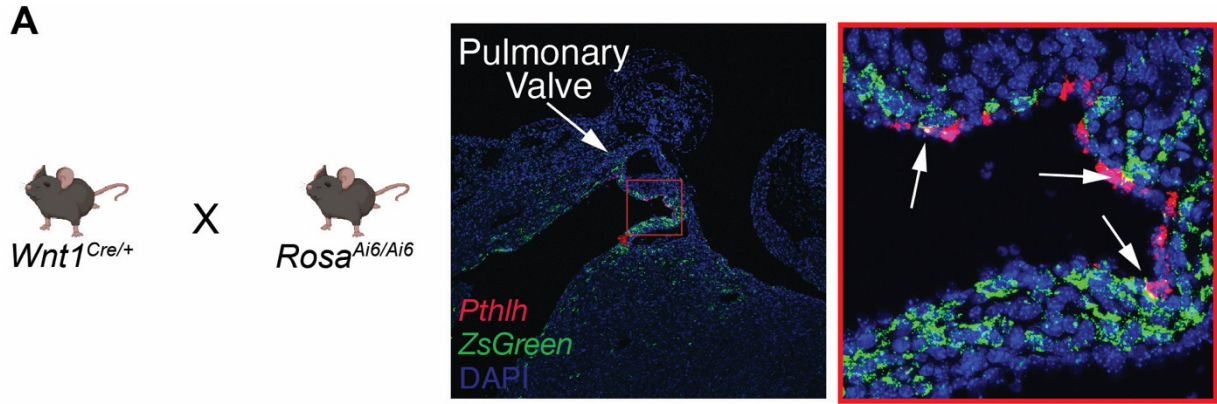
**Figure 3.3: Pthlh+ valvular endocardial cells are neural crest-derived**

**A,** *Pthlh* and *ZsGreen* expression via in situ hybridization on Wnt1[Cre/+];ROSA[Ai6/+] E18.5 mouse heart sections displaying the pulmonary valve. **B,** UMAP of *Pthlh* and *Stmn2* expression in FACS-sorted neural crest-derived cardiac cells at E17.5. **C,** UMAP of *Pthlh* and *Dhh* expression in FACS-sorted neural crest-derived cardiac and extra-cardiac cells at E8.5, E9.5, and E10.5.

tissue to capture neural crest progenitor populations[130]. Thus, in our focused re-analysis of these data, we identified *Pthlh+/Dhh+* precursor cells that lacked *Cdh5* expression (**Fig 3.3 C**). These results, in concert with our scRNAseq and RNAscope data, are highly suggestive that Pthlh+ VECs are neural crest-derived.

### 3.4 Characterization of neural crest-specific deletion of Pthlh

To test the requirement of neural crest-derived Pthlh signaling during valvulogenesis, we performed tissue-specific deletion of *Pthlh* using the Wnt1[Cre] mouse line[126,131]. Similar to the whole organism knockout, neural crest-specific deletion resulted in perinatal lethality, with zero Wnt1[Cre/+], Pthlh^{fl/fl} (ΔNC-Pthlh) animals surviving to weaning age, where as normal Mendelian ratios were observed at E18.5. Histologic analysis of ΔNC-*Pthlh* E18.5 embryonic hearts revealed a valvular dysplasia phenotype similar to that of the *Pthlh*[+] VEC ablation phenotype, characterized by thickened, "immature"-appearing leaflets, most severely impacting the semilunar valves (**Fig. 3.4 A**). Moreover, fetal echocardiography of ablation littermates also demonstrated turbulent flow through the aortic valve in 4-chamber view, suggestive of congenital aortic stenosis (**Fig. 3.4 B**) The 3-dimensional reconstruction of microCT data from ΔNC-Pthlh and control littermates revealed a highly dysplastic pulmonary valve phenotype (**Fig. 3.4 C**). Thus, loss of neural crest-derived *Pthlh* signaling phenocopies a significant portion of the phenotype observed in the Pthlh+ VEC ablation model, providing the first evidence of *Pthlh*-mediated regulation of valve development (**Fig. 3.4 D**).

**A**

*Pthlh^{fl/fl}*

X

*Wnt1^{Cre/+}; Pthlh^{fl/+}*

Control

ΔNC-Pthlh

PV

**B**

RV    Ao
LV

RV    Ao
LV

**C**

**D**

Healthy Valve

Dysplastic Valve

**E**

*Wnt1^{Cre/+}; Pthlh^{fl/+}*

X

*Pthlh^{fl/fl}*

E13.5    E18.5

Multi-omics

t-SNE2

t-SNE1
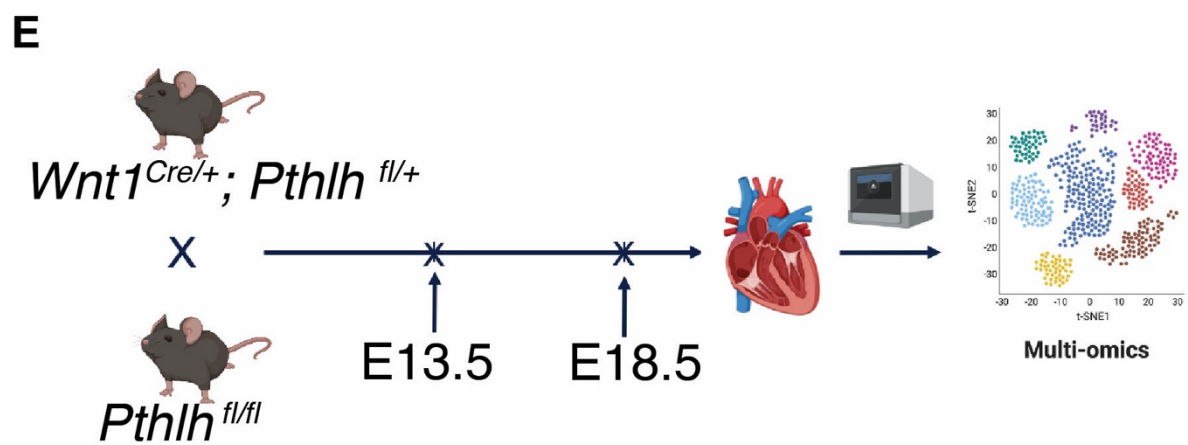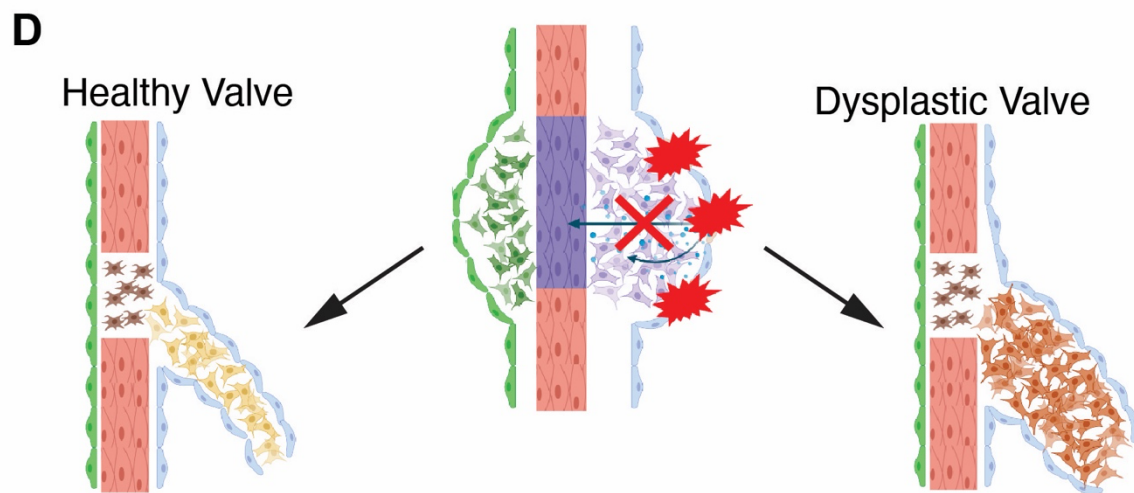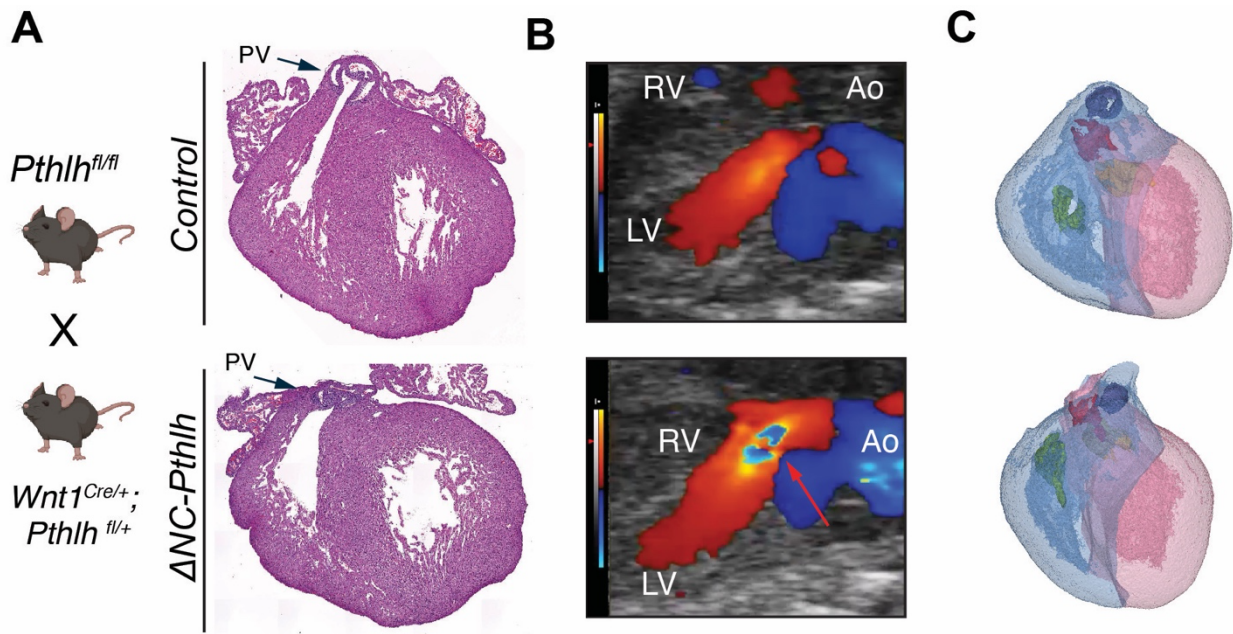
**Figure 3.4: Neural crest-derived *Pthlh* signaling is required for post-EMT valvulogenesis**
**A,** H&E-stained sections of Wnt1[Cre/+]; *Pthlh*^{fl/fl} (ΔNC-*Pthlh*) and *Pthlh*^{fl/+} (control) E18.5 pulmonary valves (PV). **B,** Fetal echocardiograms of developing semilunar valve function from control and ΔNC-*Pthlh* littermates at E18.5. **C,** 3-D reconstructions of E18.5 mouse heart micro-CT scans from control and ΔNC-*Pthlh* littermates. **D,** Cartoon representation demonstrating loss of *Pthlh*[+] VECs or *Pthlh* signaling resulting in dysplastic valve development. **E,** Cartoon representation of single-cell multi-omic analysis of E13.5 and E18.5 ΔNC-*Pthlh* vs control embryos.

**3.5 Multi-omic analysis of neural crest-specific loss of Pthlh signaling at Embryonic Day 13.5**

To interrogate the cell and non-cell autonomous transcriptional and chromatin accessibility changes secondary to neural crest-specific deletion of Pthlh, we employed the 10X Chromium Next GEM Single Cell Multiome ATAC and Gene Expression Assay (10X Multiome). To begin, we applied the multiome to three *Pthlh* delta-NC and two control embryonic hearts at both E13.5 to detect early transcriptional and epigenomic changes secondary to the loss of *Pthlh* signaling (**Fig. 3.4 E**). The hearts were micro-dissected, dissociated into single-cells, and nuclear isolation was performed. Following GEM generation, library preparation, sequencing, and quality control filtering, we generated a 33,248 nuclei Seurat object. Unsupervised clustering yielded sixteen distinct clusters of give main cell types: myocardium, endocardium, mesenchyme, epicardium, and hematopoietic (**Fig. 3.5 A**). From gross observation, it appears that both the control (CREneg) and ΔNC-*Pthlh* (CREpos) conditions contributed equally to each cluster, implying low sample-to-sample variability during sample and library preparation (**Fig. 3.5 B**). Each cluster was appropriately annotated using previously annotated marker genes and cross-referencing with our wild-type cardiogenesis atlas (**Fig. 3.5 C**).
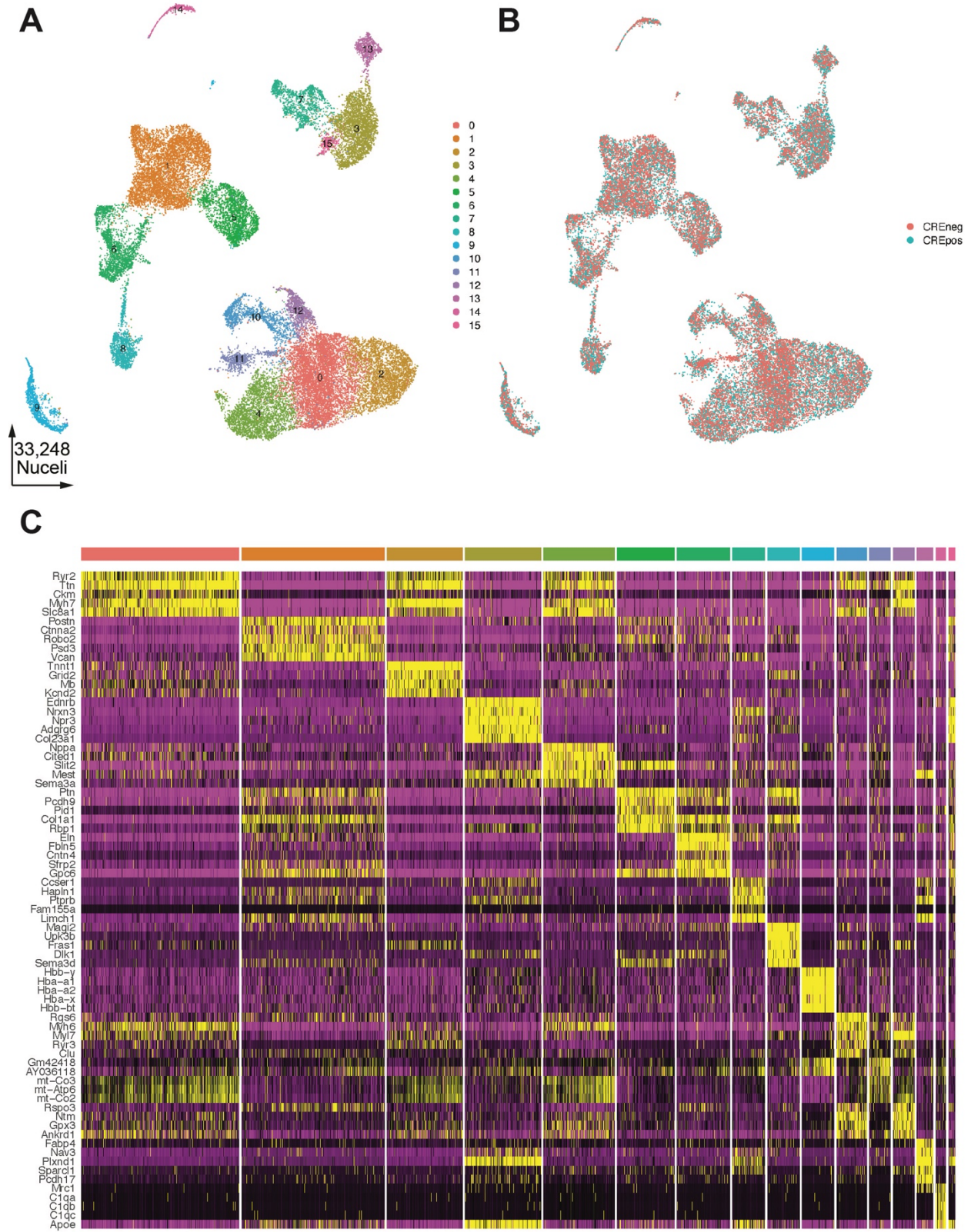
**Figure 3.5: Identification of cardiac cell types at embryonic day 13.5**

**A,** UMAP plot of all captuered cardiac cell populations colored by cluster. **B,** UMAP plot of all captured cardiac cell populations colored by genotype, CREneg vs CREpos. **C,** Expression heatmap of top 5 marker genes for each cluster.

To focus our analysis on transcriptional and chromatin accessibility changes in the developing valvular cell types, a computational dissection of these populations was performed as before using identical marker genes (**Fig. 3.6 A, B, C**). Computational sub-setting of these cell types into a new valvular cell Seurat object of 12,564 nuclei. Re-clustering resulted into a total of sixteen distinct clusters, each named based on expression of the aforementioned marker genes (**Fig 3.7 A, B**). *Pthlh* expression was restricted to the VEC_2 cluster, while *Stmn2* expression was observed in both VEC_1 and VEC_2 clusters (**Fig 3.8 A**). Differential gene expression analysis
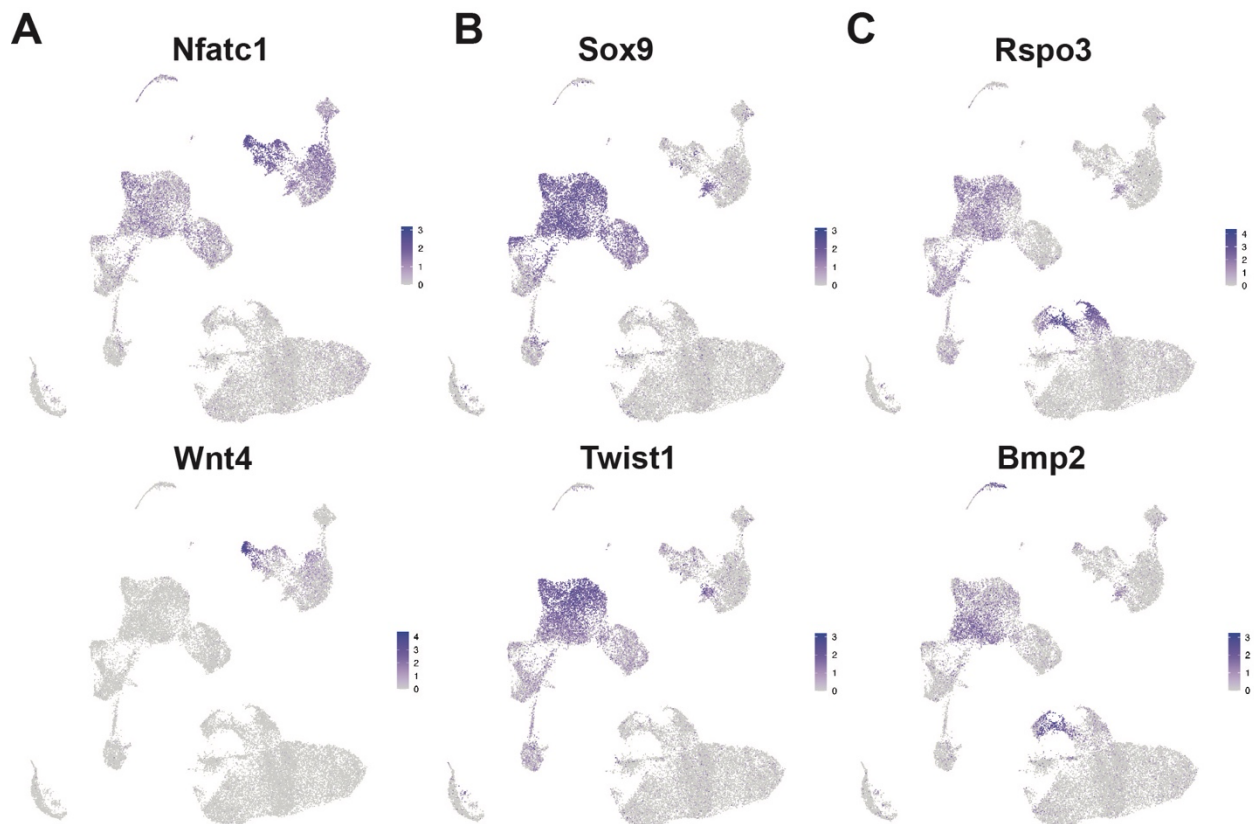


**Figure 3.6: Identification of valvular subpopulations at embryonic day 13.5**
**A,** UMAP plot of valvular endocardial marker genes, *Nfatc1* and *Wnt4*. **B,** UMAP plot of mesenchymal marker genes, *Sox9* and *Twist1*. **C,** UMAP plot of valvular myocardial marker genes, *Rspo3* and *Bmp2*.
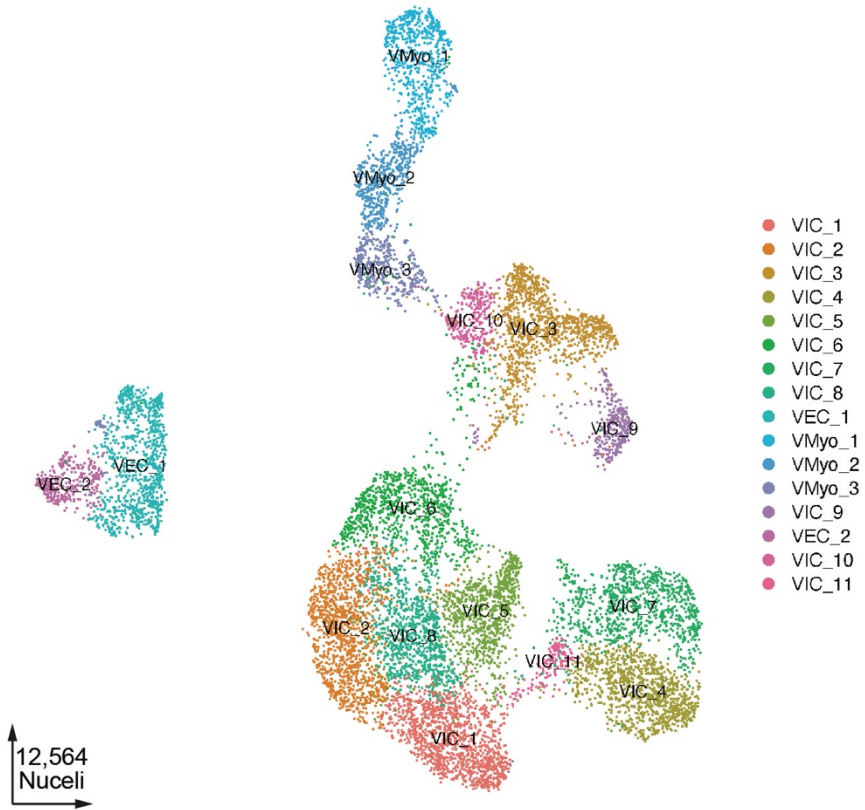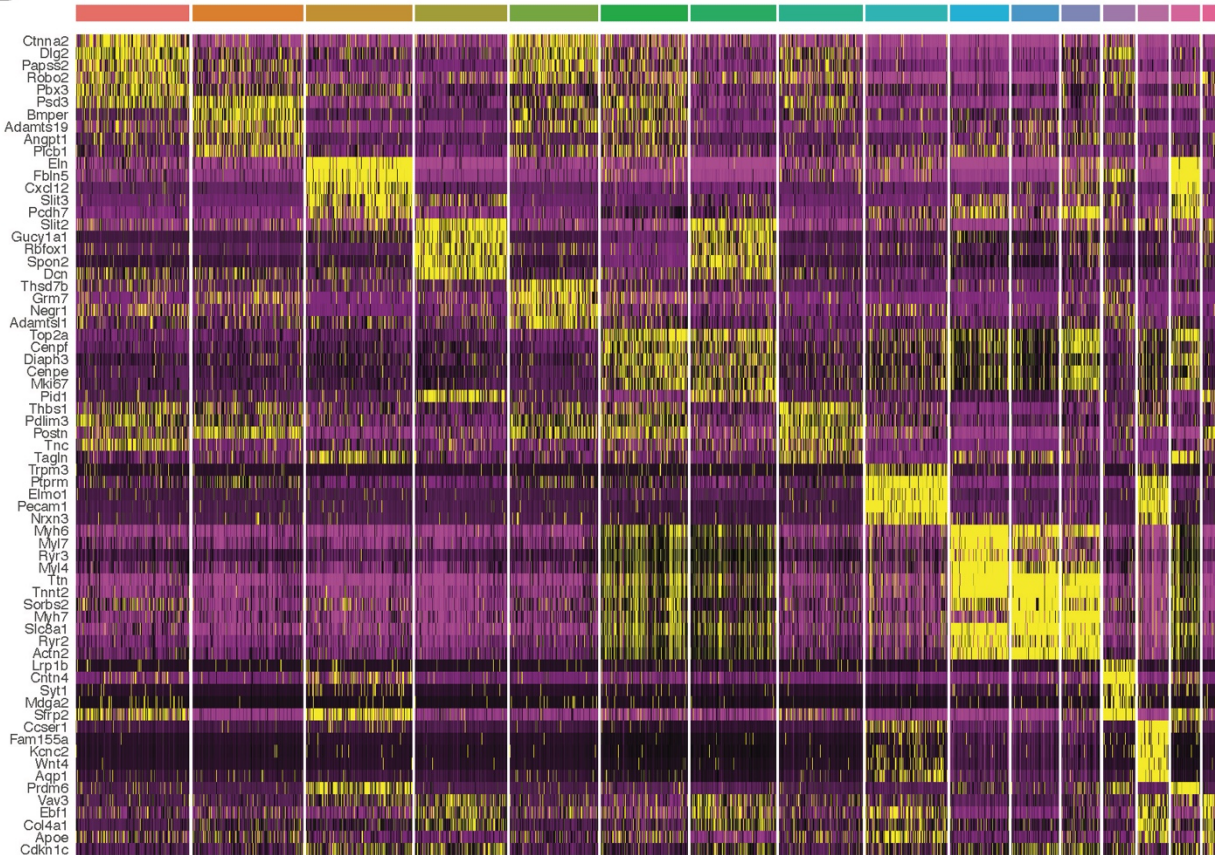
**Figure 3.7: Computational sub-setting of valvular cell types at embryonic day 13.5**
**A,** UMAP plot of valvular cell types at E13.5. **B,** Heatmap plot of top 5 marker genes for each cluster.

within the *Pthlh*[+] VEC_2 cluster between CREpos and CREneg condition yielded a total of 149 differentially expressed genes with a log fold-change greater than 0.5x (**Fig. 3.8 B**). Interestingly, loss of neural crest-derived *Pthlh* was associated with the loss of several cell type-specific marker genes including *Stmn2*, *Aqp1*, *Rbp7*. This suggests that *Pthlh* may play a cell autonomous role in the specification and maintenance of the unique transcriptional identity of *Pthlh*[+] VECs. Moreover, we also observed a down-regulation of *Jarid2*, a transcriptional repressor that has been demonstrated to interact with the Polycomb repressive complex 2 to regulate gene expression[132]. This gene has also been implicated as playing an important role in murine heart development, and putative pathogenic variants have been identified in humans with left-sided obstructive cardiac lesions such as aortic and pulmonary stenosis[133,134]. Furthermore, down-regulation of elastin (*Eln*) may have significance for two reasons. First, several studies have associated pathogenic variants in this gene with autosomal dominant inherited forms of inherited aortic stenosis[135,136,137]. Second, elastin is the predominant ECM component of the atrialis (AV valves)/ ventricularis (semilunar valves) layer of the adult valve leaflet, which is precisely where *Pthlh*+ VECs are located. We had hypothesized that disruption of *Pthlh* signaling may alter ECM composition and maturation through disruption of interaction with VICs, and this *Eln* downregulation may be supportive of this hypothesis.
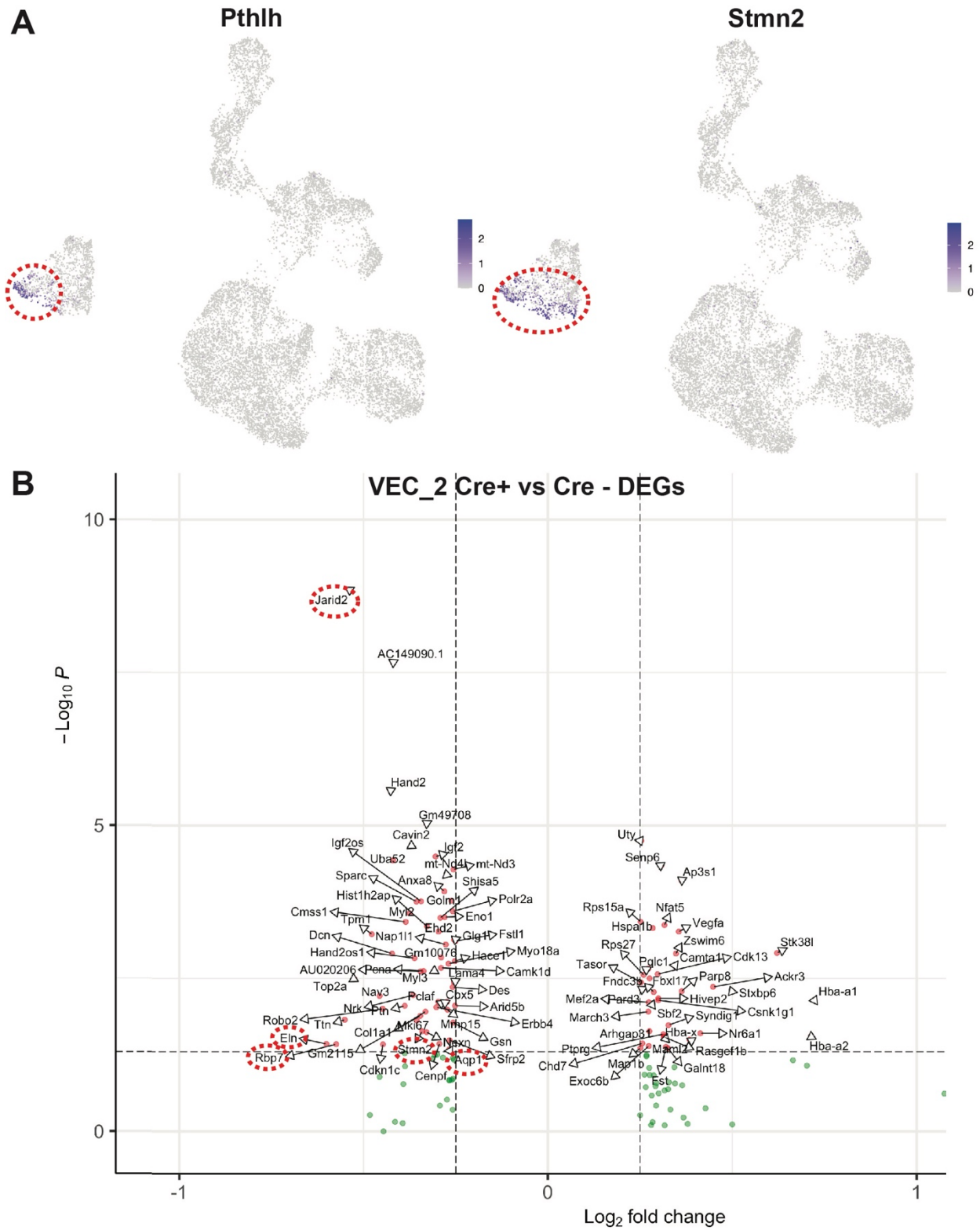
**Figure 3.8: Cell autonomous transcriptional dysregulation in *Pthlh*⁺ valvular endocardium**

**A,** UMAP plot of Pthlh and Stmn2 expression at embryonic day 13.5. **B,** Volcano plot of differentially expressed genes between CREpos and CREneg VEC_2 cells. (FCcutoff = 0.5)

We next sought to understand how loss of neural crest-derived *Pthlh* signaling impacted valvular cell-cell communication at E13.5. We again leveraged the CellChat computational pipeline to perform this analysis, comparing the CREpos and CREneg conditions to identify lost or gained cell-cell interactions. Gross comparison across all clusters identified numerous changes both in the number and strength of signaling interaction (**Fig. 3.9 A**). Notably, VMyo_1 appears to have had the largest increase in both number and strength of outgoing interactions, while VEC_1 had the largest decrease in number and strength of outgoing interactions. VIC_10 appears to have had the largest increase in number and strength of incoming interactions, while VEC_2, the *Pthlh-*expressing cluster, had the largest decrease in strength of interactions. From this analysis, we first focused our attention on VMyo_1, a population predicted to receive the *Pthlh* signal from our wild-type signal-ome analysis based on high expression of *Pth1r*.

**A** Differential number of interactions — Differential interaction strength

**B** VMyo_1 Cre+ vs Cre - DEGs

58
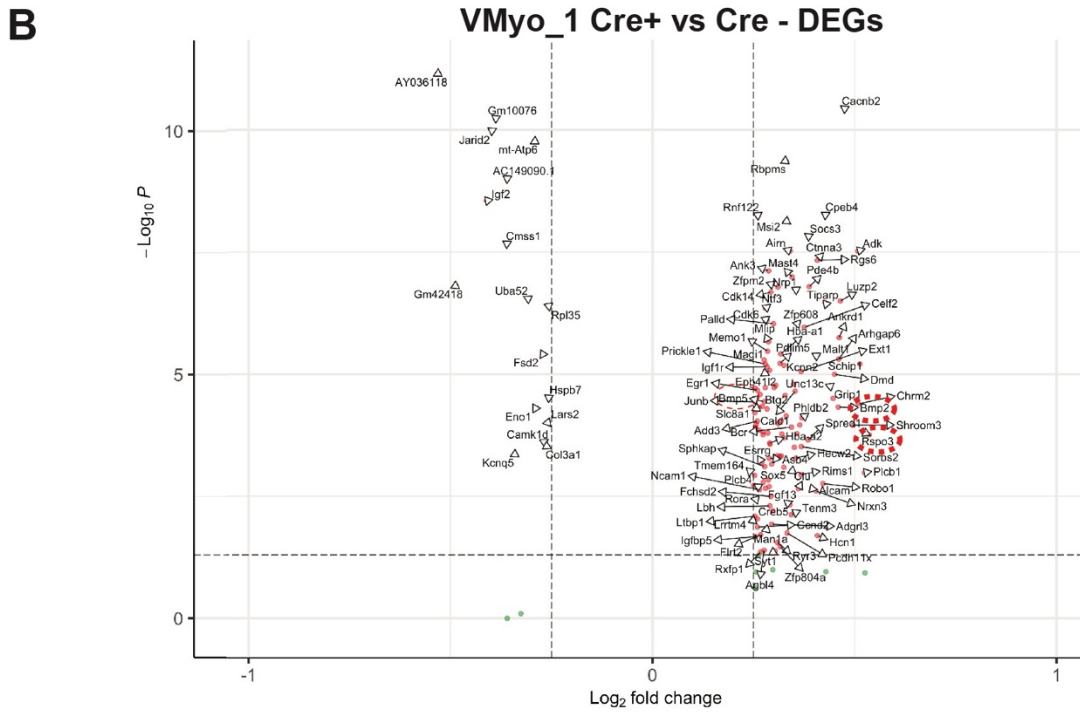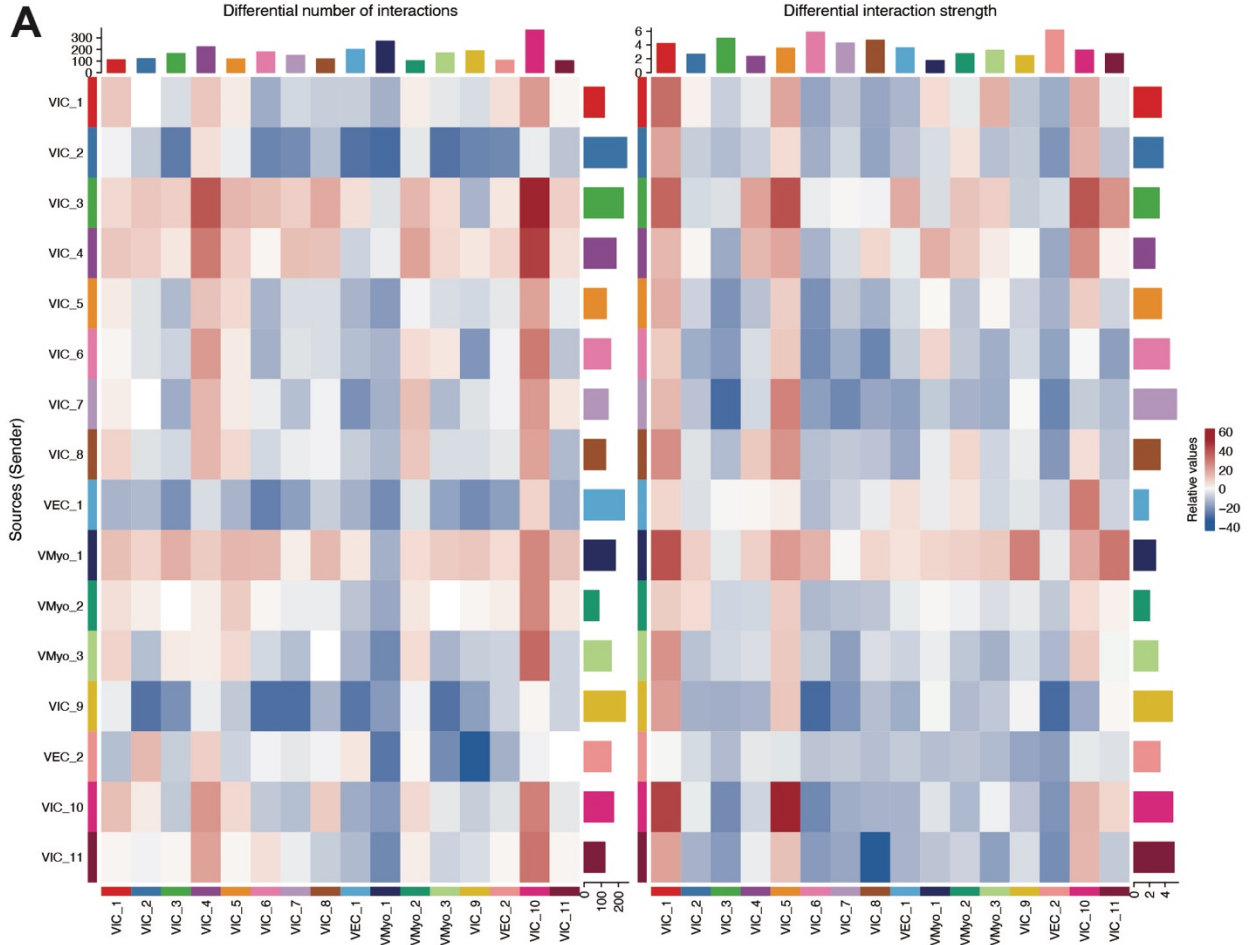
**Figure 3.9: Neural Crest-specific Pthlh-deficient Differential Cell – Cell Communication Analysis**
**A,** Heatmap plot of number (L) and strength (R) of valvular cell – cell interactions between Wnt1$^{Cre/+}$; Pthlh$^{fl/fl}$ (CREpos) and Pthlh$^{fl/+}$ (CREneg) conditions at embryonic day 13.5. **B,** Volcano plot of differentially expressed genes between CREpos and CREneg VEC_2 cells. (FCcutoff = 0.5)

Differential gene expression analysis between CREpos and CREneg conditions in VMyo_1 revealed a total of 150 differentially expressed genes with a log fold-change greater than 0.5x (**Fig. 3.9 B**). We were astonished to find that amongst the most highly differentially expressed genes were within the BMP signaling pathway: *Bmp2*, *Bmp5*, *Rspo3*, and *Tbx3*. As previously reviewed, *Pthlh* signaling has previously been shown to modulate BMP signaling in the context of mammary bud outgrowth. In this context, paracrine *Pthlh* signals up-regulate Bmpr1a in the mammary mesenchyme, sensitizing the population to *Bmp4* signaling and leading to increased *Msx2* expression, driving mesenchymal maturation. In the context of valve development, autocrine BMP signaling has been shown to be essential in the specification and maintenance of valvular myocardium to repress chamber-specific gene programs and promote *Tbx2/Tbx3* expression. Loss of neural crest-derived *Pthlh* signaling is associated with an up-regulation in these BMP pathway genes (**Fig. 3.10 A**).

Furthermore, CellChat analysis revealed a reduction in *Bmpr1a* expression in several mesenchymal clusters including VIC_7, VIC_8, and VIC_11 (**Fig. 3.10 B**). BMP signaling has also been implicated in the regulation of valvular mesenchymal growth and maturation[69]. Small increases in expression of several BMP ligands, in addition to changes in expression of the receptor in target mesenchymal populations, could cumulatively have a profound impact on valvular morphogenesis. This initial timepoint may also only reflect early changes that may be more pronounced later in valvular development. Multi-omic characterization of a later stage of

valvulogenesis at E18.5 in the setting of loss of neural crest-derived *Pthlh* signaling are currently

underway.
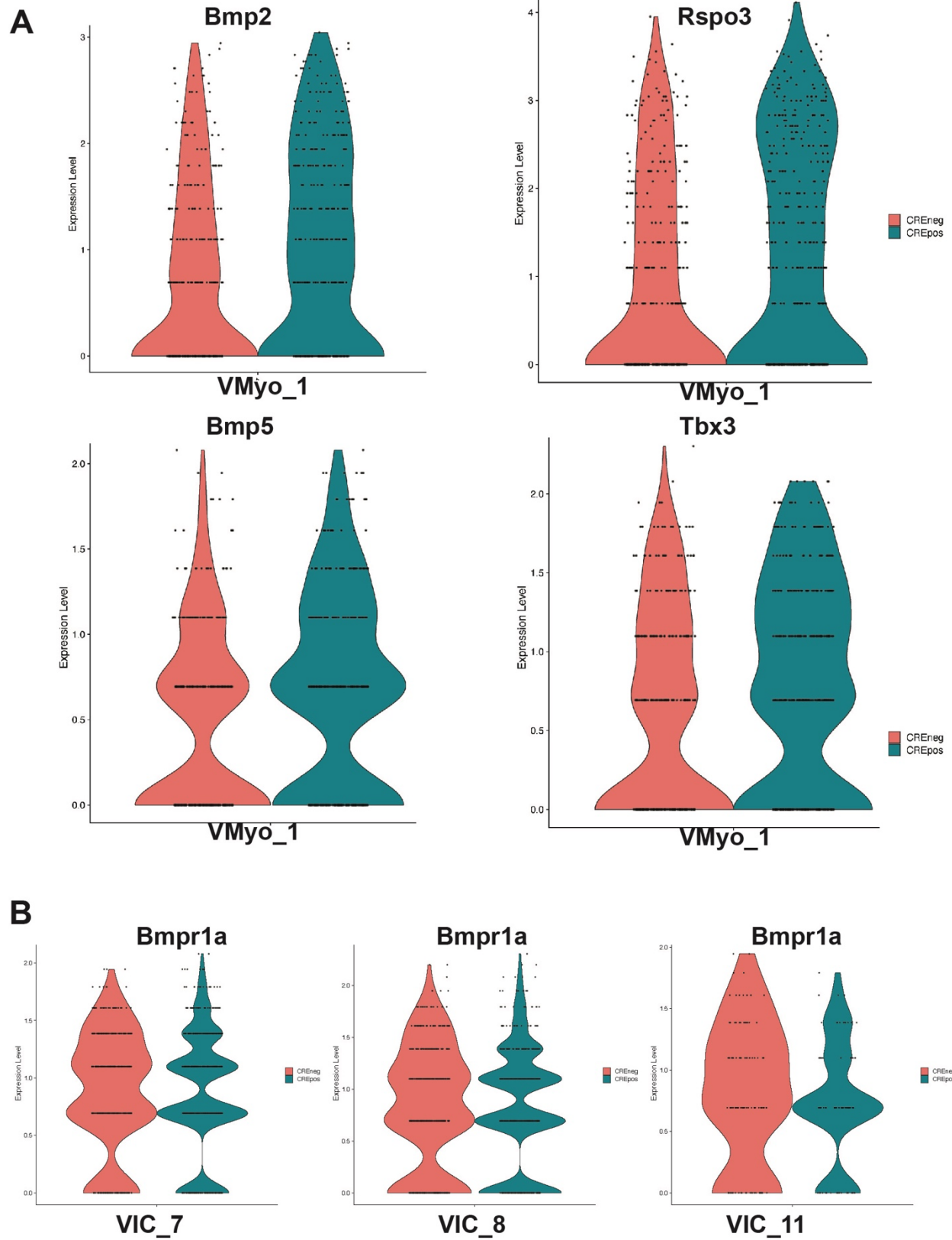
**Figure 3.10: BMP signaling dysregulation is associated with loss of *Pthlh* signaling**

**A,** Violin plots of *Bmp2, Rspo3, Bmp5, and Tbx3* expression in the VMyo_1 cluster between CREneg and CREpos conditions. **B,** Violin plots of *Bmpr1a* expression in the VIC_7, VIC_8, and VIC_11 clusters between CREneg and CREpos conditions.

Having identified transcriptional dysregulation in the BMP signaling pathway secondary to loss of neural crest-derived *Pthlh* signaling, we next investigated if we could identify any chromatin accessibility changes in the developing valvular subpopulations. One of the main advantages of using the 10X Multi-ome platform is that the RNA and ATAC data are derived from the same cell with the same cell barcode, avoiding the need for computational integration of cell type annotations, which historically are not always accurate. This is particularly of importance when studying rare populations of cells, as is the case here. We began our analysis of chromatin accessibility changes by re-clustering our cells based on their chromatin accessibility state and transferring annotation from our transcriptional Seurat object (**Fig. 3.11 A**). Of note, when clustering based on chromatin accessibility state, we observed the two endocardial clusters collapse into a single cluster, C4. We then identified marker peaks for each cluster (**Fig. 3.11 B**).
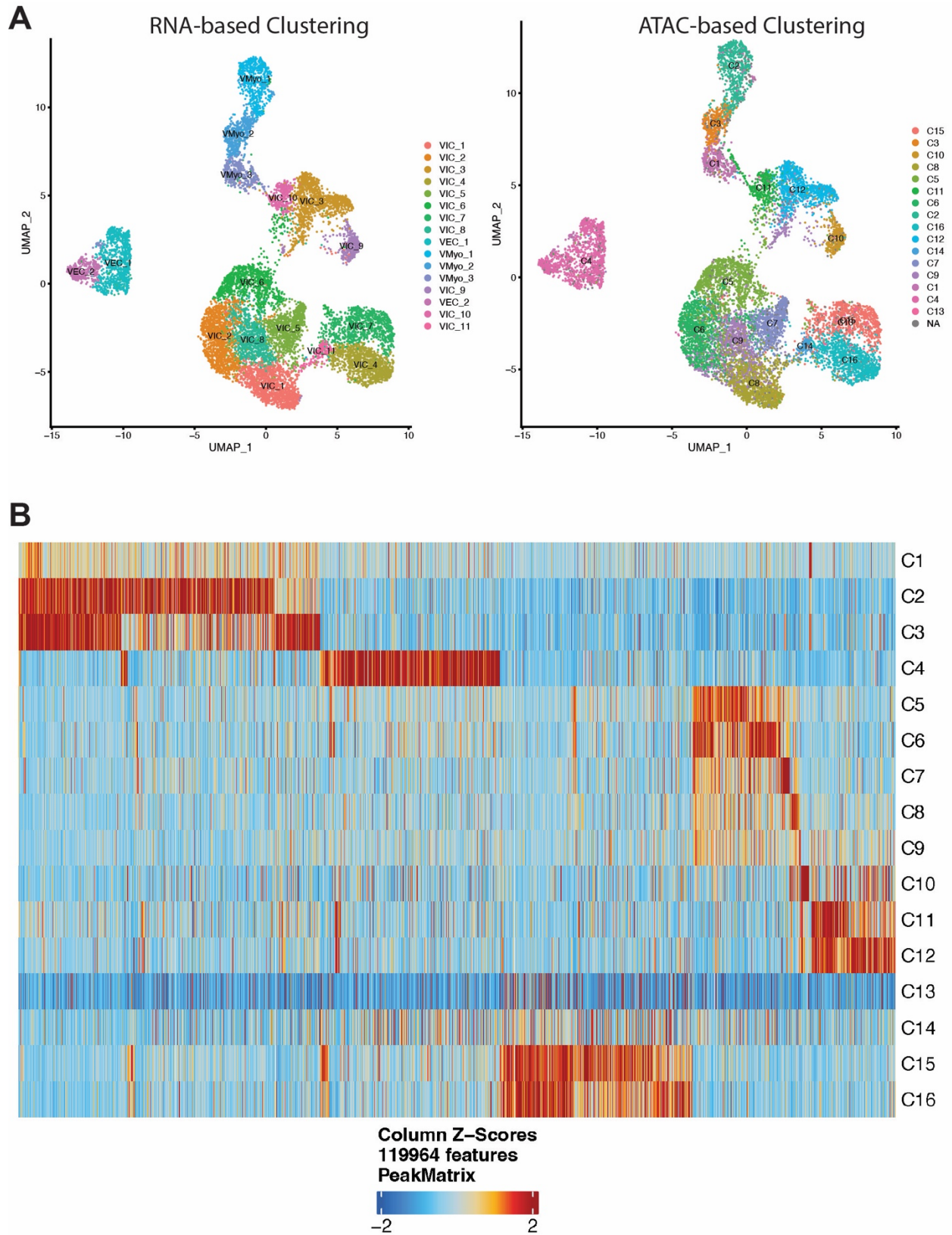
**Figure 3.11: Chromatin accessibility-based clustering of valvular cell types**

**A,** UMAP plots of RNA-based (L) and chromatin accessibility-based (R) clustering of valvular cell types at E13.5. **B,** Heatmap plot of marker peaks for each cluster.

To identify chromatin accessibility changes secondary to loss of neural crest-derived *Pthlh*, searched for differentially accessible regions (DARs) between the CREpos and CREneg conditions. From these DARs, we then performed transcription factor motif enrichment analysis to identify which transcription factors are likely to bind within these DARs. Within the DARs that are closed in the CREpos condition, we identified enrichment for *Egr*, *Ets/Etv*, and *Bach* family transcription factors (**Fig 3.12 A**). We found these to be of particular interest due to prior annotations in cardiac development and our own wild-type chromatin accessibility data. In our wild-type E12.5 multi-ome transcription factor enrichment analysis, we demonstrated that increase in accessibility to peaks with *Ets/Etv/Bach* binding sites were important differentiating markers for *Pthlh+* cells relative to valvular mesenchyme and *Pthlh-* endocardium. Thus, in the setting of loss of *Pthlh*, it was intriguing to observe loss of accessibility to these sites for candidate lineage-specifying transcription factors. Furthermore, it is known that the mid-region of *Pthlh* contains a nuclear localization signal[138], and prior studies have shown *Pthlh* to reside within the nucleoplasm of cells. This result raises interesting questions about *Pthlh* intracrine signaling and the role it may play in regulating genome architecture to regulate gene expression. Moreover, loss of *Egr2* sites, previously known as *Krox20*, was an interesting result as this gene has previously been shown to be present in a subset of neural crest cells and is important for valve development[139]. Loss of this gene is associated with thickened, immature semilunar valve leaflets, and *in situ* hybridization of *Egr2* mRNA revealed spatial localization that highly resembles the expression domain of *Pthlh*. These results provide several candidate transcription factors to study in this rare population that may play an important role in the specification and maintenance of this rare cell type's identity.
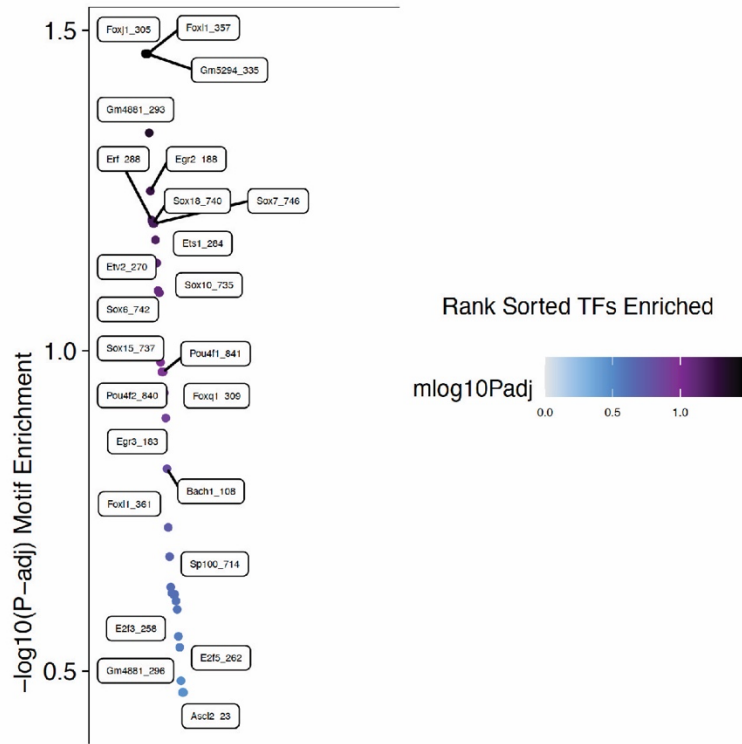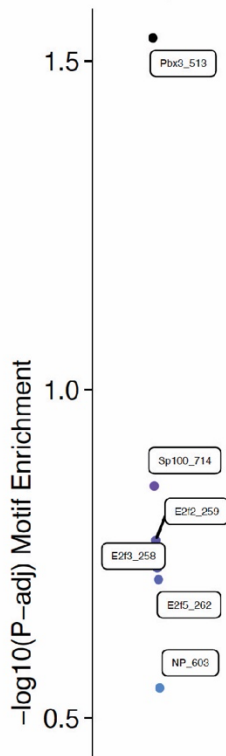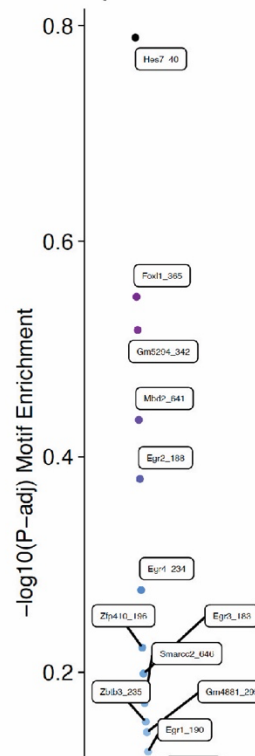
**Figure 3.12: Chromatin accessibility dysregulation secondary to loss of *Pthlh***

**A,** Transcription factor motif enrichment for closed DARs in the CREpos condition in the valvular endocardium. **B,** Transcription factor motif enrichment for closed (L) and open (R) DARs in the CREpos condition in the VMyo_1 cluster.

Given the transcriptional changes in the VMyo_1 cluster, we performed a focused analysis on this population for potential chromatin accessibility dysregulation. The top transcription factor motif enrichment in the closed DARs was for *Pbx3*. Loss of this gene is associated with cardiac malformations resembling tetraology of Fallot, overriding aorta with ventricular septal defect, and bicuspid aortic valves[140]. The top transcription factor in the open DARs was for *Hes7*, a known target of the Notch signaling pathway[141]. Notch signaling has been broadly implicated in post-EMT valvulogenesis; however, no specific-role for *Hes7* has been delineated as of yet.

## 3.6 Conclusions

Given the high spatiotemporal specificity of *Pthlh*$^+$ valvular endocardial cells and unique transcriptional and chromatin accessibility signature, we set out to functionally characterize this cell type and its marker signaling peptide. We demonstrated that *Pthlh*$^+$ valvular endocardial cells are essential for post-EMT valvulogenesis, loss of which is associated with valvular dysplasia and perinatal cyanosis and lethality. We further established that this cell type is derived from the neural crest, providing the first evidence of a neural crest-to-endocardial transition. We then demonstrated that loss of *Pthlh* from the neural crest recapitulates the *Pthlh*$^+$ valvular endocardial cells ablation phenotype, implicating a previously undescribed neuroendocrine peptide hormone signaling pathway in the regulation of post-EMT valvulogenesis. Lastly, we leveraged scRNAseq and scATACseq to identify cell autonomous loss of *Pthlh+ VEC* marker gene expression and marker peak accessibility, in addition to BMP signaling dysregulation in the valvular myocardium. In the

subsequent chapter, I will explore the role of this novel cell type in the context of human development and disease.

# Chapter 4

## *PTHLH*[+] Valvular Endocardial Cells in Human Development and Disease

**4.1 Rationale**

Single-cell analysis of murine development revealed a novel, rare valvular endocardial subpopulation that is highly secretory. This population is developmentally established and, from existing murine single-cell data, appears to persist long into postnatal valvular remodeling. We further demonstrated that (1) *Pthlh*⁺ VECs are required for proper valvulogenesis, (2) *Pthlh*⁺ VECs are derived from the neural crest, and (3) that neural crest-derived *Pthlh* signaling is a novel molecular regulator of valvulogenesis. If *PTHLH*⁺ VECs are present in human development, this would substantially increase the importance of functionally characterizing this novel cell type in the context of human development and disease. To address the prospective role of these cells in humans, we leveraged both existing human fetal heart scRNAseq data and generated new data from a 20-week human fetal heart with hypoplastic left heart syndrome (HLHS) and critical aortic stenosis. We used these data to assess the role of *PTHLH*⁺ valvular endocardial cells in human development and disease.

**4.2 Congenital Heart Disease Genetic Associations with PTHLH-positive Valvular Endocardial Cell Marker Genes**

Before analyzing scRNAseq data for this population of cells, we began with a comprehensive literature review for genetic associations between *Pthlh*⁺ VEC marker genes we identified from our murine valvulogenesis atlas and congenital heart disease. Interestingly, recent clinical genetics studies have implicated rare variants in multiple marker genes including *Ptprb* and *Wnt9b* with CHD phenotypes[142,143,144]. In the case of *PTPRB*, a recent case report documented an inherited homozygous rare variant in a highly conserved region of the gene at the exon-intron border predicted to impact splicing[142]. Mechanistic studies of the variant *in vitro* demonstrated

alternative splicing that results in a single glutamine deletion predicted to interfere with the signal peptide of the gene. Furthermore, a recent study correlating magnetic resonance images measurements of right-sided heart structures with genetic variants in 40,000 individuals in the UK Biobank identified a number of variants in the *WNT9B* locus, a gene that has previously been implicated in valvular mesenchymal compaction during murine valve development[143,48]. Additional human genetic associations between CHD and Wnt9b were identified in a recent GWAS study of CHD in a European cohort[144]. Our single cell data indicates that *Ptprb* and *Wnt9b* have greater than a 2.5x and 1.5x log-fold upregulation in *Pthlh*[+] VECs relative to *Pthlh*[-] endocardium, respectively. The presence of genetic associations of multiple murine *Pthlh*[+] VEC marker genes with CHD raises the interesting prospect that these cells may play a critical role in human valve morphogenesis and may contribute to valvular CHD pathogenesis.

## 4.3 Identifying Pthlh-positive Valvular Endocardial Cells during Human Development

To determine if this novel subpopulation of cells has any role in human valvulogenesis, we began by consulting previously published human fetal heart scRNA-seq data. We identified two independent studies that performed scRNAseq on healthy human fetal hearts across a range of developmental timepoints. In the first study, we re-processed and analyzed 146,111 cells from nine samples ranging from 90 to 122 days gestation[145]. In the second study, we re-processed 13,569 cells that were FACS-sorted for CD144, an endothelial marker, from a single 83 days gestation human fetal heart[108]. From both studies, we were able to identify a *PTHLH*[+]/*NPPC*[+] dual positive endocardial subpopulation with a transcriptional signature very similar to the one we defined in *Pthlh*[+] VECs during murine development (**Fig. 4.1 A, B**). This demonstrated the presence of a rare, *PTHLH*[+] endocardial subpopulation during human development. The timepoints represented in

these studies would correspond roughly to the end of embryonic valvulogenesis and long into the postnatal remodeling period for the murine developmental timeline[71,146]. This is consistent with prior single-cell studies of murine postnatal valvulogenesis from which we were able to identify *Pthlh*+ VECs.
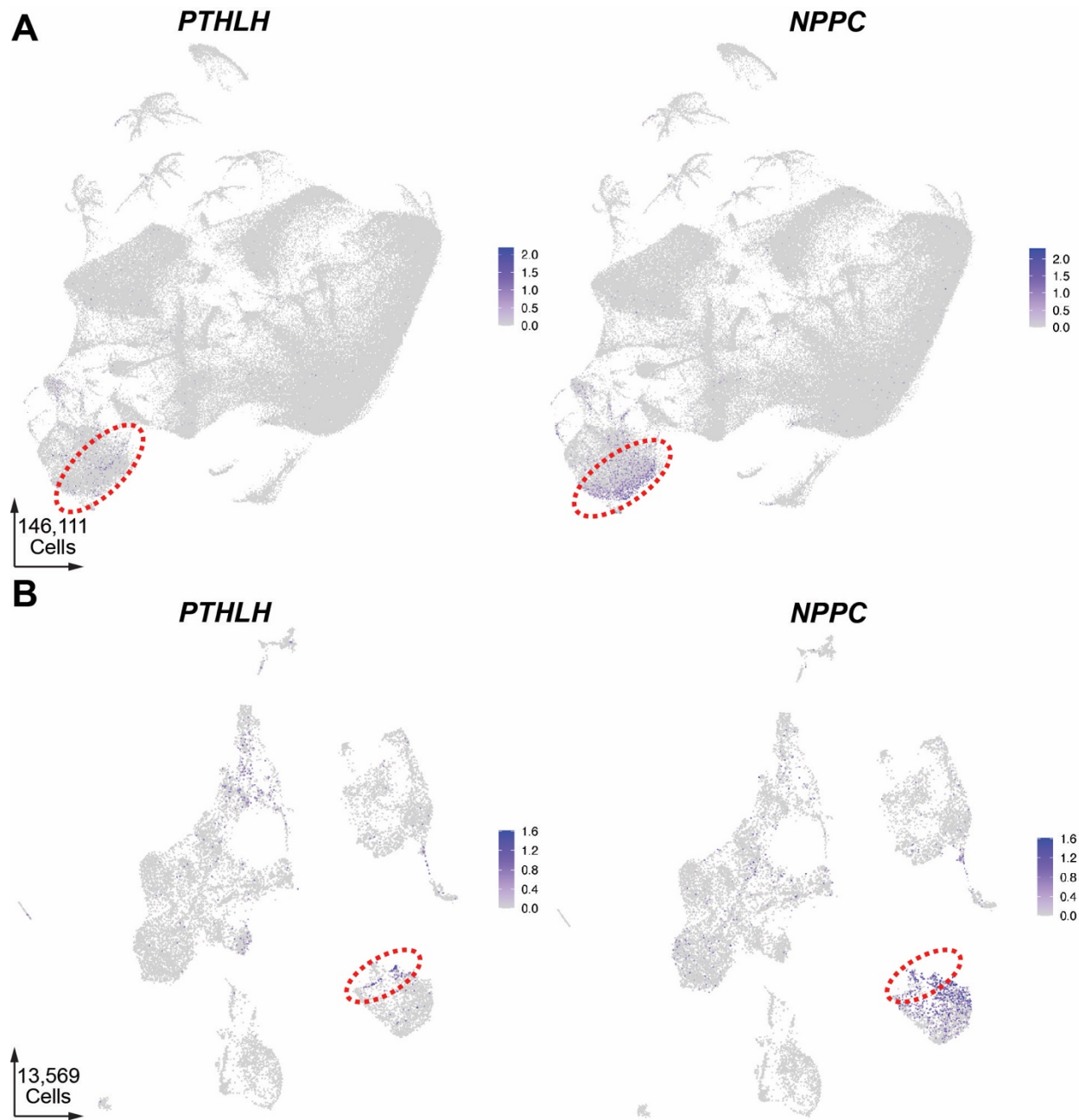
**Fig 4.1 Identification of PTHLH+ Endocardium during Human Fetal Heart Development**
**A,** UMAP plot of PTHLH and NPPC expression in endocardial cells from 9 human fetal heart samples ranging from 90 to 122 days gestation. **B,** UMAP plot of PTHLH and NPPC expression in CD144^{+} FACS-sorted endocardial cells from an 83 days gestation human fetal heart.

## 4.4 Analysis of 20-week Human Fetal Heart with Hypoplastic Left Heart Syndrome and Critical Aortic Stenosis

Given we were able to establish the presence of an analogous rare *PTHLH+* cell type in human development, we next set out to determine if this cell type had any role in the pathogenesis of human disease. As discussed briefly in Chapter 1, hypoplastic left heart syndrome (HLHS) is a severe congenital heart defect characterized by underdevelopment of left-sided heart structures including the left ventricle, aortic valve, and mitral valve. A commonly proposed hypothesis related to the pathogenesis of this syndrome, the 'no flow, no grow' hypothesis, suggests that valvular stenosis or atresia during cardiogenesis and fetal growth restricts blood flow through the developing left ventricle. The altered hemodynamics, secondary to failures in valvulogenesis, then render a hypoplastic left ventricle and downstream aorta. As a result, patients are left with a single functioning ventricle, the right ventricle, that must be surgically reconnected to systemic circulation, with venous return being re-routed to the lungs in a series of three operations. Clinically, it is common to assign subtypes of HLHS patients into three categories based on valve patency: aortic atresia/ mitral atresia (AA/MA), aortic atresia/ mitral stenosis (AA/MS), and aortic stenosis (AS/MS). These clinical subtypes have differing prevalence and clinical prognoses[147]; however, they serve to highlight how valvular morphology and the degree to valvulogenesis dysfunction can play a significant role in the pathogenesis of this highly morbid condition.

To assess the role of *PTHLH[+]* endocardial cells in the setting of disease, we performed scRNAseq on a 20 week (140 days) gestational age human fetal heart with a prenatal diagnosis of

HLHS and critical aortic stenosis via fetal echocardiography. Each of the four cardiac valves was dissected from the heart, followed by enzymatic and mechanical digestion to yield single cell suspensions (**Fig. 4.2 A**). Gem preparation was performed independently on cells from each valve to retain the critical valve-specific identity of each cell for downstream analysis. Following gem generation, library construction, pooled library sequencing, we computationally processed, quality control filtered and normalized our data to produce a 36,416 cell Seurat object containing twenty-two distinct clusters (**Fig. 4.2 B**). Clusters were annotated using previously known marker genes, and represented known valvular cell types including valve endocardium, valve mesenchyme, and resident immune cell populations. While we observed a high degree of overlap of the cells in UMAP space when displayed by valve identity, suggesting low sample-to-sample preparation variability, we did observe some clusters with valve-specific enrichment (**Fig. 4.2 C**). This could be suggestive of potential valve-specific transcriptional signatures that could be leveraged for future studies to understand valve-to-valve heterogeneity. We were successfully able to identify a *PTHLH*⁺ subset of the valvular endocardium in this sample, further validating our re-analysis of other human fetal heart scRNAseq datasets (**Fig. 4.2 D**).

To our surprise, we observed a substantial depletion in the percentage of cells expressing PTHLH in the critically stenosed aortic valve, relative to the percentage of cells expressing PTHLH in the other three non-diseased valves within the sample (**Fig. 4.2 E**). When comparing the transcriptional signature of diseased aortic valve *PTHLH*⁺ VECs against the other three valves, we observed a statistically significant downregulation of *NPPC*, an additional marker gene for this rare subpopulation. In the absence of a true healthy control, the best comparison we could make is between the two semilunar valves: the diseased aortic valve versus the healthy pulmonary valve. This *PTHLH*⁺ cell depletion in the diseased valve is an intriguing observation that may implicate

this cell type in the pathogenesis of human congenital valve disease; however, this preliminary result requires validation with additional biological replicates and proper control samples prepared in a similar fashion with preserved valvular identity information, as done in this experiment.
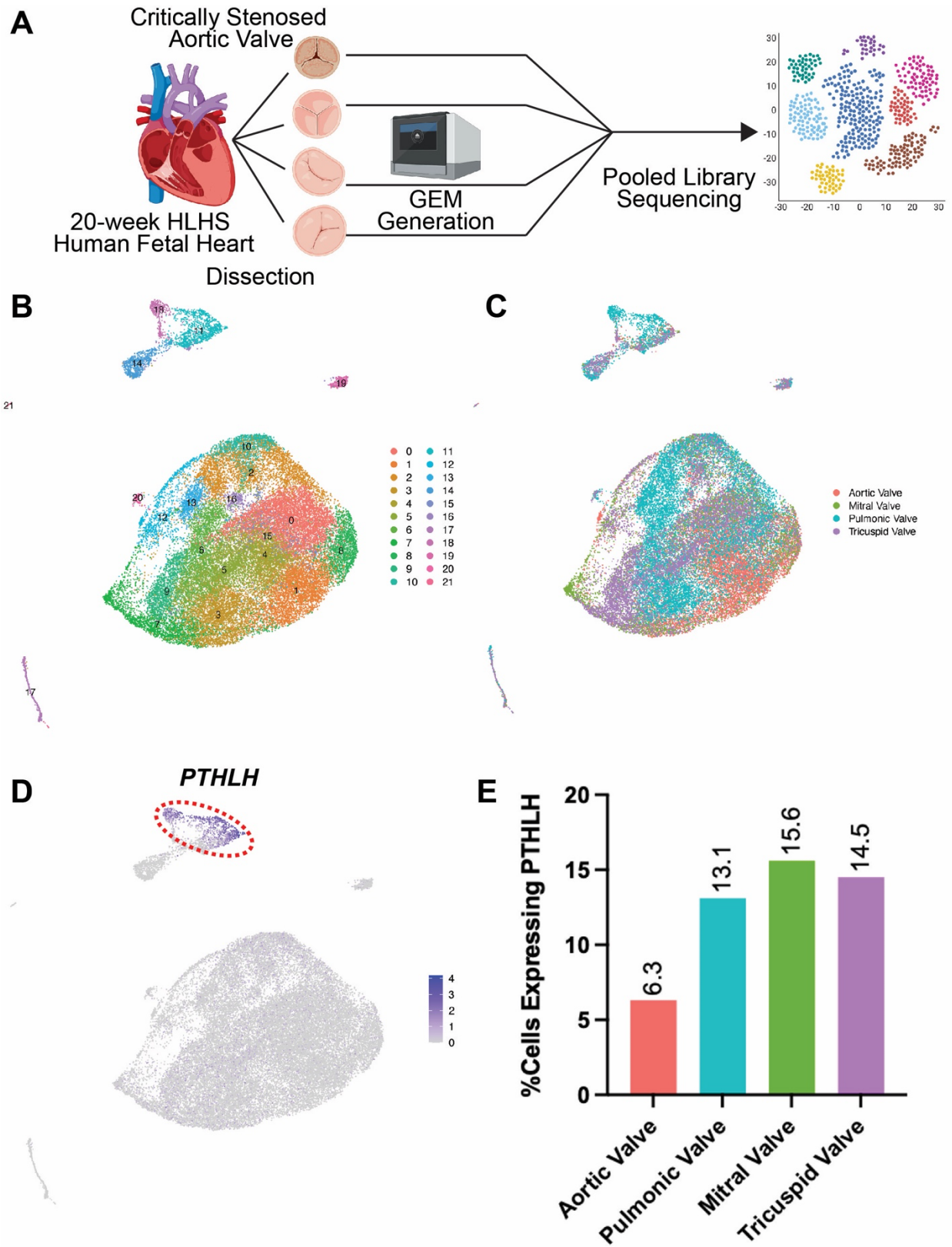
**Fig 4.2 *PTHLH*+ Valvular Endocardial Cells Depleted in Critical Stenosed Aortic Valve**

**A,** Cartoon representation of a scRNAseq experiment performed on each of the four cardiac valves from a 20-week human fetal heart with HLHS and critical aortic stenosis. **B,** UMAP plot of all captured valvular cell populations colored by cluster. **C,** UMAP plot of all captured valvular cell populations colored by cardiac valve sample identity. **D,** UMAP plot of PTHLH expression. **E,** Bar plot representing the percentage of cells in each valve expressing PTHLH.

## 4.5 Conclusions

Here, we sought to relate our findings related to $Pthlh^+$ VECs during murine development to human development and disease. Through an extensive literature review, we identified several case reports and GWAS studies linking $Pthlh^+$ VEC marker genes to human congenital heart defects. Moreover, using previously published scRNAseq data of human fetal heart development, we demonstrated that $PTHLH^+$ endocardium exists during human development. To evaluate the role of $PTHLH^+$ endocardium in the context of human disease, we generated a scRNAseq dataset from a 20-week human fetal heart with HLHS and critical aortic stenosis, preserving the identity from which each cell was derived. Our data both validated previous studies in demonstrating the presence of $PTHLH^+$ VECs during human valve development, and identified a depletion in this rare subpopulation in the diseased aortic valve relative to the other valves in the samples. Future studies in this context would necessitate more biological replicates to validate that this depletion is a feature of HLHS pathogenesis.

# Chapter 5

## Summary and Future Directions

## 5.1 Summary

In the hopes of supporting novel therapeutic development for valvular heart disease – a serious and growing health problem globally – we sought out to apply novel single cell genomic tools to better understand a poorly characterized stage of valvular development, post-EMT valvulogenesis. We began with characterization of wild-type development and, in doing so, identified previously undescribed cellular heterogeneity at the onset of this stage of development.

In our search for novel molecular regulators of post-EMT valvulogenesis, we identified two neuroendocrine peptide hormone pathways that had not been implicated in valve development. The ligand for one of these pathways, parathyroid hormone-like hormone (*Pthlh*), unexpectedly marked a rare population of cells accounting for less than 1% of the developing mouse heart at E12.5, underscoring the need for single-cell tools to make this discovery. We found that $Pthlh^+$ cells are spatially localized to the leading edge of the developing cushion at E12.5 and are further restricted to the coaptation surface of the valve leaflets at E18.5. Leveraging an atlas of wild-type cardiogenesis, we demonstrated that these cells are temporally restricted to post-EMT valvulogenesis. Transcriptionally, these cells were shown to be highly secretory marked by the expression of numerous highly-specific developmental signaling ligands. The transcriptome of this developmentally established rare cell type remains relatively stable and persists long into the postnatal remodeling period. As such, we sought to functionally characterize this cell type during development.

We established that $Pthlh^+$ valvular endocardial cells are essential for post-EMT valvulogenesis. Ablation of this population resulted in valvular dysplasia characterized by thickened, immature leaflets, and resulted in perinatal cyanosis and lethality. A combination of traditional lineage tracing approaches and re-processed previously published scRNAseq datasets

revealed that this cell type is derived from the neural crest, providing the first evidence of a neural crest-to-endocardial transition. We were then able to subsequently show that loss of *Pthlh* from the neural crest recapitulates the *Pthlh*+ valvular endocardial cells ablation phenotype, implicating a previously undescribed neuroendocrine peptide hormone signaling pathway in the regulation of post-EMT valvulogenesis.

To mechanistically dissect how neural crest-derived *Pthlh* signaling regulates post-EMT valvulogenesis, we leveraged scRNAseq and scATACseq. We identified cell autonomous loss of *Pthlh+ VEC* marker gene expression and marker peak accessibility, in addition to valvular myocardial BMP signaling dysregulation. These findings provide an important, substantive advance in our understanding have post-EMT valvulogenesis regulation and provide a number of future investigative questions that I will outline in remainder of this chapter.

Moreover, a literature review revealed that multiple marker genes for this valvular subpopulation are associated with human congenital valvulopathies. Re-processing of previously published scRNAseq human fetal heart data demonstrated that this population exists during human fetal heart development. To interrogate these cells in the setting of disease, we generated a scRNAseq dataset for each valve from a 20-week human fetal heart with HLHS and critical aortic stenosis, where we detected a depletion of this rare cell population in the diseased aortic valve with a downregulation of another marker gene. In this chapter, I will outline future avenues of investigation to carry this work forward and further uncover how these cells regulate development disease.

**5.2 Mechanistic Validation of Multi-omic profiling of neural crest-specific Pthlh signaling-deficient valves**

First, much of our analysis from the multi-omic profiling of neural crest *Pthlh*-deficient embryos centered on cell autonomous transcriptional and chromatin accessibility dysregulation. There are several experiments I propose to investigate this further. First, I discussed the prospect of *Pthlh* intracrine signaling playing a role in this dysregulation. The prospect of this *intracrine* signaling is suggested mainly due to the nuclear localization signal in the retained mid-region of the mature Pthlh peptide. Study of a novel *Pthlh* allele that lacks this nuclear localization signal *in vivo* could shed light on the requirement of intracrine signaling in the specification and maintenance of this cell type's identity. Conversely, generation of a *Pthlh* over-expression allele that could be driven in other valvular endocardium with an inducible Nfatc1CreER could demonstrate that ectopic *Pthlh* expression is capable of driving the gene programs we observed being downregulated in the setting of neural crest-specific deletion.

Second, we detected BMP signaling dysregulation in the valvular myocardium. To validate this finding, we could specifically delete *Pth1r* from the valvular myocardium using a *Tbx3CreER*, and assess for a similar pattern of BMP signaling dysregulation. Moreover, in our current perturbation model, we could perform assays for phosphorylation and nuclear localization of SMAD, the end target of BMP signaling to validate that the transcriptional changes that we have identified have a protein level consequence.

Lastly, for both of these mechanistic insights, we need to validate at a later time point. As previously mentioned, experiments are already underway to assess for transcriptional and chromatin accessibility changes at E18.5, which will help us to validate our preliminary findings at E13.5 and may provide new insights into *Pthlh*-mediated mesenchymal cell maturation.

**5.3 Investigating the role of additional Pthlh-positive Valvular Endocardial Cell Marker Genes During Murine Development**

Beyond *Pthlh*, there exist a number of potentially interesting, highly-specific genes marking this rare population. Several marker genes converge on the retinoic acid signaling pathway including *Cyp26b1*, *Crabp2*, *Rai14*, *Nr2f2*, *Rbp7*, and *Rbp1*. There exist extensive studies implicating retinoic acid-mediated regulation of cardiogenesis and valvulogenesis[148,149]. Notably, *Cyp26b1*, a gene that acts to metabolize and repress retinoic acid signaling, only exists within Pthlh+ VECs in the developing heart (data not shown). With the PthlhCreER mouse line in hand, we could perform tissue-specific deletion of a number of genes to characterize their function within this cell type and, in a greater context, valvulogenesis. Another gene that is high priority for characterization is *Ptprb*, given the recent case study identifying a likely pathogenic variant in this gene strongly associated with hypoplastic left heart syndrome.

**5.4 Exploring the role of Pthlh+ Valvular Endocardial Cells in Human Development and Disease**

While we have plenty of suggestive evidence that this population is important in human valvular development, we have yet to definitely demonstrate that this is the case. To do so would require the acquisition and single-cell interrogation of healthy and diseased human fetal heart samples. We are currently in the process of gaining access to such precious samples. In the absence of these samples, an indirect way to study this population is through histologic analysis of previously preserved samples, performing immunohistochemistry for PTHLH and other marker genes and assessing for changes in cellular metrics such as distribution and quantity.

**4.5 Exploring the role of Pthlh-positive Valvular Endocardial Cells during adult homeostasis and disease**

A preliminary analysis of the adult human heart atlas revealed that there exists a subset of *PTHLH*^{+} cells present in the adult human heart[150]. Given that *Pthlh*[+] VECs exist long into the postnatal period during mouse development, it is a natural extension of this work to investigate the role of this population in adult homeostasis and disease. Prior studies have demonstrated that genetic mechanisms leading to congenital valve disease pre-disposes the tissue to accelerated degenerative valve disease. There exist multiple models of bicuspid aortic valve disease and calcific aortic valve disease that would serve as great models to interrogate the function of this novel population during degenerative valve disease.

**4.6 Translational Directions to Overcome Congenital Heart Disease**

Lastly, the discovery of this cell type could help advance the care of patients with congenital disease in the near future. First, we have defined a transcriptional signature for a novel population of cells that we have shown to be critical to valve development. It is now possible to use this cell signature to help prioritize variants for functionalization, which has been a major bottleneck in determining new genetic etiologies of CHD. Furthermore, we have identified pathways and epigenomic regions that are dysregulated secondary to loss of *Pthlh*. These dysregulated genes and epigenomic regions could similarly function as a new lens through which to filter and prioritize functionalization of coding and noncoding variants. Through this work, we have established two new models of congenital valvulopathy that could be leveraged for pharmacologic agent screening that could aid in prevention of valvular CHD. Albeit one of the

more difficult future aims to achieve, one could consider *in vitro* experiments to differentiate *PTHLH$^+$* valvular endocardial cells and interrogate their potential therapeutic application to living tissue engineered heart valves.

# Chapter 6

## Materials and Methods

**Animal Models**

All mouse studies were carried out as stated our animal use protocol (AN189140) in accordance with all applicable ethical regulations including UCSF animal use guidelines, and the NIH Guide for the Care and Use of Laboratory Animals. The Institutional Animal Care and Use Committee granted approval for our animal use protocol. C57BL/6J wild type (JAX stock no. 000664), B6.Cg-Gt(ROSA)26Sortm6(CAG-ZsGreen1)Hze/J (Ai6) (JAX stock no. 007906), B6.Cg-Tg(Pthlh-cre/ERT2)909Nono/J (Pthlh[CreER]) (Jax stock no. 032873), B6.Cg-E2f1[Tg(Wnt1-cre)2Sor]/J (Wnt1[Cre]) (JAX stock no. 022501) mice were purchased from Jackson Laboratory (Bar Harbor, ME), Pthlh flox allele mice[1] were provided by Andrew Karaplis' lab.

**Single-cell Isolation, Library Generation, and Sequencing**

For all timed mating experiments, male and female mice were housed overnight and female mice were visually inspected for a vaginal plug in the morning. Embryos at date of plug were considered E0.5. Embryos from E12.5, E13.5, and E17.5 were prepared in the same manner. Embryos were dissected in cold PBS (Life Technologies, 14190250) with 1%FBS (ThermoFisher Scientific, 10439016). Dissected cardiac tissue was mechanically torn into several pieces with forceps prior to incubated at 37˚C in 200 µl 0.25 mg/mL Liberase (Roche, 05401020001) for 5 min, triturated with a 1000-µl pipette tip, and incubated for an additional 5 min, triturated with a 200-µl pipette tip, incubated for a final 5 min, and quenched with 600 µl PBS with 1% FBS. Cells were filtered through a 70-µm cell strainer (BD Falcon, 08-771-2), centrifuged at 150g for 3 min, and resuspended in PBS with 1% FBS. For scRNAseq, the cell suspension was prepared to recover 10K cells per sample according to the manufacturer's instructions (Chromium Single Cell 3' Reagent Kit v.3, 10X Genomics). For the 10X Genomics Gene Expression and Chromatin

Accessibility Co-Assay (scMultiome), the single-cell suspension was subjected to nuclear isolation according to the 10x nuclei isolation protocol (Nuclei Isolation for Single Cell ATAC Sequencing, CG000169, 10X Genomics). GEM generation for both assays was performed on the Chromium controller, using Chip G (PN-1000120) for scRNAseq and Chip J (PN-1000234) for scMultiome. The scRNAseq and scMultiome library preparations were performed according to the protocols described above using Chromium Single Cell 3′ Reagent Kits v3.1 (PN-1000121) and Chromium Next GEM Single Cell Multiome ATAC + Gene Expression Reagent Bundle (PN-1000283), respectively. All libraries were sequenced on the NovaSeq S4 200, in accordance with the manufacturer's protocol.

For the Wnt1$^{Cre}$;Pthlh$^{fl/fl}$ Multiome experiment, embryo tails were dissected placed in QuickExtract DNA Extraction Solution (Lucigen, QE09050) and processed according to manufacturer's protocols. Genotyping was performed by PCR using Phire Green Hot Start II DNA Polymerase (Thermo Fisher Scientific, F124L), according to manufacturer's protocols, using JAX protocol primers for Wnt1$^{Cre}$ and the following for Pthlh$^{fl}$ allele:

P1: GAGGCTAAGCCAGGAGGATT

P2: CCCCATCCTCTCTCCTCTCT

The band size for the wild type gene is 150bp and the band size for the floxed gene is ~270bp.

**Single-cell Seurat Object Preparation**

Raw sequencing data were preprocessed with the Cell Ranger v.5.0.0 pipeline for scRNAseq or Cell Ranger Arc for scMultiome (10X Genomics). Data from all samples, per experiment, was merged via cellranger-aggr or cellrangerarc-aggr and normalized to the same sequencing depth,

resulting in a single gene-barcode matrix. Further analysis was performed using Seurat v4.0 R package. Quality control metrics used to remove low quality cells were: number of genes per cells between 4,000 and 9,500, UMI count per cell between 10,000 and 100,000, and mitochondrial gene percentage between 1 and 6%. Cell cycle scores were calculated and added to the metadata for each cell and the SCTransform function was used for normalization against cell cycle score. Clustering of cells was performed with the following commands: RunPCA, RunUMAP, FindNeighbors, and FindClusters. To identify marker genes, the clusters were compared pairwise for differential gene expression using the FindAllMarkers function (min.pct = 0.45, logfc.threshold=0.4, and return.thresh (p-value cut-off) = $1 \times 10^{-10}$). Annotation of clusters was achieved via cross-referencing the resulting cluster-specific marker genes with known cell type-specific maker genes in the literature, we classified them into clusters of seven cell types. For visualization of gene expression data, the following Seurat functions were used: FeaturePlot, VlnPlot, DotPlot, and DoHeatmap.

## CellChat

Cell-cell communication analysis was performed using the R package CellChat. Seurat objects containing specific cell types and time points of interest were imported to CellChat using the function GetAssayData and createCellChat. All ligand-receptor and signaling pathways within the CellChatDB.mouse were kept for analysis. Initial pre-processing to identify over-expressed ligands and receptors was performed using the functions identifyOverExpressedGenes and identifyOverExpressedInteractions with the same settings as stated in the tutorial. Inference of cell communication was calculated with computeCommunProb and filtered by filterCommunication. Pathway level cell communication was calculated with computeCommunProbPathway and

aggregated networks were identified with aggregateNet, using standard settings. Network centrality scores were assigned with the function netAnalysis_computeCentrality. This workflow was run for both control and neural crest-specific *Pthlh*-knockout datasets independently and differential signaling analysis was then run by merging the objects with mergeCellChat. A heatmap of differential signaling, based on significantly identified pathways from above, was generated using the function netAnalysis_signalingRole_heatmap and restricting the visualization to selected pathways.

**scATACseq Data Preparation**

The Cell Ranger ARC workflow was used for all Multiome samples post sequencing (10X Genomics). Samples were first demultiplexed and fastq files were generated using the command cellranger-arc mkfastq. The command cellranger-arc count was then run to filter cell barcodes against a whitelist and align filtered fastq files to the mouse reference genome Mm10. PCR duplicates and gel bead/cell multiplets were then removed (v1.2) and transposase cut sites were counted for each sample. Unlike scRNA-seq analysis, cellranger-arc aggr was not run and instead the indexed fragments files (fragments.tsv.gz and fragments.tsv.gz.tbi) output from cellranger-atac count served as the inputs for computational analysis in ArchR[8]. Subsequent analyses were performed using ArchR v1.0.1 R package with reference to the ArchR web tutorials. For each experiment, an ArchRproject was generated through via importing the ATAC matrix and generation of an arrow file. Addition of paired transcriptional information for each cell was achieved through importing the transcriptional feature matrices per sample (import10xFeatureMatrix), altering the matrix to be compatible with ArchR (SummarizedExperiment) and appending the expression matrix onto the existing ArchRproject

(addGeneExpressionMatrix). Low quality cells were removed based on TSS enrichment score and the number of fragments per nuclei (createArrowFiles function with minTSS=7, minFrags=19952, maxFrags=1E+6), and nuclei doublets were removed through addDoubletScores and filterDoublets functions, resulting in making an ArchRproject to be analyzed. Dimensionality reduction was performed using the addIterativeLSI function. Then, clustering and the 2D embedded visualization in UMAP space were performed using the addClusters function, and the addUMAP and plotEmbedding functions, respectively. Gene body scores (GS), which were calculated by the accessibility of promoter and gene body regions of each gene and can be treated as a proxy of expression levels of a corresponding gene, were extracted to identify the cluster features using the getMarkerFeatures with useMatrix="GeneScoreMatrix". For peak calling per cluster, the addGroupCoverages and the addReproduciblePeakSet functions with peakMethod = "Macs2" were used. Peak-to-gene linkage analysis was performed in ArchR using the addPeak2GeneLinks command. Furthermore, to identify the cluster specific feature peaks, the getMarkerFeature functions with useMatrix="PeakMatrix" was used, and transcription factor binding site motif enrichment analysis on the resultant peaks was performed using HOMER[8]. For differential accessible region (DAR) analysis, peak calling was performed for each condition (CREneg or CREpos) in each cluster and differential analyses were performed using the getMarkerFeatures function by setting a cluster from CREpos as useGroups and a corresponding cluster from CREneg as bgdGroups. The statistically significant DARs were defined with FDR less than 0.05 and Log2 fold change greater than 1. Motif enrichment analyses on the detected DARs were performed using the peakAnnoEnrichment function.

**Embryo Dissection for RNAscope Assay**

Embryos used for RNAscope assay were collected through timed mating similar to methods for single cell assays. Dissected tissues were fixed overnight with 4% paraformaldehyde (50-980-487, Fisher Scientific). Tissues were subsequently washed in PBS and dehydrated in 70% EtOH overnight. Tissues were processed in paraffin overnight and sectioned onto glass slides at 5 um thickness.

**RNAscope In Situ Hybridization**

Section RNA in situ hybridization was performed in using Multiplex Fluorescent Reagent Kit v2 (Advanced Cell Diagnostics, 323100) as previously reported. Each experiment was repeated using at least three biological replicates. The *in situ* hybridization probes used in this study are as follows: Pthlh (Advanced Cell Diagnostics, 456521), Dhh (Advanced Cell Diagnostics, 415031), Wnt9b (Advanced Cell Diagnostics, 405091), Aspn (Advanced Cell Diagnostics, 502051), Ptprz1 (Advanced Cell Diagnostics, 460991), Col14a1 (Advanced Cell Diagnostics, 581941), Cthrc1 (Advanced Cell Diagnostics, 413341), Dpt (Advanced Cell Diagnostics, 561511), Sfrp2 (Advanced Cell Diagnostics, 400381), Adamts19 (Advanced Cell Diagnostics, 500981), ZsGreen (Advanced Cell Diagnostics, 461251), and Stmn2 (Advanced Cell Diagnostics, 498391). All slides were imaged on Olympus FV3000RS confocal microscope.

**Light sheet Microscopy**

For light sheet microscopy imaging, the whole mount samples were microdissected to keep the area of interest. Samples were fixed in 1% paraformaldehyde for 15 minutes at room temperature. Samples were then washed three times in PBS. Samples were incubated overnight at 37˚C in

CUBIC-L solution (TCI chemicals, T3740). After validating that the sample had adequated cleared, samples were washed three times for one hour in PBS at 37˚C. Samples were then incubated overnight in 50% PBS/ 50% Cubic R+ (M) solution (TCI chemicals, T3741). Samples were subsequently placed in 100% Cubic R+ (M) solution in a dark area until imaging. Samples were then imaged on a Zeiss Z.1 Lightsheet microscope. Images were processed with Fiji and Imaris.

# References

1. Bouma BJ, Mulder BJ. Changing landscape of congenital heart disease. *Circ Res* 2017;120:908–22.

2. Hoffman JI, Kaplan S. The incidence of congenital heart disease. J Am Coll Cardiol. 2002 Jun 19;39(12):1890-900. doi: 10.1016/s0735-1097(02)01886-7. PMID: 12084585.

3. van der Linde D, Konings EE, Slager MA, et al. Birth prevalence of congenital heart disease worldwide: a systematic review and meta-analysis. *J Am Coll Cardiol* 2011;58:2241–7.

4. Rajamannan NM, Gersh B, Bonow RO. Calcific aortic stenosis: from bench to the bedside--emerging clinical and cellular concepts. Heart. 2003 Jul;89(7):801-5. doi: 10.1136/heart.89.7.801. PMID: 12807865; PMCID: PMC1767746.

5. Liu Y, Chen S, Zuhlke L, et al. Global birth prevalence of congenital heart defects 1970-2017: updated systematic review and meta-analysis of 260 studies. *Int J Epidemiol* 2019;48:455–63.

6. Erikssen G, Liestol K, Seem E, et al. Achievements in congenital heart defect surgery: a prospective, 40-year study of 7038 patients. *Circulation* 2015;131:337–46.

7. Mandalenakis Z, Rosengren A, Skoglund K, et al. Survivorship in children and young adults with congenital heart disease in Sweden. *JAMA Intern Med* 2017;177:224–30.

8. Virani SS, Alonso A, Benjamin EJ, et al. Heart Disease and Stroke Statistics-2020 Update: A Report From the American Heart Association. Circulation. 2020 Mar 3;141(9):e139-e596. doi: 10.1161/CIR.0000000000000757. Epub 2020 Jan 29. PMID: 31992061.

9. Siffel C, Riehle-Colarusso T, Oster ME, Correa A. Survival of Children With Hypoplastic Left Heart Syndrome. Pediatrics. 2015 Oct;136(4):e864-70. doi: 10.1542/peds.2014-1427. Epub 2015 Sep 21. PMID: 26391936; PMCID: PMC4663985.

10. Bejjani AT, Wary N, Gu M. Hypoplastic left heart syndrome (HLHS): molecular pathogenesis and emerging drug targets for cardiac repair and regeneration. Expert Opin Ther Targets. 2021 Aug;25(8):621-632. doi: 10.1080/14728222.2021.1978069. Epub 2021 Sep 15. PMID: 34488532; PMCID: PMC8511342.

11. Gobergs R, Salputra E, Lubaua I. Hypoplastic left heart syndrome: a review. Acta Med Litu. 2016;23(2):86-98. doi: 10.6001/actamedica.v23i2.3325. PMID: 28356795; PMCID: PMC5088741.

12. Feinstein JA, Benson DW, Dubin AM, et al. Hypoplastic left heart syndrome: current considerations and expectations. J Am Coll Cardiol. 2012 Jan 3;59(1 Suppl):S1-42. doi: 10.1016/j.jacc.2011.09.022. Erratum in: J Am Coll Cardiol. 2012 Jan 31;59(5):544. PMID: 22192720; PMCID: PMC6110391.

13. Lloyd-Jones DM, Hong Y, Labarthe D, et al. Defining and setting national goals for cardiovascular health promotion and disease reduction: the American Heart Association's strategic Impact Goal through 2020 and beyond. Circulation. 2010 Feb 2;121(4):586-613. doi: 10.1161/CIRCULATIONAHA.109.192703. Epub 2010 Jan 20. PMID: 20089546.

14. Alsoufi B. Aortic valve replacement in children: Options and outcomes. J Saudi Heart Assoc. 2014 Jan;26(1):33-41. doi: 10.1016/j.jsha.2013.11.003. Epub 2013 Nov 13. PMID: 24578598; PMCID: PMC3936244.

15. Jover E, Fagnano M, Angelini G, Madeddu P. Cell Sources for Tissue Engineering Strategies to Treat Calcific Valve Disease. Front Cardiovasc Med. 2018 Nov 6;5:155. doi: 10.3389/fcvm.2018.00155. PMID: 30460245; PMCID: PMC6232262.

16. Zaidi S, Brueckner M. Genetics and genomics of congenital heart disease. *Circ Res* 2017;120:923–40.

17. Yasuhara J, Garg V. Genetics of congenital heart disease: a narrative review of recent advances and clinical implications. Transl Pediatr. 2021 Sep;10(9):2366-2386. doi: 10.21037/tp-21-297. PMID: 34733677; PMCID: PMC8506053.

18. Simeone RM, Devine OJ, Marcinkevage JA, et al. Diabetes and congenital heart defects: a systematic review, meta-analysis, and modeling project. Am J Prev Med. 2015 Feb;48(2):195-204. doi: 10.1016/j.amepre.2014.09.002. Epub 2014 Oct 14. PMID: 25326416; PMCID: PMC4455032.

19. Priyanka P, Vyas V, Deora S, Nag VL, Singh K. Epidemiology, etiology and clinical associations of congenital heart disease identified during congenital rubella syndrome surveillance. J Trop Pediatr. 2022 Oct 6;68(6):fmac089. doi: 10.1093/tropej/fmac089. PMID: 36306124.

20. Lee LJ, Lupo PJ. Maternal smoking during pregnancy and the risk of congenital heart defects in offspring: a systematic review and metaanalysis. Pediatr Cardiol. 2013 Feb;34(2):398-407. doi: 10.1007/s00246-012-0470-x. Epub 2012 Aug 12. PMID: 22886364.

21. Persson M, Razaz N, Edstedt Bonamy AK, et al. Maternal overweight and obesity and risk of congenital heart defects. *J Am Coll Cardiol* 2019;73:44–53.

22. Czeizel AE, Dudás I, Vereczkey A, et al. Folate deficiency and folic acid supplementation: the prevention of neural-tube defects and congenital heart defects. Nutrients. 2013 Nov 21;5(11):4760-75. doi: 10.3390/nu5114760. PMID: 24284617; PMCID: PMC3847759.

23. Khalil A, Tanos R, El-Hachem N, et al. A HAND to TBX5 Explains the Link Between Thalidomide and Cardiac Diseases. Sci Rep. 2017 May 3;7(1):1416. doi: 10.1038/s41598-017-01641-3. PMID: 28469241; PMCID: PMC5431093.

24. Yang J, Qiu H, Qu P, et al. Prenatal alcohol exposure and congenital heart defects: a meta-analysis. *PloS One*2015;10:e0130681.

25. Patorno E, Huybrechts KF, Bateman BT, et al. Lithium Use in Pregnancy and the Risk of Cardiac Malformations. N Engl J Med. 2017 Jun 8;376(23):2245-2254. doi: 10.1056/NEJMoa1612222. PMID: 28591541; PMCID: PMC5667676.

26. Priest JR, Girirajan S, Vu TH, Olson A, Eichler EE, Portman MA. Rare copy number variants in isolated sporadic and syndromic atrioventricular septal defects. Am J Med Genet A. 2012 Jun;158A(6):1279-84. doi: 10.1002/ajmg.a.35315. Epub 2012 Apr 23. PMID: 22529060; PMCID: PMC3564951.

27. Jansen FA, Hoffer MJ, van Velzen CL, Plati SK, Rijlaarsdam ME, Clur SA, Blom NA, Pajkrt E, Bhola SL, Knegt AC, de Boer MA, Haak MC. Chromosomal abnormalities and copy number variations in fetal left-sided congenital heart defects. Prenat Diagn. 2016 Feb;36(2):177-85. doi: 10.1002/pd.4767. Epub 2016 Feb 3. PMID: 26716421.

28. McDermott DA, Bressan MC, He J, et al. TBX5 genetic testing validates strict clinical criteria for Holt-Oram syndrome. Pediatr Res. 2005 Nov;58(5):981-6. doi: 10.1203/01.PDR.0000182593.95441.64. Epub 2005 Sep 23. PMID: 16183809.

29. Garg V, Kathiriya IS, Barnes R, Schluterman MK, King IN, Butler CA, Rothrock CR, Eapen RS, Hirayama-Yamada K, Joo K, Matsuoka R, Cohen JC, Srivastava D. GATA4 mutations cause human congenital heart defects and reveal an interaction with TBX5. Nature. 2003 Jul 24;424(6947):443-7. doi: 10.1038/nature01827. Epub 2003 Jul 6. PMID: 12845333.

30. Schott JJ, Benson DW, Basson CT, Pease W, Silberbach GM, Moak JP, Maron BJ, Seidman CE, Seidman JG. Congenital heart disease caused by mutations in the

transcription factor NKX2-5. Science. 1998 Jul 3;281(5373):108-11. doi: 10.1126/science.281.5373.108. PMID: 9651244.

31. Garg V, Muth AN, Ransom JF, et al. Mutations in NOTCH1 cause aortic valve disease. Nature. 2005 Sep 8;437(7056):270-4. doi: 10.1038/nature03940. Epub 2005 Jul 17. PMID: 16025100.

32. Smith KA, Joziasse IC, Chocron S, et al. Dominant-negative ALK2 allele associates with congenital heart defects. Circulation. 2009 Jun 23;119(24):3062-9. doi: 10.1161/CIRCULATIONAHA.108.843714. Epub 2009 Jun 8. PMID: 19506109.

33. Reuter MS, Jobling R, Chaturvedi RR, et al. Haploinsufficiency of vascular endothelial growth factor related signaling genes is associated with tetralogy of Fallot. Genet Med. 2019 Apr;21(4):1001-1007. doi: 10.1038/s41436-018-0260-9. Epub 2018 Sep 20. PMID: 30232381; PMCID: PMC6752294.

34. Granados-Riveron JT, Ghosh TK, Pope M, Bu'Lock F, Thornborough C, Eason J, Kirk EP, Fatkin D, Feneley MP, Harvey RP, Armour JA, David Brook J. Alpha-cardiac myosin heavy chain (MYH6) mutations affecting myofibril formation are associated with congenital heart defects. Hum Mol Genet. 2010 Oct 15;19(20):4007-16. doi: 10.1093/hmg/ddq315. Epub 2010 Jul 23. PMID: 20656787.

35. Postma AV, van Engelen K, van de Meerakker J, Rahman T, Probst S, Baars MJ, Bauer U, Pickardt T, Sperling SR, Berger F, Moorman AF, Mulder BJ, Thierfelder L, Keavney B, Goodship J, Klaassen S. Mutations in the sarcomere gene MYH7 in Ebstein anomaly. Circ Cardiovasc Genet. 2011 Feb;4(1):43-50. doi: 10.1161/CIRCGENETICS.110.957985. Epub 2010 Dec 2. PMID: 21127202.

36. McCombie WR, McPherson JD. Future Promises and Concerns of Ubiquitous Next-Generation Sequencing. Cold Spring Harb Perspect Med. 2019 Sep 3;9(9):a025783. doi: 10.1101/cshperspect.a025783. PMID: 30478095; PMCID: PMC6719590.

37. Pediatric Cardiac Genomics Consortium; Gelb B, Brueckner M, Chung W, Goldmuntz E, Kaltman J, Kaski JP, Kim R, Kline J, Mercer-Rosa L, Porter G, Roberts A, Rosenberg E, Seiden H, Seidman C, Sleeper L, Tennstedt S, Kaltman J, Schramm C, Burns K, Pearson G, Rosenberg E. The Congenital Heart Disease Genetic Network Study: rationale, design, and early results. Circ Res. 2013 Feb 15;112(4):698-706. doi: 10.1161/CIRCRESAHA.111.300297. PMID: 23410879; PMCID: PMC3679175.

38. Jin SC, Homsy J, Zaidi S, Lu Q, Morton S, DePalma SR, Zeng X, Qi H, Chang W, Sierant MC, Hung WC, Haider S, Zhang J, Knight J, Bjornson RD, Castaldi C, Tikhonoa IR, Bilguvar K, Mane SM, Sanders SJ, Mital S, Russell MW, Gaynor JW, Deanfield J, Giardini A, Porter GA Jr, Srivastava D, Lo CW, Shen Y, Watkins WS, Yandell M, Yost HJ, Tristani-Firouzi M, Newburger JW, Roberts AE, Kim R, Zhao H, Kaltman JR, Goldmuntz E, Chung WK, Seidman JG, Gelb BD, Seidman CE, Lifton RP, Brueckner M. Contribution of rare inherited and de novo variants in 2,871 congenital heart disease probands. Nat Genet. 2017 Nov;49(11):1593-1601. doi: 10.1038/ng.3970. Epub 2017 Oct 9. PMID: 28991257; PMCID: PMC5675000.

39. Srivastava D. Making or breaking the heart: from lineage determination to morphogenesis. Cell. 2006 Sep 22;126(6):1037-48. doi: 10.1016/j.cell.2006.09.003. PMID: 16990131.

40. Butcher JT, Markwald RR. Valvulogenesis: the moving target. Philos Trans R Soc Lond B Biol Sci. 2007 Aug 29;362(1484):1489-503. doi: 10.1098/rstb.2007.2130. PMID: 17569640; PMCID: PMC2440410.

41. Rosenthal N, Harvey RP, Camenisch TD, Runyan RB, Markwald RR. Chapter 6.1 Molecular Regulation of Cushion Morphogenesis. In: Heart development and regeneration. Academic; 2010. p. 363–87.

42. MacGrogan D, Luxán G, Driessen-Mol A, Bouten C, Baaijens F, de la Pompa JL. How to make a heart valve: from embryonic development to bioengineering of living valve substitutes. Cold Spring Harb Perspect Med. 2014 Nov 3;4(11):a013912. doi: 10.1101/cshperspect.a013912. PMID: 25368013; PMCID: PMC4208706.

43. Wessels A, van den Hoff MJ, Adamo RF, et al. Epicardially derived fibroblasts preferentially contribute to the parietal leaflets of the atrioventricular valves in the murine heart. Dev Biol. 2012 Jun 15;366(2):111-24. doi: 10.1016/j.ydbio.2012.04.020. Epub 2012 Apr 24. PMID: 22546693; PMCID: PMC3358438.

44. Jiang X, Rowitch DH, Soriano P, McMahon AP, Sucov HM. Fate of the mammalian cardiac neural crest. Development. 2000 Apr;127(8):1607-16. doi: 10.1242/dev.127.8.1607. PMID: 10725237.

45. Schoen FJ. Evolving concepts of cardiac valve dynamics: the continuum of development, functional structure, pathobiology, and tissue engineering. Circulation. 2008 Oct 28;118(18):1864-80. doi: 10.1161/CIRCULATIONAHA.108.805911. PMID: 18955677.

46. Hove JR, Köster RW, Forouhar AS, Acevedo-Bolton G, Fraser SE, Gharib M. Intracardiac fluid forces are an essential epigenetic factor for embryonic cardiogenesis. Nature. 2003 Jan 9;421(6919):172-7. doi: 10.1038/nature01282. PMID: 12520305.

47. Steed E, Boselli F, Vermot J. Hemodynamics driven cardiac valve morphogenesis. Biochim Biophys Acta. 2016 Jul;1863(7 Pt B):1760-6. doi: 10.1016/j.bbamcr.2015.11.014. Epub 2015 Nov 30. PMID: 26608609.

48. Goddard LM, Duchemin AL, Ramalingan H, Wu B, Chen M, Bamezai S, Yang J, Li L, Morley MP, Wang T, Scherrer-Crosbie M, Frank DB, Engleka KA, Jameson SC, Morrisey EE, Carroll TJ, Zhou B, Vermot J, Kahn ML. Hemodynamic Forces Sculpt Developing Heart Valves through a KLF2-WNT9B Paracrine Signaling Axis. Dev Cell. 2017 Nov 6;43(3):274-289.e5. doi: 10.1016/j.devcel.2017.09.023. Epub 2017 Oct 19. PMID: 29056552; PMCID: PMC5760194.

49. Fukui H, Chow RW, Xie J, Foo YY, Yap CH, Minc N, Mochizuki N, Vermot J. Bioelectric signaling and the control of cardiac cell identity in response to mechanical forces. Science. 2021 Oct 15;374(6565):351-354. doi: 10.1126/science.abc6229. Epub 2021 Oct 14. PMID: 34648325.

50. Liu AC, Joag VR, Gotlieb AI. The emerging role of valve interstitial cell phenotypes in regulating heart valve pathobiology. Am J Pathol. 2007 Nov;171(5):1407-18. doi: 10.2353/ajpath.2007.070251. Epub 2007 Sep 6. PMID: 17823281; PMCID: PMC2043503.

51. LaHaye S, Lincoln J, Garg V. Genetics of valvular heart disease. Curr Cardiol Rep. 2014;16(6):487. doi: 10.1007/s11886-014-0487-2. PMID: 24743897; PMCID: PMC4531840.

52. Ma L, Lu MF, Schwartz RJ, Martin JF. Bmp2 is essential for cardiac cushion epithelial-mesenchymal transition and myocardial patterning. Development. 2005 Dec;132(24):5601-11. doi: 10.1242/dev.02156. PMID: 16314491.

53. Camenisch TD, Spicer AP, Brehm-Gibson T, Biesterfeldt J, Augustine ML, Calabro A Jr, Kubalak S, Klewer SE, McDonald JA. Disruption of hyaluronan synthase-2 abrogates normal cardiac morphogenesis and hyaluronan-mediated transformation of epithelium to

mesenchyme. J Clin Invest. 2000 Aug;106(3):349-60. doi: 10.1172/JCI10272. PMID: 10930438; PMCID: PMC314332.

54. Liu W, Selever J, Wang D, Lu MF, Moses KA, Schwartz RJ, Martin JF. Bmp4 signaling is required for outflow-tract septation and branchial-arch artery remodeling. Proc Natl Acad Sci U S A. 2004 Mar 30;101(13):4489-94. doi: 10.1073/pnas.0308466101. Epub 2004 Mar 19. PMID: 15070745; PMCID: PMC384774.

55. Singh R, Hoogaars WM, Barnett P, Grieskamp T, Rana MS, Buermans H, Farin HF, Petry M, Heallen T, Martin JF, Moorman AF, 't Hoen PA, Kispert A, Christoffels VM. Tbx2 and Tbx3 induce atrioventricular myocardial development and endocardial cushion formation. Cell Mol Life Sci. 2012 Apr;69(8):1377-89. doi: 10.1007/s00018-011-0884-2. Epub 2011 Dec 1. PMID: 22130515; PMCID: PMC3314179.

56. Wang J, Sridurongrit S, Dudas M, Thomas P, Nagy A, Schneider MD, Epstein JA, Kaartinen V. Atrioventricular cushion transformation is mediated by ALK2 in the developing mouse heart. Dev Biol. 2005 Oct 1;286(1):299-310. doi: 10.1016/j.ydbio.2005.07.035. PMID: 16140292; PMCID: PMC1361261.

57. Gaussin V, Morley GE, Cox L, Zwijsen A, Vance KM, Emile L, Tian Y, Liu J, Hong C, Myers D, Conway SJ, Depre C, Mishina Y, Behringer RR, Hanks MC, Schneider MD, Huylebroeck D, Fishman GI, Burch JB, Vatner SF. Alk3/Bmpr1a receptor is required for development of the atrioventricular canal into valves and annulus fibrosus. Circ Res. 2005 Aug 5;97(3):219-26. doi: 10.1161/01.RES.0000177862.85474.63. Epub 2005 Jul 21. PMID: 16037571; PMCID: PMC2950023.

58. Sridurongrit S, Larsson J, Schwartz R, Ruiz-Lozano P, Kaartinen V. Signaling via the Tgf-beta type I receptor Alk5 in heart development. Dev Biol. 2008 Oct 1;322(1):208-18. doi:

10.1016/j.ydbio.2008.07.038. Epub 2008 Aug 7. PMID: 18718461; PMCID: PMC2677203.

59. Nakajima Y, Yamagishi T, Hokari S, Nakamura H. Mechanisms involved in valvuloseptal endocardial cushion formation in early cardiogenesis: roles of transforming growth factor (TGF)-beta and bone morphogenetic protein (BMP). Anat Rec. 2000 Feb 1;258(2):119-27. doi: 10.1002/(SICI)1097-0185(20000201)258:2<119::AID-AR1>3.0.CO;2-U. PMID: 10645959.

60. Zhang H, von Gise A, Liu Q, Hu T, Tian X, He L, Pu W, Huang X, He L, Cai CL, Camargo FD, Pu WT, Zhou B. Yap1 is required for endothelial to mesenchymal transition of the atrioventricular cushion. J Biol Chem. 2014 Jul 4;289(27):18681-92. doi: 10.1074/jbc.M114.554584. Epub 2014 May 15. PMID: 24831012; PMCID: PMC4081914.

61. Dickson MC, Slager HG, Duffie E, Mummery CL, Akhurst RJ. RNA and protein localisations of TGF beta 2 in the early mouse embryo suggest an involvement in cardiac development. Development. 1993 Feb;117(2):625-39. doi: 10.1242/dev.117.2.625. PMID: 7687212.

62. Jiao K, Langworthy M, Batts L, Brown CB, Moses HL, Baldwin HS. Tgfbeta signaling is required for atrioventricular cushion mesenchyme remodeling during in vivo cardiac development. Development. 2006 Nov;133(22):4585-93. doi: 10.1242/dev.02597. Epub 2006 Oct 18. PMID: 17050629.

63. Moskowitz IP, Wang J, Peterson MA, Pu WT, Mackinnon AC, Oxburgh L, Chu GC, Sarkar M, Berul C, Smoot L, Robertson EJ, Schwartz R, Seidman JG, Seidman CE. Transcription factor genes Smad4 and Gata4 cooperatively regulate cardiac valve development. [corrected]. Proc Natl Acad Sci U S A. 2011 Mar 8;108(10):4006-11. doi:

10.1073/pnas.1019025108. Epub 2011 Feb 17. Erratum in: Proc Natl Acad Sci U S A. 2011 Apr 5;108(14):5921. PMID: 21330551; PMCID: PMC3053967.

64. Timmerman LA, Grego-Bessa J, Raya A, Bertrán E, Pérez-Pomares JM, Díez J, Aranda S, Palomo S, McCormick F, Izpisúa-Belmonte JC, de la Pompa JL. Notch promotes epithelial-mesenchymal transition during cardiac development and oncogenic transformation. Genes Dev. 2004 Jan 1;18(1):99-115. doi: 10.1101/gad.276304. Epub 2003 Dec 30. PMID: 14701881; PMCID: PMC314285.

65. Dor Y, Camenisch TD, Itin A, Fishman GI, McDonald JA, Carmeliet P, Keshet E. A novel role for VEGF in endocardial cushion formation and its potential contribution to congenital heart defects. Development. 2001 May;128(9):1531-8. doi: 10.1242/dev.128.9.1531. PMID: 11290292.

66. Johnson EN, Lee YM, Sander TL, Rabkin E, Schoen FJ, Kaushal S, Bischoff J. NFATc1 mediates vascular endothelial growth factor-induced proliferation of human pulmonary valve endothelial cells. J Biol Chem. 2003 Jan 17;278(3):1686-92. doi: 10.1074/jbc.M210250200. Epub 2002 Nov 9. PMID: 12427739; PMCID: PMC2813494.

67. Wu B, Wang Y, Lui W, Langworthy M, Tompkins KL, Hatzopoulos AK, Baldwin HS, Zhou B. Nfatc1 coordinates valve endocardial cell lineage development required for heart valve formation. Circ Res. 2011 Jul 8;109(2):183-92. doi: 10.1161/CIRCRESAHA.111.245035. Epub 2011 May 19. PMID: 21597012; PMCID: PMC3132827.

68. Stankunas K, Ma GK, Kuhnert FJ, Kuo CJ, Chang CP. VEGF signaling has distinct spatiotemporal roles during heart valve development. Dev Biol. 2010 Nov 15;347(2):325-

36. doi: 10.1016/j.ydbio.2010.08.030. Epub 2010 Sep 15. PMID: 20816797; PMCID: PMC2958084.

69. Saxon JG, Baer DR, Barton JA, Hawkins T, Wu B, Trusk TC, Harris SE, Zhou B, Mishina Y, Sugi Y. BMP2 expression in the endocardial lineage is required for AV endocardial cushion maturation and remodeling. Dev Biol. 2017 Oct 1;430(1):113-128. doi: 10.1016/j.ydbio.2017.08.008. Epub 2017 Aug 6. PMID: 28790014; PMCID: PMC5948002.

70. Nakamura T, Colbert MC, Robbins J. Neural crest cells retain multipotential characteristics in the developing valves and label the cardiac conduction system. Circ Res. 2006 Jun 23;98(12):1547-54. doi: 10.1161/01.RES.0000227505.19472.69. Epub 2006 May 18. PMID: 16709902.

71. de Lange FJ, Moorman AF, Anderson RH, Männer J, Soufan AT, de Gier-de Vries C, Schneider MD, Webb S, van den Hoff MJ, Christoffels VM. Lineage and morphogenetic analysis of the cardiac valves. Circ Res. 2004 Sep 17;95(6):645-54. doi: 10.1161/01.RES.0000141429.13560.cb. Epub 2004 Aug 5. PMID: 15297379.

72. Trapnell C. Defining cell types and states with single-cell genomics. Genome Res. 2015 Oct;25(10):1491-8. doi: 10.1101/gr.190595.115. PMID: 26430159; PMCID: PMC4579334.

73. Buenrostro JD, Wu B, Litzenburger UM, Ruff D, Gonzales ML, Snyder MP, Chang HY, Greenleaf WJ. Single-cell chromatin accessibility reveals principles of regulatory variation. Nature. 2015 Jul 23;523(7561):486-90. doi: 10.1038/nature14590. Epub 2015 Jun 17. PMID: 26083756; PMCID: PMC4685948.

74. Stickels RR, Murray E, Kumar P, Li J, Marshall JL, Di Bella DJ, Arlotta P, Macosko EZ, Chen F. Highly sensitive spatial transcriptomics at near-cellular resolution with Slide-seqV2. Nat Biotechnol. 2021 Mar;39(3):313-319. doi: 10.1038/s41587-020-0739-1. Epub 2020 Dec 7. PMID: 33288904; PMCID: PMC8606189.

75. Camp JG, Platt R, Treutlein B. Mapping human cell phenotypes to genotypes with single-cell genomics. Science. 2019 Sep 27;365(6460):1401-1405. doi: 10.1126/science.aax6648. PMID: 31604266.

76. Wagner DE, Klein AM. Lineage tracing meets single-cell omics: opportunities and challenges. Nat Rev Genet. 2020 Jul;21(7):410-427. doi: 10.1038/s41576-020-0223-2. Epub 2020 Mar 31. PMID: 32235876; PMCID: PMC7307462.

77. Montoro DT, Haber AL, Biton M, Vinarsky V, Lin B, Birket SE, Yuan F, Chen S, Leung HM, Villoria J, Rogel N, Burgin G, Tsankov AM, Waghray A, Slyper M, Waldman J, Nguyen L, Dionne D, Rozenblatt-Rosen O, Tata PR, Mou H, Shivaraju M, Bihler H, Mense M, Tearney GJ, Rowe SM, Engelhardt JF, Regev A, Rajagopal J. A revised airway epithelial hierarchy includes CFTR-expressing ionocytes. Nature. 2018 Aug;560(7718):319-324. doi: 10.1038/s41586-018-0393-7. Epub 2018 Aug 1. PMID: 30069044; PMCID: PMC6295155.

78. Li J, Pan C, Zhang S, Spin JM, Deng A, Leung LLK, Dalman RL, Tsao PS, Snyder M. Decoding the Genomics of Abdominal Aortic Aneurysm. Cell. 2018 Sep 6;174(6):1361-1372.e10. doi: 10.1016/j.cell.2018.07.021. PMID: 30193110.

79. Plasschaert LW, Žilionis R, Choo-Wing R, Savova V, Knehr J, Roma G, Klein AM, Jaffe AB. A single-cell atlas of the airway epithelium reveals the CFTR-rich pulmonary

ionocyte. Nature. 2018 Aug;560(7718):377-381. doi: 10.1038/s41586-018-0394-6. Epub 2018 Aug 1. PMID: 30069046; PMCID: PMC6108322.

80. Wagner DE, Weinreb C, Collins ZM, Briggs JA, Megason SG, Klein AM. Single-cell mapping of gene expression landscapes and lineage in the zebrafish embryo. Science. 2018 Jun 1;360(6392):981-987. doi: 10.1126/science.aar4362. Epub 2018 Apr 26. PMID: 29700229; PMCID: PMC6083445.

81. Tian Y, Li Q, Yang Z, Zhang S, Xu J, Wang Z, Bai H, Duan J, Zheng B, Li W, Cui Y, Wang X, Wan R, Fei K, Zhong J, Gao S, He J, Gay CM, Zhang J, Wang J, Tang F. Single-cell transcriptomic profiling reveals the tumor heterogeneity of small-cell lung cancer. Signal Transduct Target Ther. 2022 Oct 5;7(1):346. doi: 10.1038/s41392-022-01150-4. PMID: 36195615; PMCID: PMC9532437.

82. González-Silva L, Quevedo L, Varela I. Tumor Functional Heterogeneity Unraveled by scRNA-seq Technologies. Trends Cancer. 2020 Jan;6(1):13-19. doi: 10.1016/j.trecan.2019.11.010. Epub 2020 Jan 3. Erratum in: Trends Cancer. 2021 Mar;7(3):265. PMID: 31952776.

83. Perez RK, Gordon MG, Subramaniam M, Kim MC, Hartoularos GC, Targ S, Sun Y, Ogorodnikov A, Bueno R, Lu A, Thompson M, Rappoport N, Dahl A, Lanata CM, Matloubian M, Maliskova L, Kwek SS, Li T, Slyper M, Waldman J, Dionne D, Rozenblatt-Rosen O, Fong L, Dall'Era M, Balliu B, Regev A, Yazdany J, Criswell LA, Zaitlen N, Ye CJ. Single-cell RNA-seq reveals cell type-specific molecular and genetic associations to lupus. Science. 2022 Apr 8;376(6589):eabf1970. doi: 10.1126/science.abf1970. Epub 2022 Apr 8. PMID: 35389781; PMCID: PMC9297655.

84. Ziffra RS, Kim CN, Ross JM, Wilfert A, Turner TN, Haeussler M, Casella AM, Przytycki PF, Keough KC, Shin D, Bogdanoff D, Kreimer A, Pollard KS, Ament SA, Eichler EE, Ahituv N, Nowakowski TJ. Single-cell epigenomics reveals mechanisms of human cortical development. Nature. 2021 Oct;598(7879):205-213. doi: 10.1038/s41586-021-03209-8. Epub 2021 Oct 6. PMID: 34616060; PMCID: PMC8494642.

85. Hao Y, Hao S, Andersen-Nissen E, Mauck WM 3rd, Zheng S, Butler A, Lee MJ, Wilk AJ, Darby C, Zager M, Hoffman P, Stoeckius M, Papalexi E, Mimitou EP, Jain J, Srivastava A, Stuart T, Fleming LM, Yeung B, Rogers AJ, McElrath JM, Blish CA, Gottardo R, Smibert P, Satija R. Integrated analysis of multimodal single-cell data. Cell. 2021 Jun 24;184(13):3573-3587.e29. doi: 10.1016/j.cell.2021.04.048. Epub 2021 May 31. PMID: 34062119; PMCID: PMC8238499.

86. Granja, J. M. *et al.* ArchR is a scalable software package for integrative single-cell chromatin accessibility analysis. *Nat Genet* **53**, 403-411, doi:10.1038/s41588-021-00790-6 (2021).

87. Hulin A, Hortells L, Gomez-Stallons MV, O'Donnell A, Chetal K, Adam M, Lancellotti P, Oury C, Potter SS, Salomonis N, Yutzey KE. Maturation of heart valve cell populations during postnatal remodeling. Development. 2019 Mar 12;146(12):dev173047. doi: 10.1242/dev.173047. PMID: 30796046; PMCID: PMC6602342.

88. O'Donnell A, Yutzey KE. Mechanisms of heart valve development and disease. Development. 2020 Jul 3;147(13):dev183020. doi: 10.1242/dev.183020. PMID: 32620577; PMCID: PMC7338271.

89. Dye B, Lincoln J. The Endocardium and Heart Valves. Cold Spring Harb Perspect Biol. 2020 Dec 1;12(12):a036723. doi: 10.1101/cshperspect.a036723. PMID: 31988139; PMCID: PMC7382980.

90. de la Pompa JL, Timmerman LA, Takimoto H, Yoshida H, Elia AJ, Samper E, Potter J, Wakeham A, Marengere L, Langille BL, Crabtree GR, Mak TW. Role of the NF-ATc transcription factor in morphogenesis of cardiac valves and septum. Nature. 1998 Mar 12;392(6672):182-6. doi: 10.1038/32419. PMID: 9515963.

91. Alfieri CM, Cheek J, Chakraborty S, Yutzey KE. Wnt signaling in heart valve development and osteogenic gene induction. Dev Biol. 2010 Feb 15;338(2):127-35. doi: 10.1016/j.ydbio.2009.11.030. Epub 2009 Dec 1. PMID: 19961844; PMCID: PMC2814915.

92. Akiyama H, Chaboissier MC, Behringer RR, Rowitch DH, Schedl A, Epstein JA, de Crombrugghe B. Essential role of Sox9 in the pathway that controls formation of cardiac valves and septa. Proc Natl Acad Sci U S A. 2004 Apr 27;101(17):6502-7. doi: 10.1073/pnas.0401711101. Epub 2004 Apr 19. PMID: 15096597; PMCID: PMC404074.

93. Chakraborty S, Wirrig EE, Hinton RB, Merrill WH, Spicer DB, Yutzey KE. Twist1 promotes heart valve cell proliferation and extracellular matrix gene expression during development in vivo and is expressed in human diseased aortic valves. Dev Biol. 2010 Nov 1;347(1):167-79. doi: 10.1016/j.ydbio.2010.08.021. Epub 2010 Sep 6. PMID: 20804746; PMCID: PMC2950232.

94. Cambier L, Plate M, Sucov HM, Pashmforoush M. Nkx2-5 regulates cardiac growth through modulation of Wnt signaling by R-spondin3. Development. 2014

Aug;141(15):2959-71. doi: 10.1242/dev.103416. PMID: 25053429; PMCID: PMC4197672.

95. Jin, S. *et al.* Inference and analysis of cell-cell communication using CellChat. *Nat Commun* **12**, 1088, doi:10.1038/s41467-021-21246-9 (2021).

96. Martin TJ, Sims NA, Seeman E. Physiological and Pharmacological Roles of PTH and PTHrP in Bone Using Their Shared Receptor, PTH1R. Endocr Rev. 2021 Jul 16;42(4):383-406. doi: 10.1210/endrev/bnab005. PMID: 33564837.

97. Fischer JP, Els-Heindl S, Beck-Sickinger AG. Adrenomedullin - Current perspective on a peptide hormone with significant therapeutic potential. Peptides. 2020 Sep;131:170347. doi: 10.1016/j.peptides.2020.170347. Epub 2020 Jun 20. PMID: 32569606.

98. Hens JR, Dann P, Zhang JP, Harris S, Robinson GW, Wysolmerski J. BMP4 and PTHrP interact to stimulate ductal outgrowth during embryonic mammary development and to inhibit hair follicle induction. Development. 2007 Mar;134(6):1221-30. doi: 10.1242/dev.000182. Epub 2007 Feb 14. PMID: 17301089.

99. Hiremath M, Wysolmerski J. Parathyroid hormone-related protein specifies the mammary mesenchyme and regulates embryonic mammary development. J Mammary Gland Biol Neoplasia. 2013 Jun;18(2):171-7. doi: 10.1007/s10911-013-9283-7. Epub 2013 May 3. PMID: 23640717; PMCID: PMC3696739.

100. Chen YH, Ishii M, Sucov HM, Maxson RE Jr. Msx1 and Msx2 are required for endothelial-mesenchymal transformation of the atrioventricular cushions and patterning of the atrioventricular myocardium. BMC Dev Biol. 2008 Jul 30;8:75. doi: 10.1186/1471-213X-8-75. PMID: 18667074; PMCID: PMC2518925.

101. Schipani E, Provot S. PTHrP, PTH, and the PTH/PTHrP receptor in endochondral bone development. Birth Defects Res C Embryo Today. 2003 Nov;69(4):352-62. doi: 10.1002/bdrc.10028. PMID: 14745975.

102. Minina E, Kreschel C, Naski MC, Ornitz DM, Vortkamp A. Interaction of FGF, Ihh/Pthlh, and BMP signaling integrates chondrocyte proliferation and hypertrophic differentiation. Dev Cell. 2002 Sep;3(3):439-49. doi: 10.1016/s1534-5807(02)00261-7. PMID: 12361605.

103. Wuelling M, Kaiser FJ, Buelens LA, Braunholz D, Shivdasani RA, Depping R, Vortkamp A. Trps1, a regulator of chondrocyte proliferation and differentiation, interacts with the activator form of Gli3. Dev Biol. 2009 Apr 1;328(1):40-53. doi: 10.1016/j.ydbio.2009.01.012. Epub 2009 Jan 14. PMID: 19389374.

104. Karaplis AC, Luz A, Glowacki J, Bronson RT, Tybulewicz VL, Kronenberg HM, Mulligan RC. Lethal skeletal dysplasia from targeted disruption of the parathyroid hormone-related peptide gene. Genes Dev. 1994 Feb 1;8(3):277-89. doi: 10.1101/gad.8.3.277. PMID: 8314082.

105. Mizuhashi K, Ono W, Matsushita Y, Sakagami N, Takahashi A, Saunders TL, Nagasawa T, Kronenberg HM, Ono N. Resting zone of the growth plate houses a unique class of skeletal stem cells. Nature. 2018 Nov;563(7730):254-258. doi: 10.1038/s41586-018-0662-5. Epub 2018 Oct 31. PMID: 30401834; PMCID: PMC6251707.

106. Hallett SA, Matsushita Y, Ono W, Sakagami N, Mizuhashi K, Tokavanich N, Nagata M, Zhou A, Hirai T, Kronenberg HM, Ono N. Chondrocytes in the resting zone of the growth plate are maintained in a Wnt-inhibitory environment. Elife. 2021 Jul 26;10:e64513. doi: 10.7554/eLife.64513. PMID: 34309509; PMCID: PMC8313235.

107. Qian J, Colbert MC, Witte D, Kuan CY, Gruenstein E, Osinska H, Lanske B, Kronenberg HM, Clemens TL. Midgestational lethality in mice lacking the parathyroid hormone (PTH)/PTH-related peptide receptor is associated with abrupt cardiomyocyte death. Endocrinology. 2003 Mar;144(3):1053-61. doi: 10.1210/en.2002-220993. PMID: 12586782.

108. Miao Y, Tian L, Martin M, Paige SL, Galdos FX, Li J, Klein A, Zhang H, Ma N, Wei Y, Stewart M, Lee S, Moonen JR, Zhang B, Grossfeld P, Mital S, Chitayat D, Wu JC, Rabinovitch M, Nelson TJ, Nie S, Wu SM, Gu M. Intrinsic Endocardial Defects Contribute to Hypoplastic Left Heart Syndrome. Cell Stem Cell. 2020 Oct 1;27(4):574-589.e8. doi: 10.1016/j.stem.2020.07.015. Epub 2020 Aug 17. PMID: 32810435; PMCID: PMC7541479.

109. de Soysa, T. Y. *et al.* Single-cell analysis of cardiogenesis reveals basis for organ-level developmental defects. *Nature* **572**, 120-124, doi:10.1038/s41586-019-1414-x (2019).

110. Ranade SS, Whalen S, Zlatanova I, Nishino T, van Soldt B, Ye L, et al. Single cell epigenetics reveal cell-cell communication networks in normal and abnormal cardiac morphogenesis. Biorxiv. 2022

111. Schachterle W, Rojas A, Xu SM, Black BL. ETS-dependent regulation of a distal Gata4 cardiac enhancer. Dev Biol. 2012 Jan 15;361(2):439-49. doi: 10.1016/j.ydbio.2011.10.023. Epub 2011 Oct 26. PMID: 22056786; PMCID: PMC3246565.

112. Hua LL, Vedantham V, Barnes RM, Hu J, Robinson AS, Bressan M, Srivastava D, Black BL. Specification of the mouse cardiac conduction system in the absence of Endothelin signaling. Dev Biol. 2014 Sep 15;393(2):245-254. doi: 10.1016/j.ydbio.2014.07.008. Epub 2014 Jul 19. PMID: 25050930; PMCID: PMC4143461.

113. Wang F, Flanagan J, Su N, Wang LC, Bui S, Nielson A, Wu X, Vo HT, Ma XJ, Luo Y. RNAscope: a novel in situ RNA analysis platform for formalin-fixed, paraffin-embedded tissues. J Mol Diagn. 2012 Jan;14(1):22-9. doi: 10.1016/j.jmoldx.2011.08.002. PMID: 22166544; PMCID: PMC3338343.

114. Jiang L, Yin M, Wei X, Liu J, Wang X, Niu C, Kang X, Xu J, Zhou Z, Sun S, Wang X, Zheng X, Duan S, Yao K, Qian R, Sun N, Chen A, Wang R, Zhang J, Chen S, Meng D. Bach1 Represses Wnt/β-Catenin Signaling and Angiogenesis. Circ Res. 2015 Jul 31;117(4):364-375. doi: 10.1161/CIRCRESAHA.115.306829. Epub 2015 Jun 29. Erratum in: Circ Res. 2015 Oct 9;117(9):e79. PMID: 26123998; PMCID: PMC4676728.

115. Chakraborty S, Cheek J, Sakthivel B, Aronow BJ, Yutzey KE. Shared gene expression profiles in developing heart valves and osteoblast progenitor cells. Physiol Genomics. 2008 Sep 17;35(1):75-85. doi: 10.1152/physiolgenomics.90212.2008. Epub 2008 Jul 8. PMID: 18612084; PMCID: PMC2536828.

116. Voehringer D, Liang HE, Locksley RM. Homeostasis and effector function of lymphopenia-induced "memory-like" T cells in constitutively T cell-depleted mice. J Immunol. 2008 Apr 1;180(7):4742-53. doi: 10.4049/jimmunol.180.7.4742. PMID: 18354198; PMCID: PMC2670614.

117. Lesciotto KM, Motch Perrine SM, Kawasaki M, Stecko T, Ryan TM, Kawasaki K, Richtsmeier JT. Phosphotungstic acid-enhanced microCT: Optimized protocols for embryonic and early postnatal mice. Dev Dyn. 2020 Apr;249(4):573-585. doi: 10.1002/dvdy.136. Epub 2019 Nov 28. PMID: 31736206; PMCID: PMC7125040.

118. Madisen L, Zwingman TA, Sunkin SM, Oh SW, Zariwala HA, Gu H, Ng LL, Palmiter RD, Hawrylycz MJ, Jones AR, Lein ES, Zeng H. A robust and high-throughput Cre reporting

and characterization system for the whole mouse brain. Nat Neurosci. 2010 Jan;13(1):133-40. doi: 10.1038/nn.2467. Epub 2009 Dec 20. PMID: 20023653; PMCID: PMC2840225.

119. Krus KL, Strickland A, Yamada Y, Devault L, Schmidt RE, Bloom AJ, Milbrandt J, DiAntonio A. Loss of Stathmin-2, a hallmark of TDP-43-associated ALS, causes motor neuropathy. Cell Rep. 2022 Jun 28;39(13):111001. doi: 10.1016/j.celrep.2022.111001. PMID: 35767949; PMCID: PMC9327139.

120. Vincent JP, Mazella J, Kitabgi P. Neurotensin and neurotensin receptors. Trends Pharmacol Sci. 1999 Jul;20(7):302-9. doi: 10.1016/s0165-6147(99)01357-7. PMID: 10390649.

121. Fujisawa M, Kanai Y, Nam SY, Maeda S, Nakamuta N, Kano K, Kurohmaru M, Hayashi Y. Expression of Prnp mRNA (prion protein gene) in mouse spermatogenic cells. J Reprod Dev. 2004 Oct;50(5):565-70. doi: 10.1262/jrd.50.565. PMID: 15514463.

122. Klim JR, Williams LA, Limone F, Guerra San Juan I, Davis-Dusenbery BN, Mordes DA, Burberry A, Steinbaugh MJ, Gamage KK, Kirchner R, Moccia R, Cassel SH, Chen K, Wainger BJ, Woolf CJ, Eggan K. ALS-implicated protein TDP-43 sustains levels of STMN2, a mediator of motor neuron growth and repair. Nat Neurosci. 2019 Feb;22(2):167-179. doi: 10.1038/s41593-018-0300-4. Epub 2019 Jan 14. PMID: 30643292; PMCID: PMC7153761.

123. Chiellini C, Grenningloh G, Cochet O, Scheideler M, Trajanoski Z, Ailhaud G, Dani C, Amri EZ. Stathmin-like 2, a developmentally-associated neuronal marker, is expressed and modulated during osteogenesis of human mesenchymal stem cells. Biochem Biophys Res Commun. 2008 Sep 12;374(1):64-8. doi: 10.1016/j.bbrc.2008.06.121. Epub 2008 Jul 9. PMID: 18611392.

124. Bahn S, Mimmack M, Ryan M, Caldwell MA, Jauniaux E, Starkey M, Svendsen CN, Emson P. Neuronal target genes of the neuron-restrictive silencer factor in neurospheres derived from fetuses with Down's syndrome: a gene expression study. Lancet. 2002 Jan 26;359(9303):310-5. doi: 10.1016/S0140-6736(02)07497-4. PMID: 11830198.

125. Rehman Y, Wazir HD, Akbar A, Khan AM, Hussain I, Afridi A, Gul H, Sadia H. Congenital Heart Disease and Its Association in Children With Down Syndrome. Cureus. 2022 Sep 14;14(9):e29176. doi: 10.7759/cureus.29176. PMID: 36258963; PMCID: PMC9568679.

126. Lewis AE, Vasudevan HN, O'Neill AK, Soriano P, Bush JO. The widely used Wnt1-Cre transgene causes developmental phenotypes by ectopic activation of Wnt signaling. Dev Biol. 2013 Jul 15;379(2):229-34. doi: 10.1016/j.ydbio.2013.04.026. Epub 2013 May 3. PMID: 23648512; PMCID: PMC3804302.

127. Sörensen I, Adams RH, Gossler A. DLL1-mediated Notch activation regulates endothelial identity in mouse fetal arteries. Blood. 2009 May 28;113(22):5680-8. doi: 10.1182/blood-2008-08-174508. Epub 2009 Jan 14. PMID: 19144989.

128. Danielian PS, Muccino D, Rowitch DH, Michael SK, McMahon AP. Modification of gene activity in mouse embryos in utero by a tamoxifen-inducible form of Cre recombinase. Curr Biol. 1998 Dec 3;8(24):1323-6. doi: 10.1016/s0960-9822(07)00562-3. PMID: 9843687.

129. Chen W, Liu X, Li W, Shen H, Zeng Z, Yin K, Priest JR, Zhou Z. Single-cell transcriptomic landscape of cardiac neural crest cell derivatives during development. EMBO Rep. 2021 Nov 4;22(11):e52389. doi: 10.15252/embr.202152389. Epub 2021 Sep 27. PMID: 34569705; PMCID: PMC8567227.

130. De Bono, C., Liu, Y., Ferrena, A. *et al.* Single-cell transcriptomics uncovers a non-autonomous *Tbx1*-dependent genetic program controlling cardiac neural crest cell development. *Nat Commun* **14**, 1551 (2023). https://doi.org/10.1038/s41467-023-37015-9

131. He B, Deckelbaum RA, Miao D, Lipman ML, Pollak M, Goltzman D, Karaplis AC. Tissue-specific targeting of the pthrp gene: the generation of mice with floxed alleles. Endocrinology. 2001 May;142(5):2070-7. doi: 10.1210/endo.142.5.8146. PMID: 11316774.

132. Li G, Margueron R, Ku M, Chambon P, Bernstein BE, Reinberg D. Jarid2 and PRC2, partners in regulating gene expression. Genes Dev. 2010 Feb 15;24(4):368-80. doi: 10.1101/gad.1886410. Epub 2010 Feb 1. PMID: 20123894; PMCID: PMC2816736.

133. Li AH, Hanchard NA, Furthner D, Fernbach S, Azamian M, Nicosia A, Rosenfeld J, Muzny D, D'Alessandro LCA, Morris S, Jhangiani S, Parekh DR, Franklin WJ, Lewin M, Towbin JA, Penny DJ, Fraser CD, Martin JF, Eng C, Lupski JR, Gibbs RA, Boerwinkle E, Belmont JW. Whole exome sequencing in 342 congenital cardiac left sided lesion cases reveals extensive genetic heterogeneity and complex inheritance patterns. Genome Med. 2017 Oct 31;9(1):95. doi: 10.1186/s13073-017-0482-5. PMID: 29089047; PMCID: PMC5664429.

134. Parker LE, Landstrom AP. Genetic Etiology of Left-Sided Obstructive Heart Lesions: A Story in Development. J Am Heart Assoc. 2021 Jan 19;10(2):e019006. doi: 10.1161/JAHA.120.019006. Epub 2021 Jan 12. PMID: 33432820; PMCID: PMC7955312.

135. Angelov SN, Zhu J, Hu JH, Dichek DA. What's the Skinny on Elastin Deficiency and Supravalvular Aortic Stenosis? Arterioscler Thromb Vasc Biol. 2017 May;37(5):740-742. doi: 10.1161/ATVBAHA.117.309257. PMID: 28446468; PMCID: PMC5472477.

136. Hinton RB, Adelman-Brown J, Witt S, Krishnamurthy VK, Osinska H, Sakthivel B, James JF, Li DY, Narmoneva DA, Mecham RP, Benson DW. Elastin haploinsufficiency results in progressive aortic valve malformation and latent valve disease in a mouse model. Circ Res. 2010 Aug 20;107(4):549-57. doi: 10.1161/CIRCRESAHA.110.221358. Epub 2010 Jun 24. PMID: 20576933; PMCID: PMC2928934.

137. Min S, Kinnear C, D'Alessandro LCA, Bouwmeester J, Yao R, Chiasson D, Keeley F, Mital S. Genetic Diagnosis and the Severity of Cardiovascular Phenotype in Patients With Elastin Arteriopathy. Circ Genom Precis Med. 2020 Dec;13(6):e002971. doi: 10.1161/CIRCGEN.120.002971. Epub 2020 Sep 22. PMID: 32960096; PMCID: PMC7748044.

138. Klopocki E, Hennig BP, Dathe K, Koll R, de Ravel T, Baten E, Blom E, Gillerot Y, Weigel JF, Krüger G, Hiort O, Seemann P, Mundlos S. Deletion and point mutations of PTHLH cause brachydactyly type E. Am J Hum Genet. 2010 Mar 12;86(3):434-9. doi: 10.1016/j.ajhg.2010.01.023. Epub 2010 Feb 18. PMID: 20170896; PMCID: PMC2833367.

139. Odelin G, Faure E, Coulpier F, Di Bonito M, Bajolle F, Studer M, Avierinos JF, Charnay P, Topilko P, Zaffran S. Krox20 defines a subpopulation of cardiac neural crest cells contributing to arterial valves and bicuspid aortic valve. Development. 2018 Jan 3;145(1):dev151944. doi: 10.1242/dev.151944. PMID: 29158447.

140. Stankunas K, Shang C, Twu KY, Kao SC, Jenkins NA, Copeland NG, Sanyal M, Selleri L, Cleary ML, Chang CP. Pbx/Meis deficiencies demonstrate multigenetic origins of congenital heart disease. Circ Res. 2008 Sep 26;103(7):702-9. doi:

10.1161/CIRCRESAHA.108.175489. Epub 2008 Aug 21. PMID: 18723445; PMCID: PMC2633052.

141. Bessho Y, Miyoshi G, Sakata R, Kageyama R. Hes7: a bHLH-type repressor gene regulated by Notch and expressed in the presomitic mesoderm. Genes Cells. 2001 Feb;6(2):175-85. doi: 10.1046/j.1365-2443.2001.00409.x. PMID: 11260262.

142. Jia Y, Chen J, Zhong J, He X, Zeng L, Wang Y, Li J, Xia S, Ye E, Zhao J, Ke B, Li C. Novel rare mutation in a conserved site of PTPRB causes human hypoplastic left heart syndrome. Clin Genet. 2023 Jan;103(1):79-86. doi: 10.1111/cge.14234. Epub 2022 Oct 12. PMID: 36148623.

143. Pirruccello JP, Di Achille P, Nauffal V, Nekoui M, Friedman SF, Klarqvist MDR, Chaffin MD, Weng LC, Cunningham JW, Khurshid S, Roselli C, Lin H, Koyama S, Ito K, Kamatani Y, Komuro I; BioBank Japan Project; Jurgens SJ, Benjamin EJ, Batra P, Natarajan P, Ng K, Hoffmann U, Lubitz SA, Ho JE, Lindsay ME, Philippakis AA, Ellinor PT. Genetic analysis of right heart structure and function in 40,000 people. Nat Genet. 2022 Jun;54(6):792-803. doi: 10.1038/s41588-022-01090-3. Epub 2022 Jun 13. PMID: 35697867.

144. Lahm H, Jia M, Dreßen M, Wirth F, Puluca N, Gilsbach R, Keavney BD, Cleuziou J, Beck N, Bondareva O, Dzilic E, Burri M, König KC, Ziegelmüller JA, Abou-Ajram C, Neb I, Zhang Z, Doppler SA, Mastantuono E, Lichtner P, Eckstein G, Hörer J, Ewert P, Priest JR, Hein L, Lange R, Meitinger T, Cordell HJ, Müller-Myhsok B, Krane M. Congenital heart disease risk loci identified by genome-wide association study in European patients. J Clin Invest. 2021 Jan 19;131(2):e141837. doi: 10.1172/JCI141837. PMID: 33201861; PMCID: PMC7810487.

145. Cao J, O'Day DR, Pliner HA, Kingsley PD, Deng M, Daza RM, Zager MA, Aldinger KA, Blecher-Gonen R, Zhang F, Spielmann M, Palis J, Doherty D, Steemers FJ, Glass IA, Trapnell C, Shendure J. A human cell atlas of fetal gene expression. Science. 2020 Nov 13;370(6518):eaba7721. doi: 10.1126/science.aba7721. PMID: 33184181; PMCID: PMC7780123.

146. Buijtendijk MFJ, Barnett P, van den Hoff MJB. Development of the human heart. Am J Med Genet C Semin Med Genet. 2020 Mar;184(1):7-22. doi: 10.1002/ajmg.c.31778. Epub 2020 Feb 12. PMID: 32048790; PMCID: PMC7078965.

147. Fruitman DS. Hypoplastic left heart syndrome: Prognosis and management options. Paediatr Child Health. 2000 May;5(4):219-25. doi: 10.1093/pch/5.4.219. PMID: 20177524; PMCID: PMC2817797.

148. Wiesinger A, Boink GJJ, Christoffels VM, Devalla HD. Retinoic acid signaling in heart development: Application in the differentiation of cardiovascular lineages from human pluripotent stem cells. Stem Cell Reports. 2021 Nov 9;16(11):2589-2606. doi: 10.1016/j.stemcr.2021.09.010. Epub 2021 Oct 14. PMID: 34653403; PMCID: PMC8581056.

149. Wiesinger A, Boink GJJ, Christoffels VM, Devalla HD. Retinoic acid signaling in heart development: Application in the differentiation of cardiovascular lineages from human pluripotent stem cells. Stem Cell Reports. 2021 Nov 9;16(11):2589-2606. doi: 10.1016/j.stemcr.2021.09.010. Epub 2021 Oct 14. PMID: 34653403; PMCID: PMC8581056.

150. Litviňuková M, Talavera-López C, Maatz H, Reichart D, Worth CL, Lindberg EL, Kanda M, Polanski K, Heinig M, Lee M, Nadelmann ER, Roberts K, Tuck L, Fasouli ES,

DeLaughter DM, McDonough B, Wakimoto H, Gorham JM, Samari S, Mahbubani KT, Saeb-Parsy K, Patone G, Boyle JJ, Zhang H, Zhang H, Viveiros A, Oudit GY, Bayraktar OA, Seidman JG, Seidman CE, Noseda M, Hubner N, Teichmann SA. Cells of the adult human heart. Nature. 2020 Dec;588(7838):466-472. doi: 10.1038/s41586-020-2797-4. Epub 2020 Sep 24. PMID: 32971526; PMCID: PMC7681775.

**Publishing Agreement**

It is the policy of the University to encourage open access and broad distribution of all theses, dissertations, and manuscripts. The Graduate Division will facilitate the distribution of UCSF theses, dissertations, and manuscripts to the UCSF Library for open access and distribution.  UCSF will make such theses, dissertations, and manuscripts accessible to the public and will take reasonable steps to preserve these works in perpetuity.

I hereby grant the non-exclusive, perpetual right to The Regents of the University of California to reproduce, publicly display, distribute, preserve, and publish copies of my thesis, dissertation, or manuscript in any form or media, now existing or later derived, including access online for teaching, research, and public service purposes.

DocuSigned by:

*Alexander Merriman*

48AF1E6041AE405...          Author Signature

4/28/2023

Date